

MECHANICAL RESPONSE OF CHEMICALLY TREATED SULFATE-RICH CLAY

UNDER MULTIPLE TRIAXIAL STRESS PATH

by

AZADEH ASGHARIASTANEH

DISSERTATION

Submitted in partial fulfillment of the requirements

for the degree of Doctor of Philosophy at

The University of Texas at Arlington

August 2021

Supervising Committee:

Dr. Laureano R. Hoyos (CE), Supervising Professor

Dr. Xinbao Yu (CE), Co-Supervising Professor

Dr. Sahadat Hossain (CE)

Dr. Saibun Tjuatja (EE)

Dr. Diego D. Pérez-Ruiz (Courtesy Membership)

Copyright © by Azadeh Asghariastaneh 2021

All Rights Reserved

ACKNOWLEDGEMENTS

I would like to thank my advisor, Dr. Laureano R. Hoyos, for his guidance and support throughout my master's and Ph.D. programs. He supported me through this journey with his valuable guidance and recommendations. I also like to extend my gratitude to my co-advisor, Dr. Xinbao Yu, for his support and help during my study and for giving me the opportunity to utilize his research group's lab facilities. I would also like to thank Dr. Diego Pérez-Ruiz for his guidance and support and for transferring his valuable knowledge regarding lab devices. I would also like to express my appreciation to other committee members, Dr. Sahadat Hossain and Dr. Saibun Tjautja, for their valuable suggestions for my thesis.

I appreciate all my friends' and colleagues' help during my studies, including Nice, Gang, Maedot, Roya, Omid, Asif, Sabrina, Prabesh, Azijul, and Shi. I also thank Mr. Apostolov from the Geocomp company for his valuable guidance and help throughout my experimental efforts.

My husband's, Maziar Mahdavi's, support is deeply appreciated, and I am grateful for the lifelong encouragement and help of my parents, Abolghasem Asghariastaneh and Atefeh Sabouri, and my siblings (Ahmad, Elham, Alaleh and Afsaneh).

ABSTRACT

MECHANICAL RESPONSE OF CHEMICALLY TREATED SULFATE-RICH CLAY UNDER MULTIPLE TRIAXIAL STRESS PATH

Azadeh Asghariastaneh, Ph.D.

The University of Texas at Arlington, 2021

Supervising Professors: Laureano R. Hoyos (Advisor), Xinbao Yu (Co-Advisor)

Expansive clayey soils, which are abundant in arid and semi-arid areas, including the state of Texas, can lead to excessive distress in pavements, foundations, embankments, earth retaining systems and other civil infrastructure that is either made of or supported by this type of soils. Calcium-based stabilizers, such as lime, cement and fly ash, have become popular soil stabilizers due to their ready availability and relatively low cost; however, myriad cases of failures of pavements and foundation built over sulfate-rich treated clay have led researchers to search for more efficient substitutes for calcium-based stabilizers. A very limited number of studies, however, have investigated the mechanical response of chemically treated clay under the wide range of multiple stress path that the soil is likely to undergo during the construction, post-construction and/or soil excavation stages.

In the present research work, a thorough assessment of the behavior of chemically treated expansive clay was accomplished by experimentally characterizing its mechanical response under multiple triaxial stress path, which can ultimately contribute to the postulation of more robust constitutive models for untreated and treated sulfate-rich expansive soils. A fully servo-controlled triaxial system was utilized to test natural and treated samples of highly plastic, sulfate-rich clay under unconsolidated-undrained hydrostatic compression (HC), proportional loading (PL), conventional triaxial compression (CTC), triaxial compression (TC) and triaxial extension (TE) stress path.

Test results were used to experimentally calibrate key mechanical properties and constitutive parameters of natural and treated soils, including the assessment of critical state lines and compaction induced yield loci. The results showed that both 5% Type V cement + 15% Class F fly ash, and 6% lime + 4% Class F fly ash, can yield optimum performance in terms of volumetric stiffness, shear strength and critical state response of sulfate-rich expansive clay. However, in more practical terms, the mixture of 6% lime + 4% Class F fly ash would be most suitable as a treatment given the increased ductility that is manifestly observed from the stress-strain-stiffness response of lime-fly ash treated soil.

TABLE OF CONTENTS

| | |
|---|----|
| CHAPTER 1 | 1 |
| BACKGROUND AND SCOPE | 1 |
| 1.1 Introduction..... | 1 |
| 1.2 Justification..... | 3 |
| 1.3 Main Objectives | 4 |
| 1.4 Thesis Organization | 5 |
| CHAPTER 2 | 7 |
| LITERATURE REVIEW: CONVENTIONAL TESTING | 7 |
| CHAPTER 3 | 28 |
| LITERATURE REVIEW: MULTIPLE TRIAXIAL TESTING | 28 |
| CHAPTER 4 | 42 |
| EXPERIMENTAL PROGRAM AND MATERIALS..... | 42 |
| 4.1 Test Soil and Sulfate Content | 42 |
| 4.2 Chemical Treatments | 47 |
| 4.3 Experimental Variables..... | 49 |
| 4.4 Triaxial System: Main Components and Added Features | 50 |
| 4.5 Repeatability of Test Results | 53 |
| CHAPTER 5 | 54 |

| | |
|---|-----|
| ANALYSIS OF RESULTS: CONVENTIONAL TRIAXIAL TESTING | 54 |
| 5.1 Stress-Strain Response: Natural and Treated Clay | 54 |
| 5.2 Mohr Circles at Failure: Natural and Treated Clay | 60 |
| 5.3 Failure Envelopes: Natural and Treated Clay | 66 |
| CHAPTER 6 | 68 |
| ANALYSIS OF RESULTS: MULTIPLE TRIAXIAL TESTING | 68 |
| 6.1 Stress path and Stress-Strain-Work Response: Natural and Treated Clay | 68 |
| 6.2 Proportional Loading (PL) Stress path | 92 |
| 6.4 Unconsolidated-Undrained Critical State Lines: Natural and Treated Clay | 96 |
| 6.5 Yielding in Compression and Extension: Natural and Treated Clay | 104 |
| 6.6 Calibration of Constitutive Parameters | 111 |
| CHAPTER 7 | 114 |
| TRUE TRIAXIAL TESTING: PRELIMINARY RESULTS | 114 |
| 7.1 Cubical Device: Main Components | 114 |
| 7.2 Response of Chemically Treated Clay | 116 |
| CHAPTER 8 | 119 |
| CONCLUSIONS AND FUTURE WORK | 119 |
| 8.1 Summary | 119 |
| 8.2 Conclusions | 119 |

| | |
|--|-----|
| 8.3 Recommendations for Future Work..... | 121 |
| References..... | 122 |

CHAPTER 1

BACKGROUND AND SCOPE

1.1 Introduction

Expansive soils are problematic due to their propensity for shrinking and swelling, which leads to significant distress in geotechnical infrastructures, such as cracks in pavements and pipelines and excessive settlement or heaving of the foundations of residential or commercial buildings. Expansive soils are primarily found in arid and semi-arid places such as Australia, Canada, China, South Africa, India, and the United States (U.S.). In the U.S., the civil infrastructure in Texas is one of the most severely affected by the swelling and shrinking of expansive soils (He, 2019). Myriad cases have been reported of residential units that sustained significant damage because of non-uniform foundation deflections that were a direct result of their being built on expansive soil. Expansive clays are vulnerable to moisture variations caused by pipe leaks, watering, heavy rain, seasonal weather changes, and evaporation that can exacerbate the soil shrinkage and thus magnify the non-uniform deflections. Figure 1.1, for instance, shows a residential unit in Australia that experienced multiple cracks in the walls and ceilings due to excessive foundation deflection that was mostly caused by watering their garden (Li et al., 2014).



Figure 1.1 Exposed cracks in a residential building founded on expansive soil (Li et al., 2014)

Chemical stabilization has been proven to be a feasible solution for suppressing the swelling effects of expansive clayey soil. The stabilizers are divided into two categories: traditional stabilizers (lime, cement, and fly ash) and by-product stabilizers (enzymes, geopolymers, and ionic-based stabilizers) (He, 2019).

Chemical treatment of sulfate-rich expansive soils, particularly with lime- and cement-based methods, has been utilized often due to its relatively low cost and availability. Over the last few decades, however, the prevalence of pavement failures caused by excessive heaving and/or shrinking of lime- and cement-treated subgrade soils with moderate-to-high sulfate content have led researchers to search for a viable alternative. Investigations were conducted to assess the feasibility and effectiveness of using calcium-based stabilizers in sulfate-rich soils and researchers concluded, with solid experimental evidence, that the excessive heave phenomenon can be attributed to a crystal named *Ettringite*, which is formed from the reaction of free alumina and sulfate in the natural soil with the calcium in the stabilizer, as depicted in Figure 1.2 (Semane, 2014; Knop et al., 2016; Puppala et al., 2019).

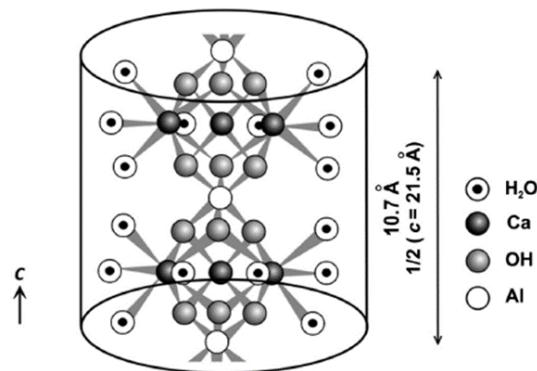


Figure 1.2 Schematic illustration of ettringite molecular structure (Puppala et al., 2019)

In addition to the specific type of chemical stabilizer, other variables such as curing and mellowing times were investigated to assess their effects on the swell reduction and strength gain of treated expansive clays. It was observed that longer curing and mellowing periods resulted in higher lime consumption by the clay particles in lime-treated soil, and the long-term chemical reaction in lime-treated soils required a longer mellowing duration to stabilize the soil than did the cement-treated clay.

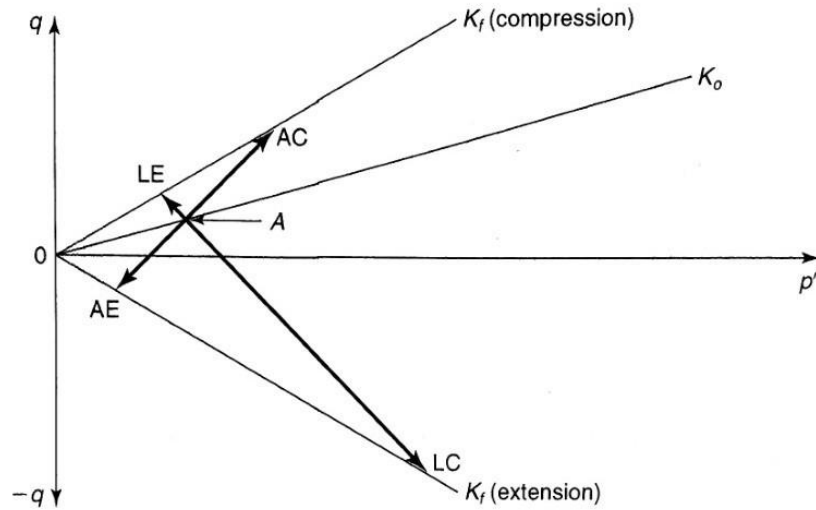
1.2 Justification

Abundant studies have been conducted on the performance of different treatment methods in counteracting the detrimental effects of calcium-based stabilizers. These studies, many of which compare the strength parameters of stabilized and natural soil, are discussed in detail in the literature review.

Ascertaining the exact stress state of the soil in the field is vital to obtaining reliable strength parameters for treated soils. For this research, a conventional and a true triaxial apparatus were used, as other frequently utilized devices, like oedometers or direct shear, are not capable of applying both the soil stress history and the potential shear stresses that the soil undergoes in the field. The triaxial device is also beneficial for subjecting test specimens to either isotropic stress or some other stress condition with a different ratio of axial to radial effective stress. These stress conditions are named stress path and are discussed in more detail in Chapter 3.

Most of the related studies in the reviewed literature focused on axial compression stress path, which are not necessarily suitable since the treated soil in the field may undergo a wide range of different stress path other than just axial compression. Figure 1.3 presents

a conceptual schematic of the variable stress path that are most feasible in the field, where q represents deviatoric stress, p represents mean stress, and point A represents the in-situ stress state of the soil prior to loading.



| Symbol | Geotechnical engineering example |
|-------------------------|--|
| AC: Axial compression | Foundation loading – increase σ_v , σ_h constant |
| LE: Lateral extension | Active earth pressure – decrease σ_h , σ_v constant |
| AE: Axial extension | Unloading (excavation) – decrease σ_v , σ_h constant |
| LC: Lateral compression | Passive earth pressure – increase σ_h , σ_v constant |

Figure 1.3 Stress path during drained loadings on normally consolidated clay and sand (Holtz and Kovacs, 1981)

1.3 Main Objectives

Most of the previous studies focused on the beneficial and detrimental effects of lime- and cement-based treatment methods in terms of Atterberg limits, swell-shrink potential, and unconfined compressive strength of the treated soils. An accurate prediction of treated soil behavior in the field requires a more thorough characterization of its mechanical response under multiple triaxial stress path, which constitutes a chief motivation for the present research work. To

achieve this goal, cylindrical samples of natural and chemically treated sulfate-rich clay were subjected to hydrostatic compression (HC), conventional triaxial compression (CTC), triaxial compression (TC) and triaxial extension (TE), and proportional loading (PL) stress path, utilizing a fully automated triaxial device. Test results were used to experimentally calibrate some of the key constitutive parameters of natural and treated soils, hence assessing the most effective treatment method for highly plastic, sulfate-rich clay.

1.4 Thesis Organization

This dissertation is composed of eight chapters: background and scope (Chapter 1), literature review on conventional testing of chemically treated soil (Chapter 2), literature review on triaxial and true triaxial testing of soils (Chapter 3), experimental program and variables (Chapter 4), analysis of results from conventional triaxial stress path (Chapter 5), analysis of results from multiple triaxial stress path (Chapter 6), true triaxial stress path and preliminary results for two test conducted using true triaxial (Chapter 7), and conclusions and future work (Chapter 8).

Chapter 1 includes an introduction to the research, its justification, the main objective, and the thesis organization, and describes the problems associated with expansive soils and their conventional treatment methods.

Chapter 2 provides a literature review of conventional testing of chemically treated soil, including previous studies on expansive clay stabilization, as well as a discussion of the strength parameters, such as unconfined compressive strength, resilient modulus, etc.

Chapter 3 consists of the justification for the research and an illustration of the stress path in a principal stress space, triaxial plane, q-p plane, and octahedral plane. Previous studies conducted on the variable stress path are also reported in this chapter.

Chapter 4 includes the experimental program and variables. The soil basic tests are reported, based on the soil's classification, and a table that summarizes the test variables for all the treatment methods is presented. The repeatability of test results is discussed in the last part of the chapter.

Chapter 5 presents an analysis of the experimental results, including the stress-strain response curves, Mohr circles from conventional compression triaxial tests (CTC), failure envelopes, and undrained cohesion and friction angle for each treatment. This chapter also includes a table that summarizes all of the strength parameters, such as cohesion and friction angle.

Chapter 6 is devoted to a thorough analysis of all test results from multiple triaxial stress path. Results are used to experimentally calibrate key constitutive parameters of natural and treated soils, as well as to assess the corresponding critical state lines and compaction induced yield loci.

Chapter 7 documents the preliminary results obtained from true triaxial testing. The true triaxial device used in this work is described briefly, and results from a short series of hydrostatic compression (HC) tests on statically compacted, 3-in. per side, cubical samples of natural and treated soil are presented.

Chapter 8 summarizes the main conclusions drawn from this research effort and makes recommendations for future research that could contribute to a better understanding of the most effective stabilizations methods under multiple triaxial stress path.

CHAPTER 2

LITERATURE REVIEW: CONVENTIONAL TESTING

Expansive soil has been treated for decades to suppress its swelling characteristic that adversely impacts infrastructures such as pavements, foundations, etc. Cracks are one of the most common occurrences that are caused by an expansion in bases or subgrades containing expansive soil. In addition to treating the soil to reduce the potential swelling, the treatment method selected should also contribute to increasing the soil's shear strength, stiffness, resistance to moisture, stability, and durability (TxDOT, Treatment Guidelines for Soils and Base in Pavement Structures, 2019).

Lime, cement and fly ash have been studied extensively and are considered the best-performing stabilizers. Their effectiveness is impacted, however, by the soil's chemical reactions with the stabilizer type, which boosts the soil's strength and decreases its moisture sensitivity. Lime and Class F fly ash are appropriate for high-PI materials, while cement and Class C fly ash is more effective in stabilizing medium- and low-PI soils (TxDOT, Treatment Guidelines for Soils and Base in Pavement Structures, 2019). Figure 2.1 is an illustration of the pulverizing effect of lime on clay particles.



**Figure 2.1 Clay soil before and after treatment with lime
(TxDOT, Treatment Guidelines for Soils and Base in Pavement Structures, 2019)**

Sulfate-rich expansive soils have been stabilized with lime and cement to mitigate their swelling and shrinking behaviors that result from cyclic wetting and drying (Talluri 2013). The significant distress that pavements and foundations built over these soils experience, however, has prompted further research on the effectiveness of mixing these traditional additives with non-calcium-based stabilizers, such as type F fly ash, blast furnace slag (BFS), silica fume (SF), natural pozzolana, and MKG polymers (Zhang et al., 2015; Jha et al., 2016; Cheshami et al., 2017; Puppala et al., 2019). To assess the effectiveness of mixing traditional and non-calcium-based stabilizers, many researchers have investigated their effect on the key characteristics of treated soils, such as the swell-shrink potential, unconfined compressive strength, and small-strain stiffness gains (Hoyos and Puppala, 2009; Hoyos et al., 2012; Semane, 2014; Hoyos et al., 2006; Jha et al., 2017, McCartney and Hoyos, 2018). By observing that some additives only performed well in soils with relatively low sulfate content, i.e., less than 8,000 ppm, the researchers concluded that the sulfates content (ppm) in natural soil is a critical factor (Talluri, 2013; Semane, 2014; Knop et al., 2016). It should also be noted that the moisture content of treated soil strongly influences the performance of the stabilizer (Hoyos et al., 2004).

A series of dynamic tests were conducted with a resonant column device to investigate the effects of the stabilizer type and moisture content on the stiffness of high-sulfate expansive clay (Hoyos et al., 2004). The results presented in Figure 2.2 show that the G_{max} (shear modulus) values were affected by the moisture content; the highest G_{max} was for 10% cement (V) treated soil with 95% wet of optimum (Hoyos et al., 2004).

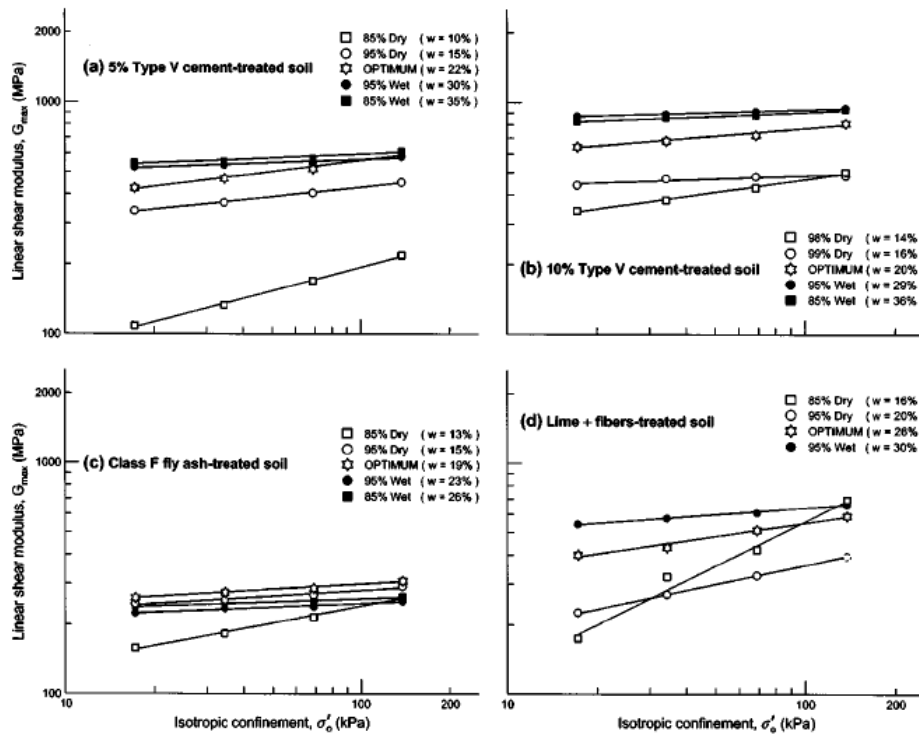


Figure 2.2 Variation of G_{max} with σ'_0 for specimens treated with: (a) 5% type v cement, (b) 10% type v cement, (c) Class F fly ash, and (d) lime + fibers (Hoyos et al., 2004)

The strength of the soil is another key parameter to consider in choosing the best-performing stabilizer. In research performed on high-sulfate expansive clay from Arlington, Texas, Sirivitmaitrie (2009) addressed the effects of different stabilizer types on the UCS and M_r . The stabilizers included 8% type v cement, 20% ground granulated blast furnace slag (GGBFS), 15%

Class F fly ash with 5% type v cement, and 8% lime with 0.15 polypropylene fibrillated fibers. The results indicated that 15% Class F fly ash with 5% type v cement and 8% type v cement gained the most CBR and M_r values (Sirivitmaitrie, 2009). Furthermore, the investigations on the total long-term cost of these treatments showed that the costs were similar for 5% type v cement, 8% type V cement, and lime-treated soil, and lower than GGBFS and lime plus fiber (Sirivitmaitrie, 2009).

The results of the experiments conducted by Sirivitmaitrie (2009) agreed well with the results of a study conducted by Vasudev (2007), wherein 26 months post-construction, he assessed the performance of various treatment methods on a section of a road built over expansive soil. The comprehensive results based on his experiments are presented in Figure 2.3.

| Study Type | Type V Cement | Cement and Fly ash | GGBFS | Lime and Fibers | Lime (Control) |
|-------------------------|---------------|--------------------|-------|-----------------|----------------|
| Instrumentation Studies | H | H | M | M | M |
| Elevation Studies | M | H | H | M | L |
| DCP Studies | H | H | M | L | L |
| Laboratory Studies | H | H | H | M | L |
| Mineralogical Studies | M | M | M | L | L |

Note- H – High Performance; M – Medium Performance; L – Low Performance

Figure 2.3 Summary of qualitative performance of stabilizers (Vasudev, 2007)

The curing period also contributes to the stabilizer's performance, and the temperature at which it is cured, and the duration of the curing can affect the strength of the stabilized soil. This effect was studied by Chittoori (2009), who performed UCS tests on CH soils from Fort Worth

and Paris, Texas and CL soils from Bryan and El Paso, Texas. All the soil samples were stabilized with 8% lime, except for the ones from Fort Worth that were treated with 6% lime. According to the UCS values, which are presented in Figure 2.4, increasing the curing temperature decreased the strength gain of the soil (Chittoori, 2009).

The effect of mineralogy on the durability of the treatment methods was analyzed, utilizing wetting/ drying tests, and the results proved that durability is a concern for stabilized clayey soil if the dominant mineral is montmorillonite (Chittoori, 2009).

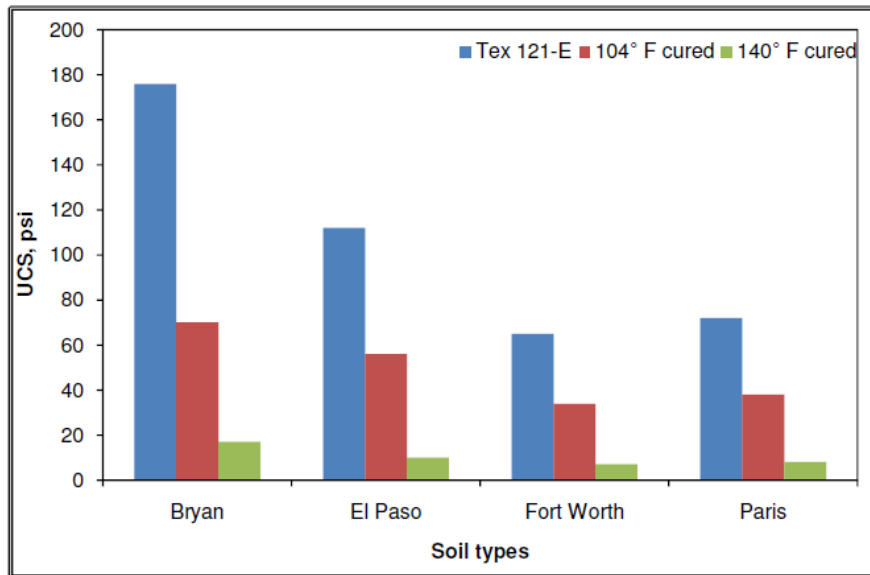


Figure 2.4 Effect of curing temperature on the UC strength of all four soils (Chittoori, 2009)

Pedarla (2009) also proved that clay mineralogy has a remarkable impact on the long-term durability of stabilized soil. He replicated moisture flocculation and rainfall by using the leachate apparatus to wet and dry the soil and performed UCS tests on soils treated with 6% cement and 8% lime to investigate the mineralogy effect. The results demonstrated that 6% cement contributes to the best durability performance when added to clays with different percentages of

montmorillonite content (Pedarla, 2009). The result of the UCS test is reported in Figure 2.5 as the percentage of strength that was retained after 14 leachate cycles.

| Soil | Additive | Average calcium concentration (ppm) | % of lime/cement leached out after 14 cycles | % strength retained after 14 cycles |
|------|-----------|-------------------------------------|--|-------------------------------------|
| M20 | 6% Lime | 375 | 0.75 | 88 |
| | 8% Lime | 526 | 0.98 | 95 |
| | 3% Cement | 217 | 0.43 | 90 |
| | 6% Cement | 614 | 0.91 | 97 |
| M40 | 6% Lime | 435 | 0.40 | 99 |
| | 8% Lime | 652 | 0.80 | 97 |
| | 3% Cement | 478 | 0.41 | 98 |
| | 6% Cement | 641 | 0.58 | 97 |
| M50 | 6% Lime | 478 | 0.88 | 96 |
| | 8% Lime | 641 | 1.15 | 98 |
| | 3% Cement | 470 | 0.43 | 97 |
| | 6% Cement | 599 | 0.83 | 99 |
| M60 | 6% Lime | 430 | 0.31 | 97 |
| | 8% Lime | 535 | 0.68 | 98 |
| | 3% Cement | 447 | 0.70 | 96 |
| | 6% Cement | 704 | 0.83 | 98 |

Figure 2.5 Retained properties of soils after 14 leachate cycles (Pedarla, 2009)

Many researchers have investigated the effect of curing time on chemically treated soils. According to Pinilla et al. (2011), the resilient modulus (stiffness) of an Oklahoma grained soil treated with cement kiln dust and Class C fly ash was significantly increased by extending the curing time. The exponential relationship between the resilient modulus and the curing time (days) for CL soil treated with Class C fly ash is presented in Figure 2.6.

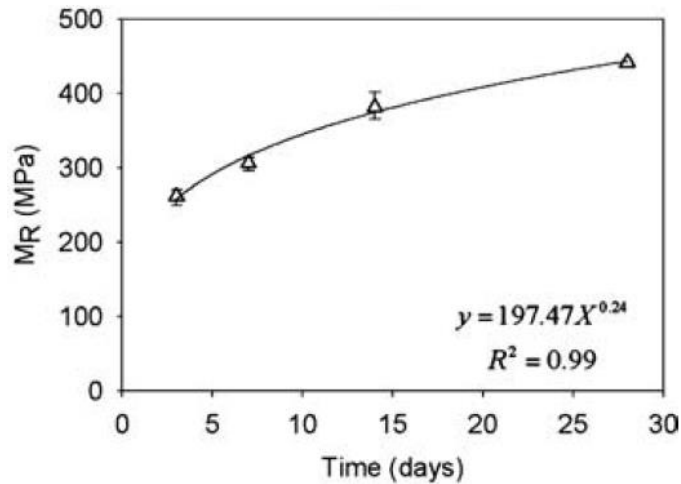


Figure 2.6 Effect of number of curing days on resilient modulus of CFS clay (Pinilla et al., 2011)

The mellowing period, which depends on the soil and stabilizer type, also has a significant impact on the strength gain of stabilized clay. For instance, lime-treated soil requires a minimum mellowing period of 1 to 4 days, because the moisture resistance is the result of the alternation of the soil particles mechanism, which happens slowly over time (TxDOT, Treatment Guidelines for Soils and Base in Pavement Structures, 2019). To address the mellowing period's importance, Gaily (2012) conducted experiments to investigate the effect of increasing the mellowing period from 0 to 3 days for 6% lime-stabilized clay with variable sulfate contents. The UCS test results revealed that increasing the mellowing time intensified the strength of the soil with 30000 ppm sulfate; however, strength improvement was not significant in soil containing more than 30000 ppm sulfate. He also analyzed the effect of mellowing on the loss of sulfate content (Figure 2.7) and found that the results were the same as those he observed for the sulfate heave.

| Soil | Initial | 0 day mellowing | | | | 3 days mellowing | | | |
|-----------|---------|----------------------|--------|--------|--------|----------------------|--------|--------|--------|
| | Sulfate | Final sulfate levels | | | | Final sulfate levels | | | |
| | (ppm) | OMC | % loss | WOMC | % loss | OMC | % loss | WOMC | % loss |
| Austin | 36,000 | 24,600 | 32 | *N/A | *N/A | 18,800 | 48 | *N/A | *N/A |
| Childress | 44,000 | 23,000 | 48 | 26,600 | 40 | 29,600 | 33 | 12,400 | 72 |
| Dallas | 12,000 | 1,600 | 87 | 1,800 | 85 | 2,200 | 82 | 1,600 | 87 |
| FM1417 | 24,000 | 2,600 | 89 | 2,800 | 88 | 3,600 | 85 | 4,000 | 83 |
| Riverside | 20,000 | 2,000 | 90 | 2,200 | 89 | 3,200 | 84 | 3,600 | 82 |
| US82 | 12,000 | 1,800 | 85 | 1,600 | 87 | 4,400 | 63 | 4,000 | 67 |

* Note: Due to the limited availability of Austin type soil, fewer tests were performed.

Figure 2.7 Percentage of sulfate loss in 6% lime-treated, high-sulfate soils (Gaily, 2012)

The long-term strength gain from cement stabilization has been studied by many researchers. Pakbaz and Alipour (2012) estimated the strength of 4% to 10% cement-treated, low-PI clay by measuring the UCS and pre-consolidation pressure. The variables in their study were cement content, number of curing days, and initial water content. According to the consolidation test results, the pre-consolidation stress values increased as the cement content increased (Pakbaz and Alipour, 2012), and the samples with the lowest water content had higher pre-consolidation pressures, as depicted in Figure 2.8. Consequently, UCS tests were conducted on samples treated with different amounts of cement and variable water contents and cured for 28 days. As shown in Figure 2.9, the highest amount of cement (10%), aligned with the lowest water content (30%), reached the highest unconfined compressive strength, which was approximately 3000 kPa (Pakbaz and Alipour, 2012).

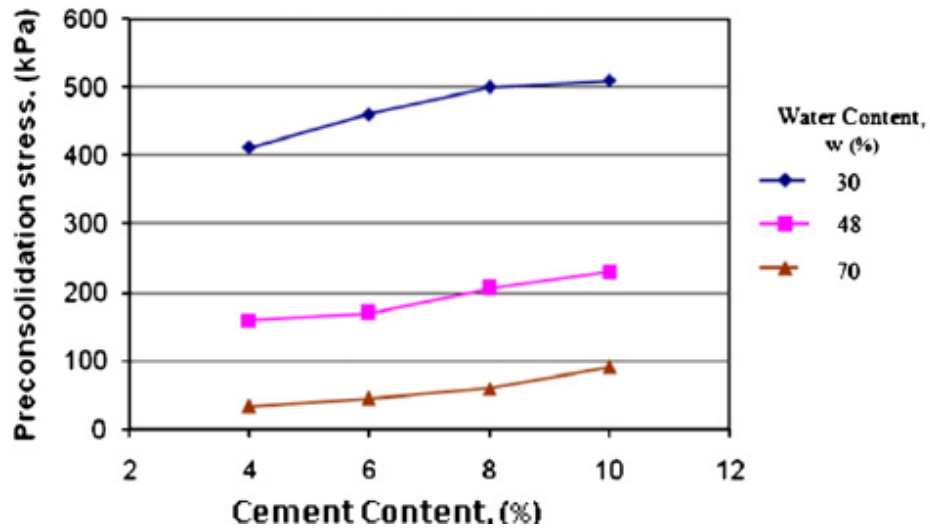


Figure 2.8 The effect of cement content and water content on preconsolidation stress (Pakbaz and Alipour, 2012)

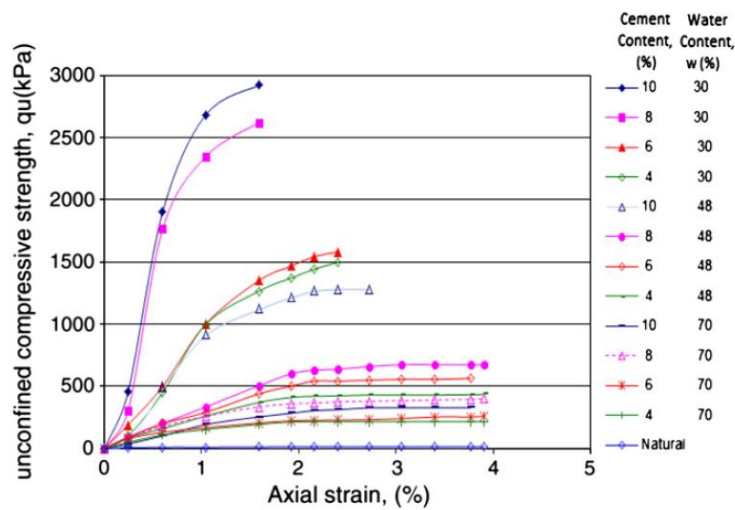


Figure 2.9 The stress-strain relationship of treated and untreated soil at different initial water and cement contents and after 28 days of curing (Pakbaz and Alipour, 2012)

High-sulfate soils that have been stabilized with calcium-based stabilizers such as lime frequently contain ettringite. Talluri (2013) conducted bender element tests on lime-treated

expansive clay containing high sulfate before and after 9 days of curing and observed that although the shear modulus of lime-treated soil was higher than that of the natural soil, the G_{max} of lime-treated samples reduced after 9 days, as indicated in Figure 2.10. This led him to conclude that a reduction in the shear modulus ettringite, due to the material softening (Talluri 2013).

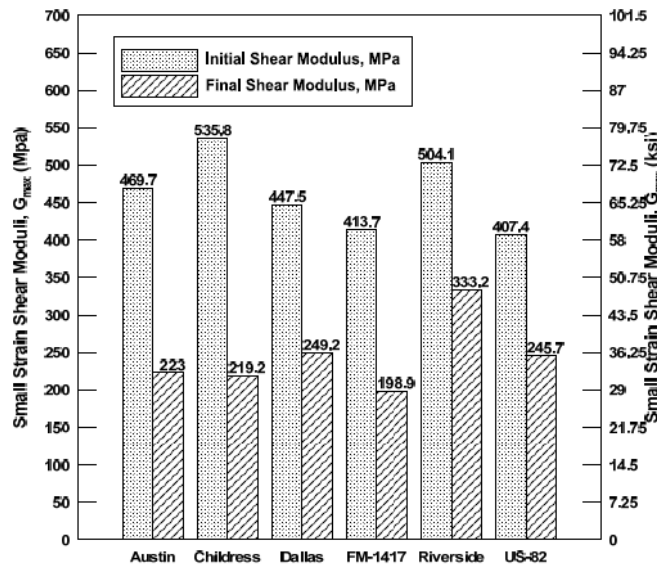


Figure 2.10 Initial and final shear modulus at OMC (Talluri, 2013)

Lucian (2013) investigated the influence of the period of mellowing on the strength of expansive clayey sand stabilized with lime and cement and found that a two-stage stabilization was beneficial since the cement increased the strength of the expansive soil abruptly after mixing, while the lime required a longer duration to achieve the maximum strength. Triaxial compression CU tests were performed on soil mellowed for 4 days and treated with different percentages of lime, followed by the addition of 2% cement and 28 days of curing. The friction angle and cohesion increased after the 4-hour mellowing period, and the strength parameters increased as the lime percentages intensified (Lucian, 2013). The triaxial strength parameters and the shape of the

sample after the test are depicted in Figures 2.11 and 2.12, respectively. According to the consolidated undrained tests, soil treated with 6% lime demonstrated the highest shear strength and cohesion (Lucian, 2013). The stress-strain responses of untreated and treated soils are compared and presented in Figure 2.13.

| | Untr. Soil | 4% Lime | 6% Lime | 8% Lime |
|------------------------|---------------|------------|------------|------------|
| Φ' [°] | 14 | 31 | 32 | 33 |
| c [kN/m ²] | 17 | 152 | 300 | 187 |

Figure 2.11 Triaxial strength parameters (Lucian, 2013)



Figure 2.12 Triaxial compression (CU) samples after the test (Lucian, 2013)

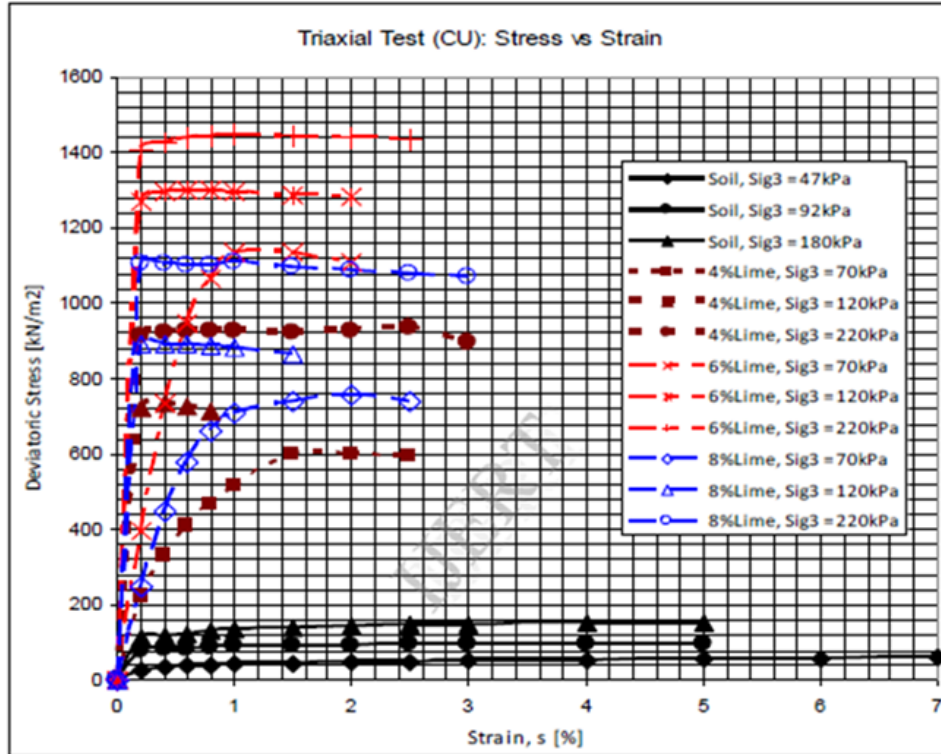


Figure 2.13 Results of CU triaxial compression on natural soil samples and lime-treated soil samples (Lucian,2013)

Khemissa and Mahamedi (2014) utilized direct shear and CBR to investigate the strength parameters of expansive, over-consolidated clay soil from Algeria that had been treated with lime and cement. Their tests showed that 8% cement plus 4% fly ash were the most effective stabilizers (Khemissa and Mahamedi, 2014). The shear strength values for different combinations of cement and lime are presented in Figure 2.14.

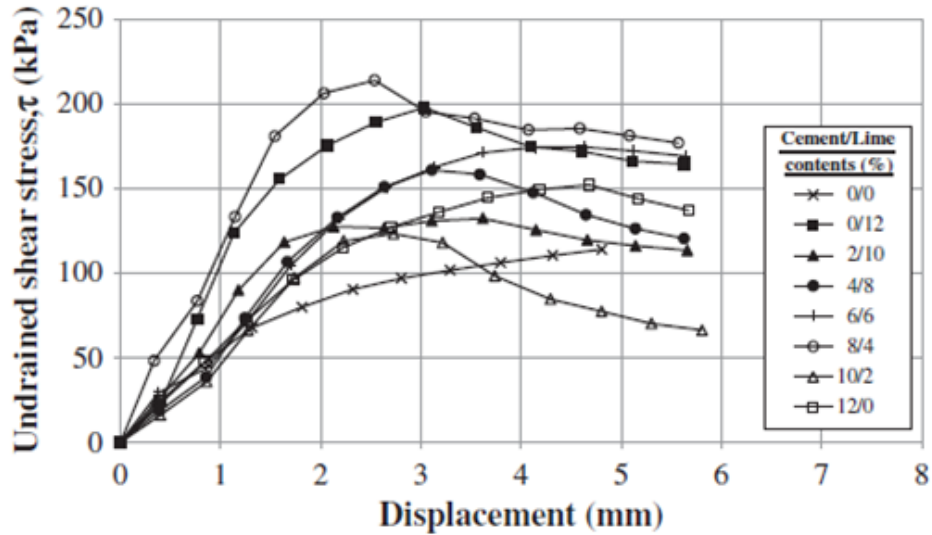


Figure 2.14 Undrained shear curves for a mixture of various cement and lime contents (Khemissa and Mahamedi, 2014)

The stiffness of stabilized soil is another noticeable criterion in selecting the best-performing soil for a long duration. A series of resonant column tests were conducted by Semane (2014) on the stiffness of stabilized soils after different mellowing durations. The soil for their study was sulfate-rich expansive clay from Sherman, Texas and the selected treatment methods were the addition of 6% lime and 4% lime + 8% FA. According to the test results, 4% lime + 8% FA with three days mellowing showed the best stiffness result (Semane, 2014). The adverse effects of increasing the durations of mellowing and curing for this treatment explain the material softening, which is illustrated in Figures 2.15 and 2.16, respectively (Semane, 2014).

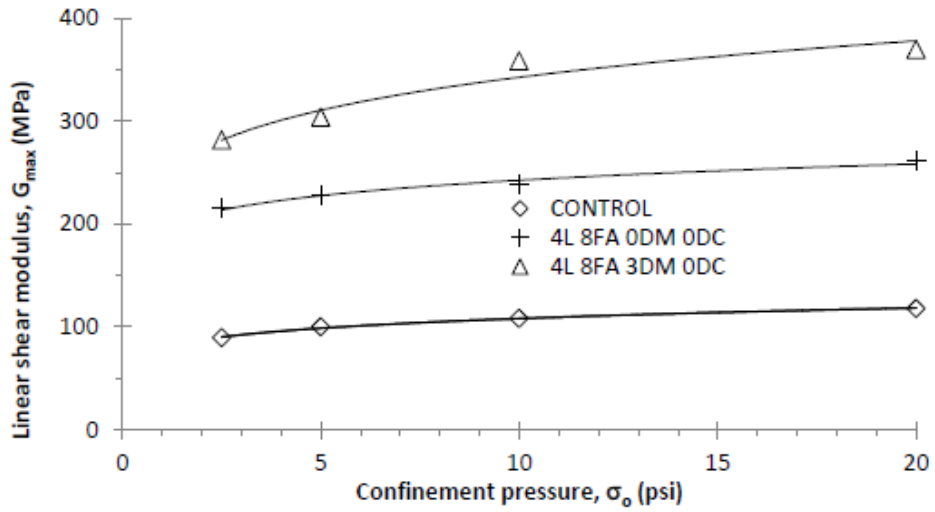


Figure 2.15 Effect of mellowing period on stiffness properties of control and soil treated with 4% lime + 8% fly ash (Semane, 2014)

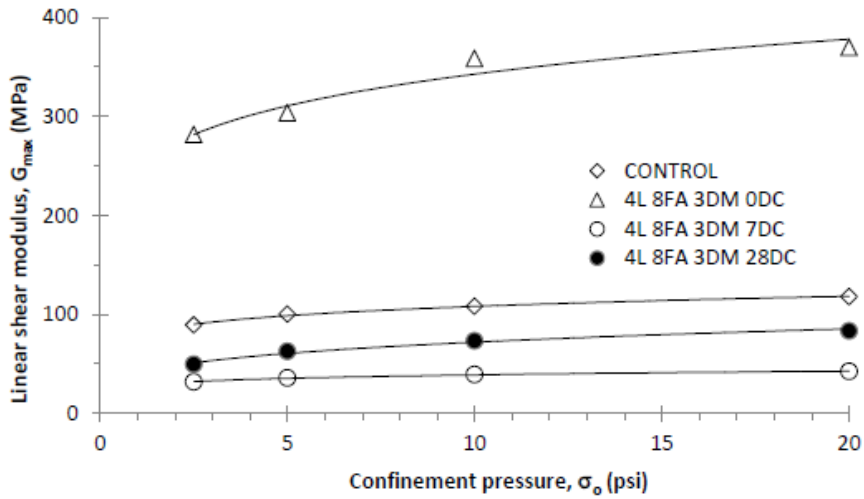


Figure 2.16 Effect of curing time on stiffness properties of control and soil treated with 4% lime + 8% fly ash (Semane, 2014)

More recently, based on resonant column testing conducted by Asghariastaneh (2017), the shear modulus was found to be highest in high-plastic clay treated with 6% lime + 4% fly ash after 14 days of curing under the highest confining pressure, as shown in Figure 2.17.

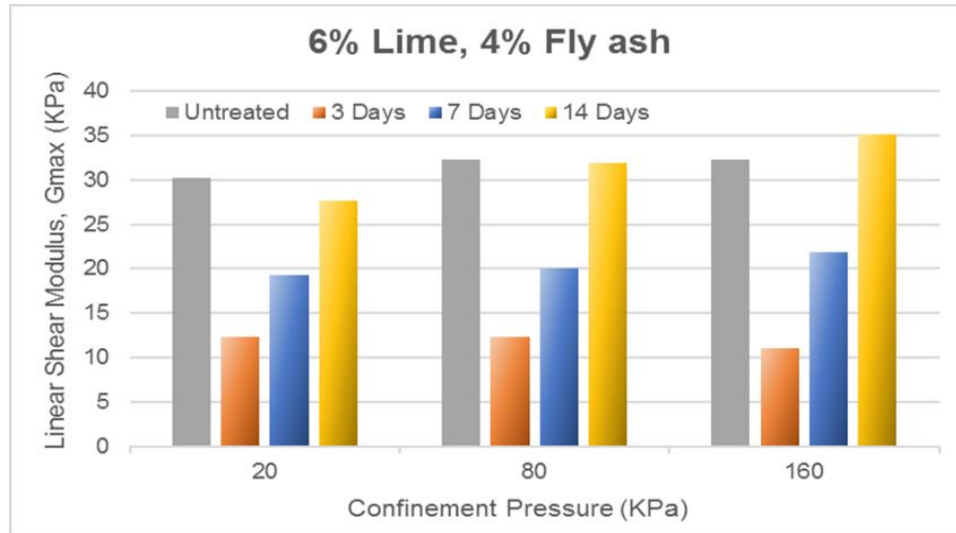


Figure 2.17 Effect of number of curing (days) on shear modulus of clay treated with lime- fly ash (Asghariastaneh, 2017).

While cement, lime, and fly ash are the most popular additives, researchers are investigating more environmentally friendly stabilizers that may have the potential to suppress the swelling effect of problematic soils. Unconsolidated, undrained triaxial compression tests were conducted on black cotton soil that had been treated with 5%, 10%, 15%, and 20 % rice husk ash (Jain et al., 2020). According to the results, the secant modulus and the peak deviator stress intensified as the stabilizer content increased. The variations of the peak deviator stress are presented in Figure 2.18. In addition, the undrained cohesion reached its maximum value when 10% RHA was added, while the undrained cohesion exhibited no specific pattern, as depicted in Figure 2.19.

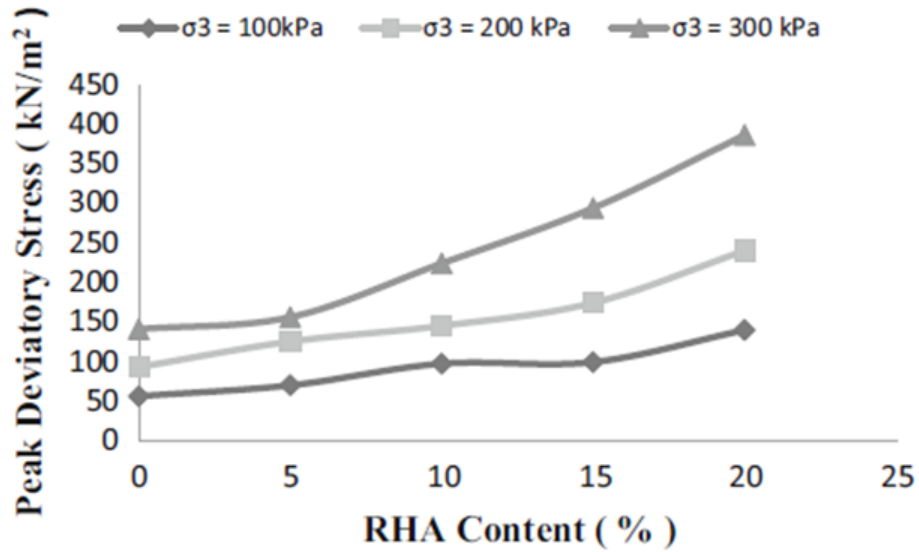


Figure 2.18 Variation in peak deviator stress with varying RHA content at different cell pressures (Jain et al., 2020)

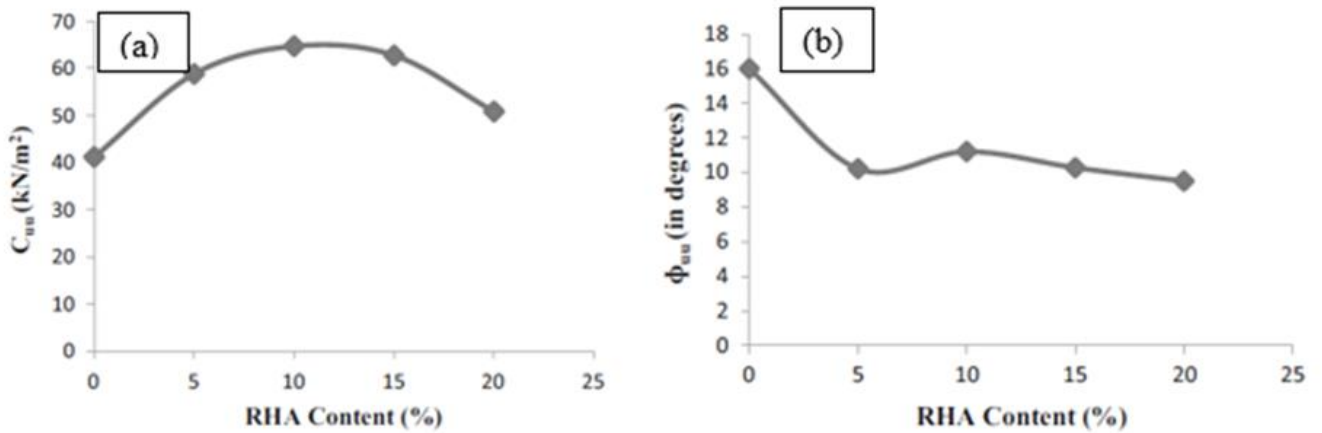


Figure 2.19 Variation in C_{uu} with RHA content: a) %, b) Variation in φ_{uu} with RHA content (%) (Jain et al., 2020)

Cement and environmentally friendly additives, including natural zeolite and recycled polyester fiber (PET), were combined and the UCS test was performed to evaluate its effectiveness in stabilizing loess. According to Mariri et al. (2019), the addition of PET can overcome the brittle

behavior of cement- and zeolite-treated soil (Mariri et al., 2019). Mariri et al. (2019) also studied the relationship between the water content and the UCS for 4% and 8% cement-treated soil, which is presented in Figure 2.20. The results showed that the most strength was achieved when the compaction water content was 1.2 times the optimum moisture content.

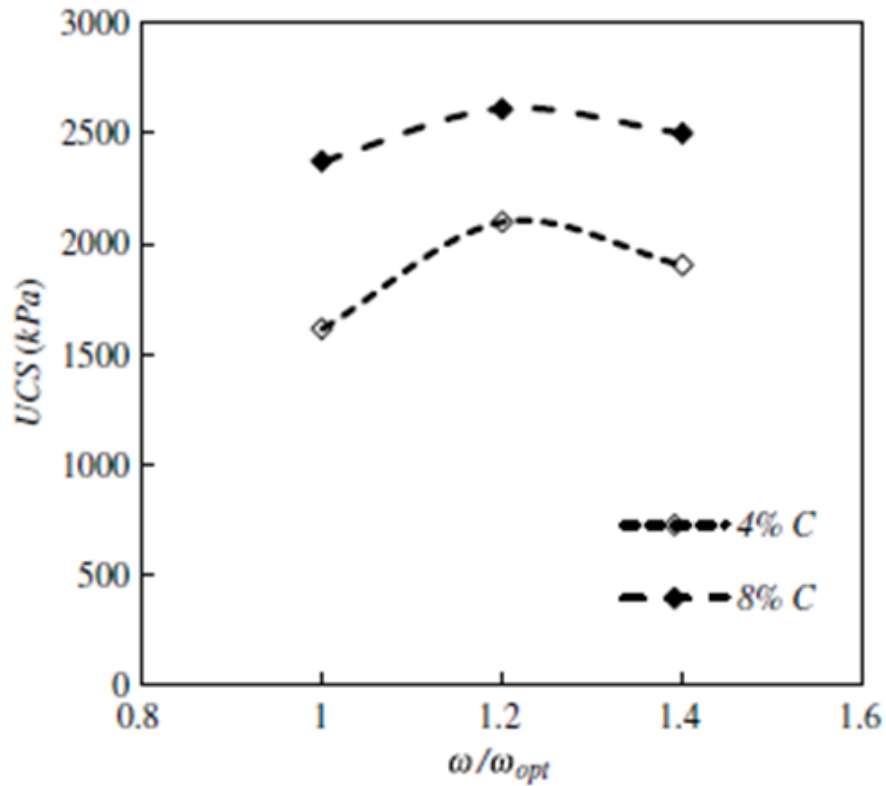


Figure 2.20 Variations in UCS with water content ratio for 28 days of curing (Mariri et al., 2019)

The popularity and necessity of environmentally friendly additives led researchers to investigate the strength properties of variable compounds. Lime sludge, a by-product of the paper industry, was utilized in a study conducted by Phanikumar and Raju (2020). CBR and UCS tests were conducted to study the effect of curing time and type of additive on the strength properties and revealed that 12% lime sludge did not decrease the swell index significantly. Therefore, 10%

cement was added to the lime-sludge-treated soil, and the strength increase was impressive: an approximate 118% increase of UCS and 293% of CBR (Phanikumar and Raju, 2020). Figure 2.21 presents the effects of additives on CBR after 28 days of curing (Phanikumar and Raju, 2020).

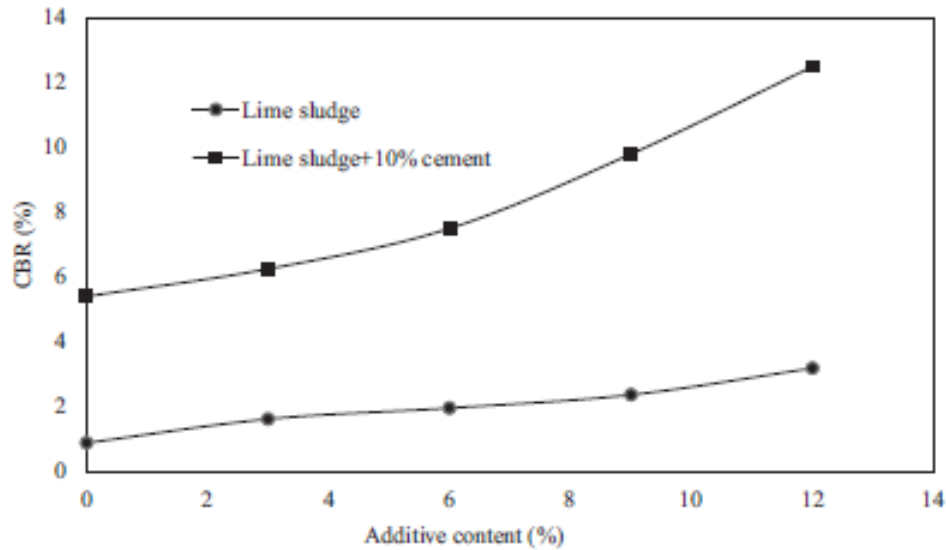


Figure 2.21 Effect of additives on soaked CBR (Phanikumar and Raju, 2020)

Gao et al (2020) conducted triaxial shear tests to investigate the influence of nano-silica grouting on the strength of the slip zone inside the slope of the Lvliang Airport. Overall, the friction angle and cohesion were improved by an increase in additive content, as illustrated in Figure 2.22. In addition, 15% to 20% nano-silica was found to be the threshold content for stabilizing the slope at an optimized cost (Gao et al., 2020).

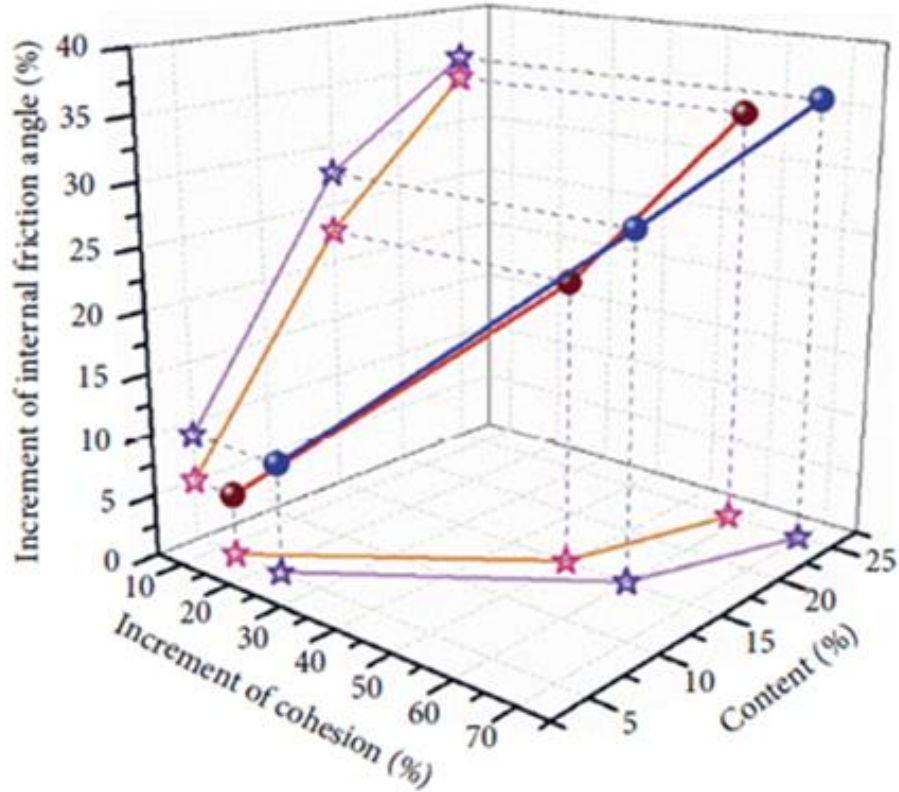


Figure 2.22 Increments of cohesion and internal friction angle of grouting samples compared with undisturbed sample (Gao et al., 2020)

As corroborated by this brief literature review, most of the previous studies on strength parameters focused on the beneficial and/or detrimental effects of lime- and cement-based treatment methods on the unconfined compressive strength, CBR, conventional triaxial, and small-strain stiffness (shear or resilient modulus) of sulfate-rich soils. An accurate prediction of the behavior of treated soil in the field, however, would require a more thorough characterization of its mechanical response under multiple stress path. Table 2.1 is a comprehensive summary of the previous studies conducted on the strength parameters of chemically stabilized clay that are mentioned in this chapter.

Table 2.1 Previous studies on Strength Parameters of Chemically Treated Clay

| Author (Year) | Soil Type | Treatment Method | Test Type | Properties |
|---------------------------------|------------------|--|--------------------------------------|----------------------------------|
| Hoyos et al. (2004) | CH | 5% cement (V), 10% cement (V), Class F fly ash, lime + fibers | Resonant column | G_{max} |
| Sirivitmaitrie (2009) | CH | 8% type V cement, 20% GGBFS, 15% Class F fly ash +5% cement (V), 8% cement (V) | UCS test setup. M_r test setup. | UCS, CBR, M_r |
| Chittoori (2009) | CH, CL | 8% lime, 6% lime | UCS test device | UCS |
| Pedarla (2009) | Clay | 6% cement, 8% lime | UCS test device | UCS |
| Pinilla et al. (2011) | CL | Cement kiln dust and Class C fly ash | M_r test set up | M_r |
| Gaily (2012) | CL | 6% Lime | UCS test device | UCS |
| Pakbaz and Alipour (2012) | Clay | 4% cement, 6% cement, 8% cement, 10% cement | UCS test device Oedometer | UCS, σ_p |
| Talluri (2013) | CH | Lime | Bender element | G_{max} |
| Lucian (2013) | CH | 4% lime, 6% lime, 8% lime | Triaxial device | CU |
| Khemissa and Mahamedi (2014) | CH | Cement + lime | Direct shear, CBR test device | Undrained shear strength, CBR |
| Semane (2014) | CH | 6% lime, 4% lime+8% fly ash | Resonant column | G_{max} |
| Asghariastaneh (2017) | CH | 6% lime + 4% fly ash | Resonant column | G_{max} |

**Table 2.1 Previous studies on Strength Parameters of Chemically Treated Clay
(Continued)**

| Author (Year) | Soil Type | Treatment Method | Test Type | Properties |
|----------------------------|------------------|--|------------------------------------|--------------------------------------|
| Mariri et al. (2019) | CL | 4% cement, 8% cement, cement + natural zeolite, cement + zeolite | UCS test device | UCS |
| Jain et al. (2020) | Clay | 0.5%, 10%, 15%, and 20 % rice husk ash | Triaxial device | Peak deviator stress, C_u , Φ |
| Phanikumar and Raju (2020) | CH | 12% lime sludge, 12% lime sludge +10% cement | UCS test device CBR test device | UCS |
| Gao et al. (2020) | Clay | 3% nano silica, 5% nano silica | GD triaxial shear test | C , φ |

CHAPTER 3

LITERATURE REVIEW: MULTIPLE TRIAXIAL TESTING

Conventional geotechnical testing devices allow for the application of loads along limited paths/modes of deformation, such as one-dimensional, hydrostatic, or axisymmetric. In nature, however, pavement subgrades and shallow foundation soils may be subjected to three-dimensional stress gradients, as illustrated in Figure 3.1. Accurate predictions of the stress-strain response of soils, therefore, require that the constitutive relations be valid for all the principal stress path that are likely to be experienced in the field.

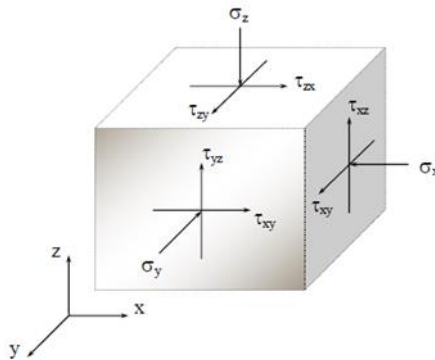


Figure 3.1 Multiaxial stress state of infinitesimal soil element (Perez-Ruiz, 2009)

A triaxial device is utilized to dictate the variable stress path that are applied to the soil in the field; consequently, it is possible to predict the stress-strain behavior of soils under different stress path from the test results. Figure 3.2 demonstrates the variable stress path that can be modeled with the triaxial device, and Figure 3.3 demonstrates the Mohr circle and stress path in

the q-p plane that can be obtained from the outputs of the triaxial shear test. Some common field stability situations and the laboratory model are presented in Figure 3.4.

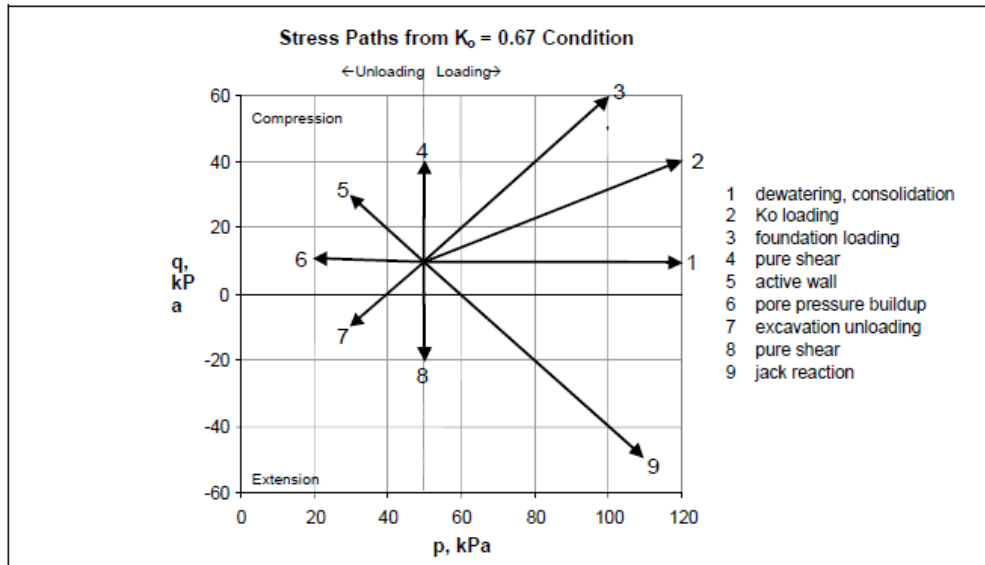


Figure 3.2 Stress path diagram for running stress path tests
(www.geocomp.com, TRIAXIAL V2.3 User's Manual, 2018)

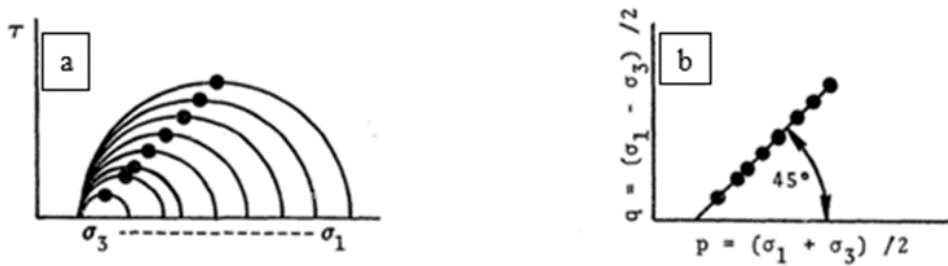


Figure 3.3 (a) Mohr circle representation, (b) Stress-path representation of stress states
(Cammack, 1978)

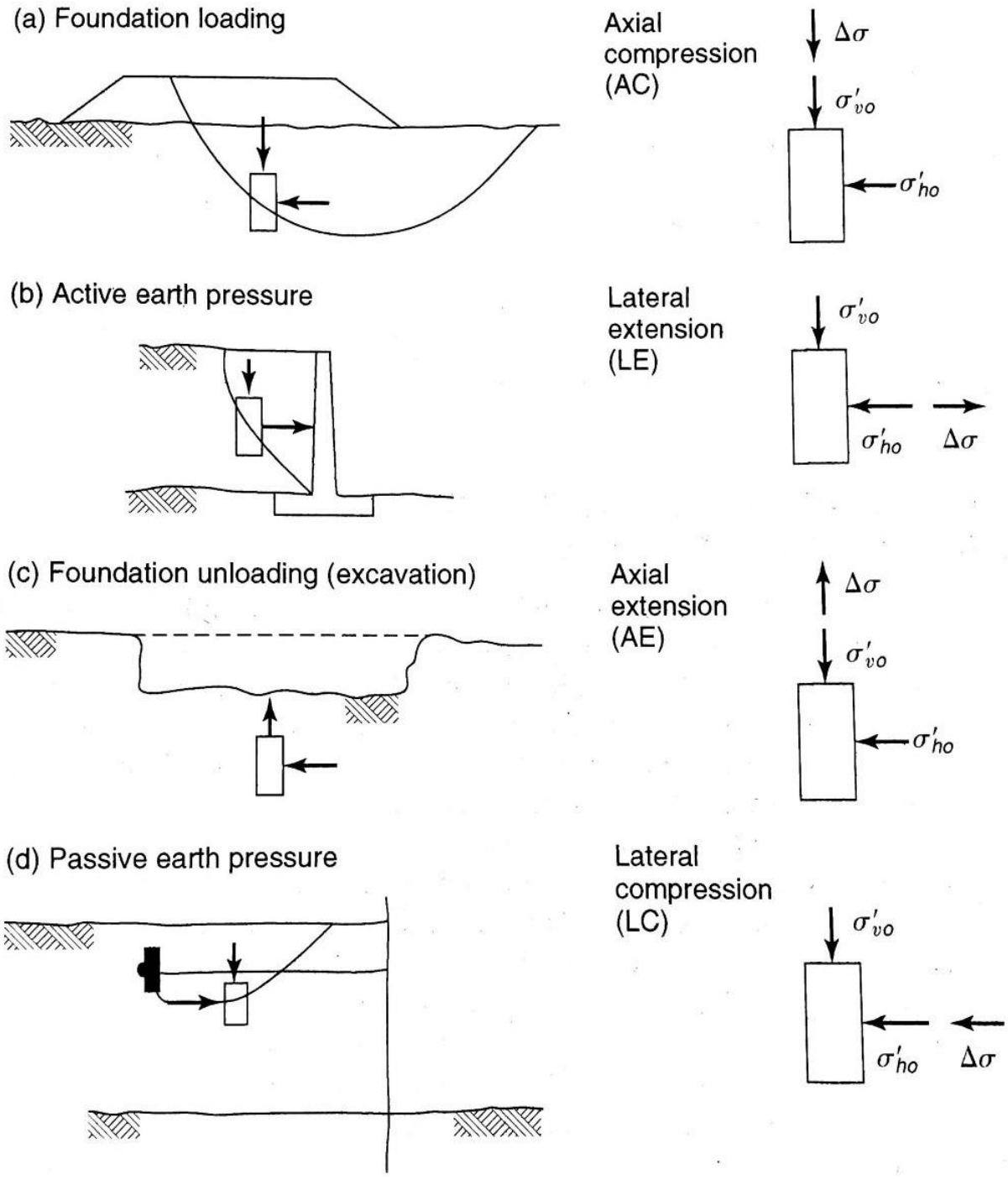


Figure 3.4 Common field stability scenarios and laboratory model
(Holtz and Kovacs, 1981)

A true triaxial (cubical) apparatus also plays a fundamental role in characterizing the stress-strain-strength of soils, as it is capable of inducing a wide range of simple-to-complex multiaxial stress path. Figure 3.5 shows a conceptual illustration of simple-to-complex multiaxial stress path that are not readily achievable with a conventional oedometer or triaxial apparatus.

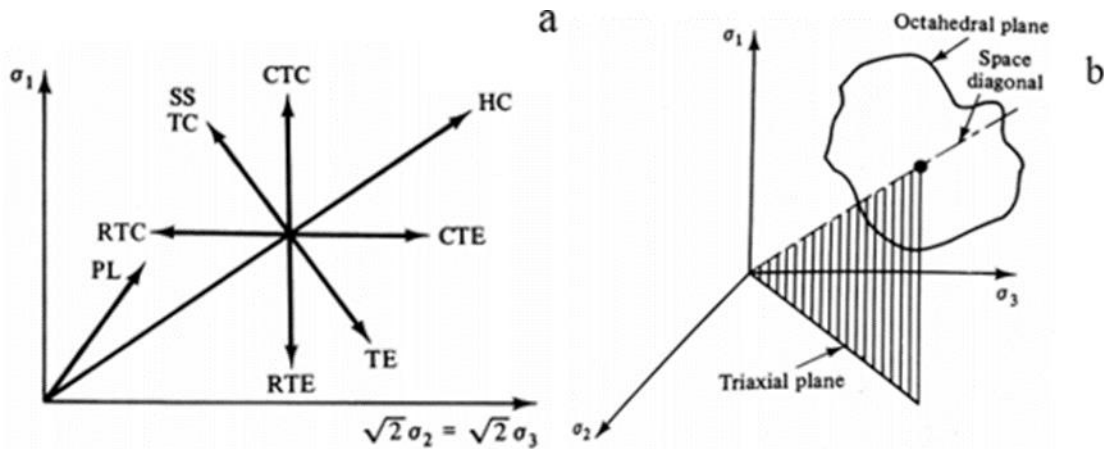


Figure 3.5 Multi-axial stress path: (a) Triaxial plane, (b) Principal stress space

The present work focuses on cylindrical samples of chemically treated clay that have been subjected to hydrostatic compression (HC), conventional triaxial compression (CTC), triaxial compression (TC), triaxial extension (TE) stress path, and proportional loading (PL) in a two-dimensional space. A preliminary test was conducted with a true triaxial device to compare the bulk modulus of cement-treated high-PI clay with natural soil, which is discussed in Chapter 7. It can be observed in Figure 3.5 that HC testing involves applying equal pressure in all three principal directions while not applying shear stress. Dewatering or consolidation is an example of this stress path in the field. During CTC testing, the major principal stress σ_1 increases while the minor principal stress (σ_3) remains constant and p increases, such as in foundation loading. During TC testing, σ_1 increases while σ_3 decreases so that the mean stress p (pure shear) remains constant.

Conversely, during TE testing or pure shear, σ_3 increases, while σ_1 decreases, and the mean stress or p remains constant. Finally, during the PL loading, the soil is consolidated with unequal horizontal and vertical stresses, with a constant k ratio.

Triaxial testing allows for thorough experimental calibrations of key constitutive parameters of soils. One of these parameters is the slope of the critical state line M , as defined by the ratio q/p in Eq. 1, where q is the deviatoric stress and p is the mean stress in Eqs. 2 and 3, respectively.

$$M = \frac{q}{p} \quad (1)$$

$$q = \frac{\sigma_1 - \sigma_3}{2} \quad (2)$$

$$p = \frac{\sigma_1 + \sigma_3}{2} \quad (3)$$

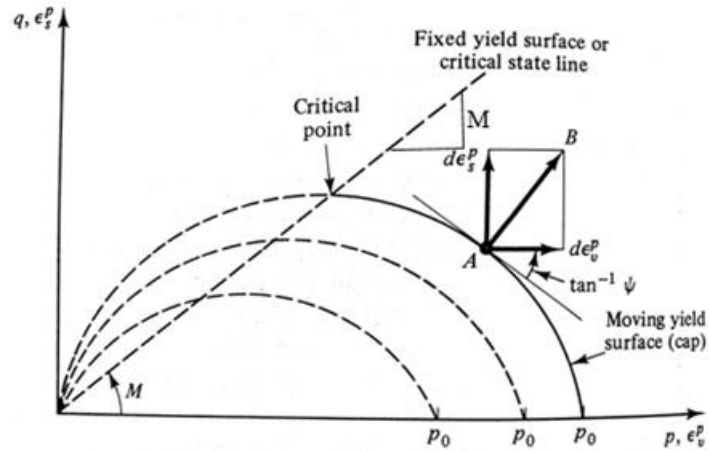
Consolidation stress path are not always axisymmetric, and the vertical and horizontal stresses can increase with variable K_0 ratios, denoting the coefficient of rest pressure shown in Eq. 4. In this study, this value was calculated using Eq. 5 for the variable treatment method, and the friction angle was obtained from the Mohr circles from the CTC stress path presented in Chapter 5. During proportional loading, the ratio of q/p is constant and equal to η , as shown in Eq.6.

$$k_0 = \frac{\sigma_h}{\sigma_v} \quad (4)$$

$$k_0 = 1 - \sin(\theta) \quad (5)$$

$$\eta = \frac{q}{p} = \frac{(1-k_0)}{(1+k_0)} \quad (6)$$

In the critical state, the values of the mean stress (p) and deviatoric stresses (q) obtained from testing the stress path of all the natural and chemically treated samples can be plotted on the q - p plane to assess the effects of the chemical treatment on the size of the yield surfaces and the slope of the critical state lines, as conceptually illustrated in Figure 3.6.



**Figure 3.6 Conceptual illustration of moving yield surface and critical state line
(Desai and Siriwardane, 1984)**

After processing the experimental data generated from each test in this study, the fundamental stress-strain response variables, such as deviatoric stress (q), mean stress (p), and axial strain increment (ϵ_a) were obtained from the test results. The stress-strain response curves were plotted and are reported in Chapters 5 and 6. In addition, the key constitutive parameters such as shear modulus (G), modulus of elasticity (E) were determined and compared for different curing times, confining pressures, and stress path.

Shear modulus (G) measures the soil's elastic shear stiffness and is defined as the shear stress to shear strain ratio. Modulus of elasticity (E) is a material's resistance to deforming

elastically, and bulk modulus (K) is a measure of the material's resistance to compression. Figure 3.7 demonstrates how G and E are inferred from q - ϵ_a curves.

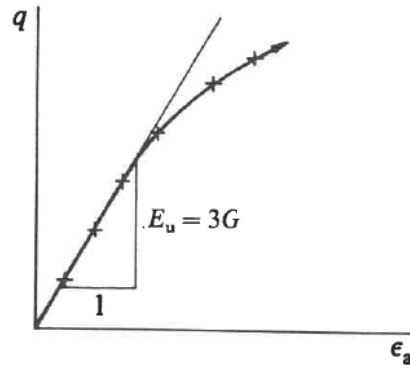


Figure 3.7 Elastic constants assessed from CTC testing (Desai and Siriwardane, 1984)

Finally, the yield loci obtained from all the stress path of natural and chemically treated samples of clay, under each confining pressure, were plotted on the q - p plane for comparison purposes. An example of a yield locus based on the Tresca and von Mises criteria is shown in Figure 3.8.

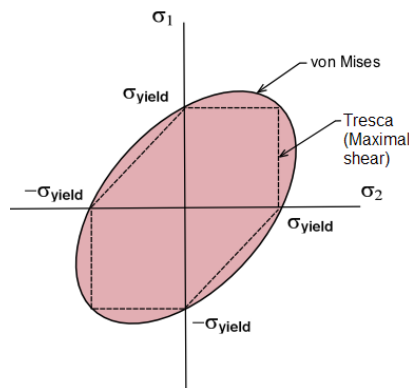


Figure 3.8 Tresca and von Mises yield criterion in 2D (planar) loading conditions (Wikipedia)

Conventional triaxial devices and CTC stress path were utilized in most of the previous studies on the behavior of chemically treated clay. A few studies, however, utilized the true triaxial

device and other stress path, and they are summarized below. The literature review focuses on work reported over the last two decades.

The three types of true triaxial devices that have been introduced since the early 1930s are categorized based upon the specific boundary conditions imposed on the cubical sample: (1) rigid or strain-controlled boundary type, (2) flexible or stress-controlled boundary type, and (3) mixed boundary type (Perez, 2009). Matsuoka et al. (2002) tested 10 cm cubical silty soil samples using the rigid or strain-controlled boundary type of true triaxial device that had inflexible loading plates, as shown in Figure 3.9. Perez-Ruiz (2009) conducted true triaxial testing on 7.62 cm cubical samples of unsaturated silty sand using a mixed boundary type of true triaxial device that allowed him to assess the size of the yield loci of compacted SP-SC soil for different matric suction conditions. The experimental and predicted yield loci of compacted SP-SC soil presented in Figure 3.10 are the results of their testing.

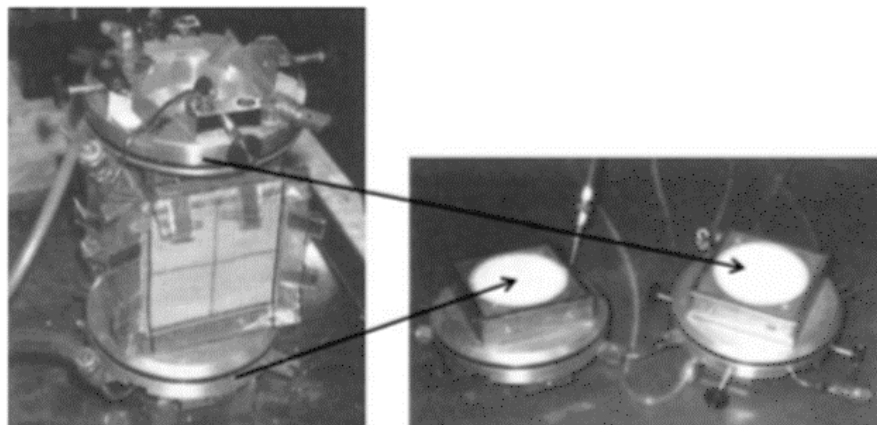


Figure 3.9 True triaxial device with rigid plates (Matsuoka et al., 2002)

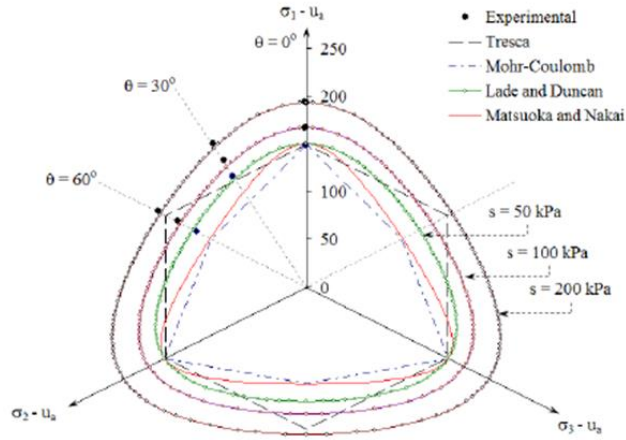


Figure 3.10 Experimental and predicted yield loci of compacted SP-SC soil (Perez-Ruiz, 2009)

Ye et al. (2013) conducted true triaxial testing on saturated samples of normally consolidated (NC) and over-consolidated (OC) clays. They used a mixed boundary type of true triaxial device, which allowed them to compare the experimental failure envelopes assessed for different load angles with the Matsuoka-Nakai failure criterion, as shown in Figure 3.11.

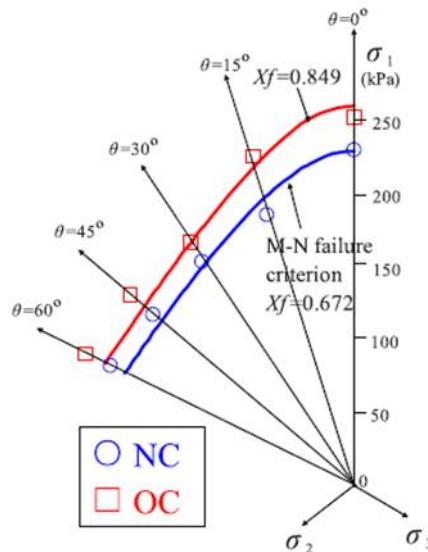


Figure 3.11 Experimental and predicted failure envelopes of normally (NC) and over-consolidated (OC) clays (Ye et al., 2013)

As illustrated in Figure 3.12, soils undergo unloading stress path with variable K_0 ratios during excavation. Huang et al. 2018 conducted a set of triaxial compression tests with constant p (TC) and K_0 consolidation unloading to investigate the difference between lateral and axial unloading. The results showed that the stress-strain responses of both stress path exhibited nonlinearity, but the failure modes were different, in that the axial unloading showed elongated failure, while the lateral unloading presented compression-shear failure (Huang et al., 2018). They established a formula for strain-stress curves for K_0 consolidation unloading, which agreed well with the data from the experiments, as presented in Figure 3.13.

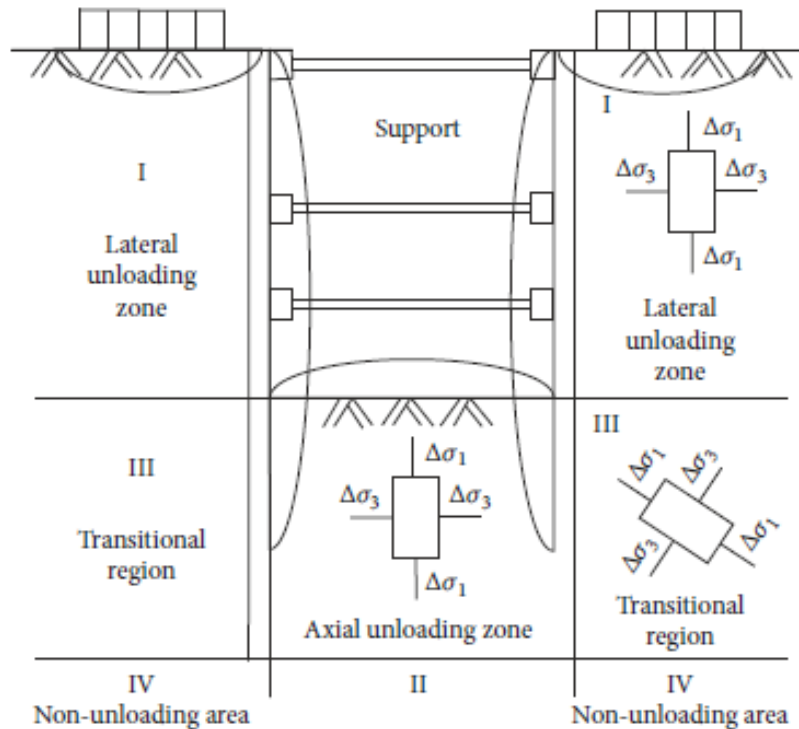


Figure 3.12 Soil stress state within the influencing scope of the foundation Pit (Huang et al., 2018)

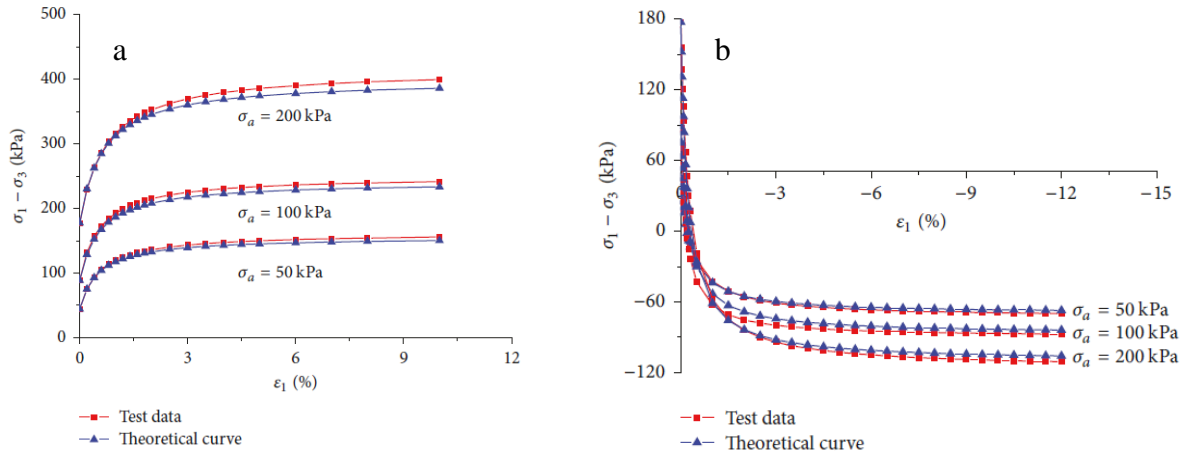


Figure 3.13 Theoretical model versus testing results for silty clay condition:

(a) Under lateral unloading condition, (b) Theoretical model versus testing results for silty clay condition under axial unloading condition (Huang et al., 2018)

The researchers found that the tangent modulus of the soil increased as the consolidation pressure intensified (Huang et al., 2018). Formulas for initial tangent modulus in unloading stress path were developed based on modifications of the Duncan-Chang model (Huang et al., 2018).

Some researchers have modeled the stress path that apply to soil elements in the field. For instance, Li et al. (2018) utilized the discrete element method (DEM) to simulate a triaxial compression test under constant P on a QH-E lunar soil simulant. The results resembled the conventional triaxial compression tests and showed that the simulated deviatoric stress-strain response was divided into hardening, softening descending, and residual strain stages and that the shear strength and residual strength intensified as the confining pressure increased (Li et al., 2018). The exported curve from the triaxial test for $p=150$ kPa agreed well with the corresponding simulation, as presented in Figure 3.14.

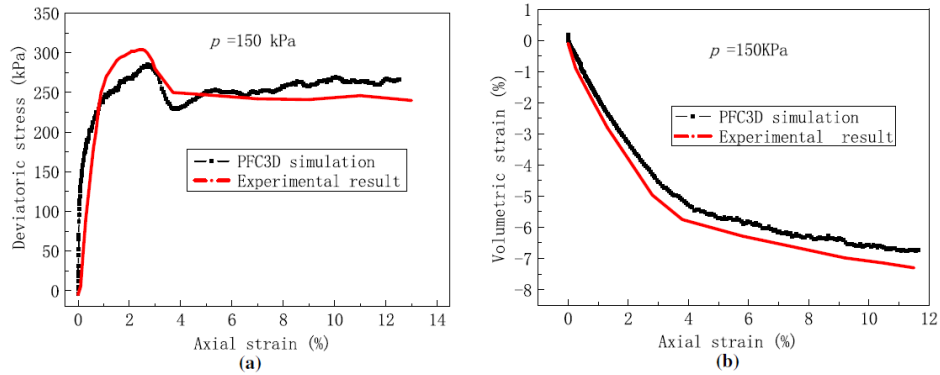


Figure 3.14 Comparison between experimental and simulation curves under P stress of 150 KPa: (a) deviatoric stress versus axial strain curves, (b) volumetric strain versus axial strain curves (Li et al., 2018)

Another study was performed by Zhang et al. (2020) to simulate different stress path induced by surcharge loading, lateral excavation, and lateral unloading with axial loading. Consolidated undrained tests were conducted on Guiyang red clay under CTC, RTC, and TC stress path, using a test device that was a pressure chamber with an axial load piston. The stress-strain responses for the different stress path are presented in Figure 3.15.

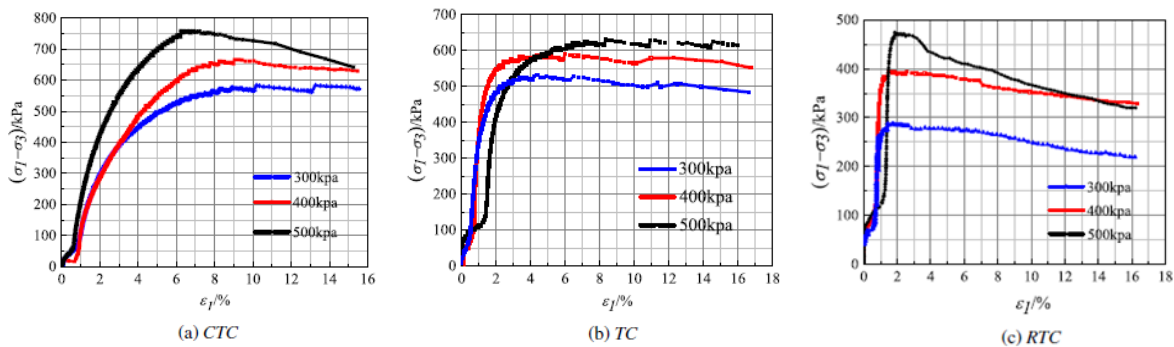


Figure 3.15 Stress-strain response of different stress path of Guiyang red clay (CU test) (Zhang et al., 2020)

The results revealed that the stress path had a greater influence on cohesion than on friction angles (Zhang et al., 2020). Both values are reported in Figure 3.16, which demonstrates the obtained Mohr circles. The peak shear stress was the largest for the path with increasing P and increased as the initial confining pressure rose, as illustrated in Figure 3.17.

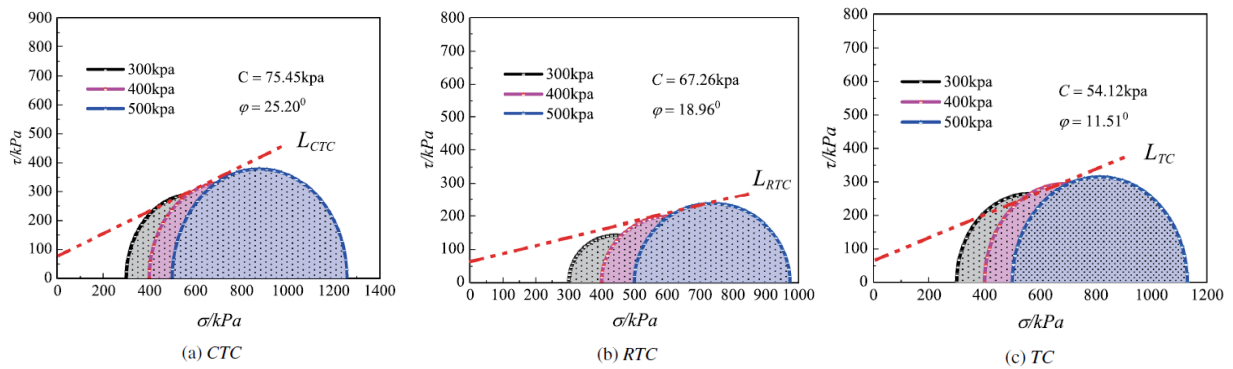


Figure 3.16 Mohr circle of stress under different stress path (CU test) (Zhang et al., 2020)

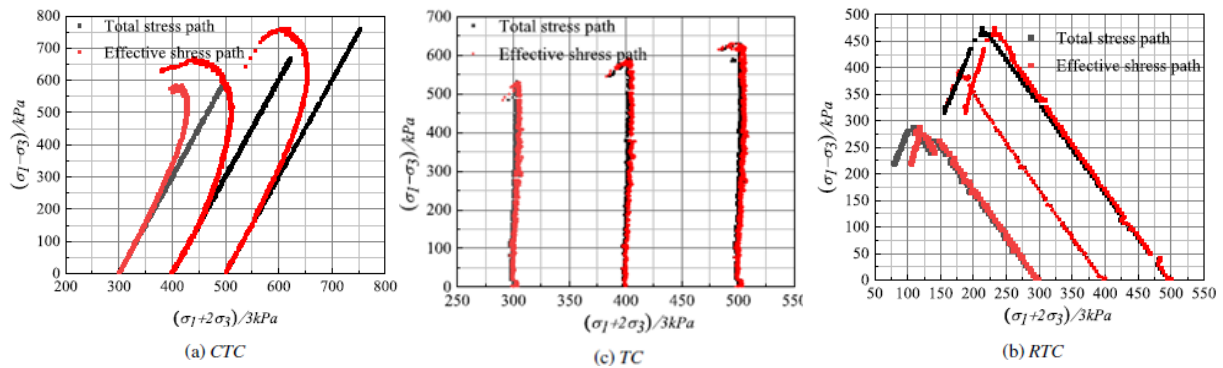


Figure 3.17 Stress-strain response of different stress path of Guiyang red clay (CU test) (Zhang et al., 2020)

In summary, a limited number of experimental investigations have been conducted that assess the effectiveness of chemical treatment on sulfate-rich soils after being tested under multiple

stress path. The present research effort is devoted to providing valuable insight into this critical problem.

CHAPTER 4

EXPERIMENTAL PROGRAM AND MATERIALS

4.1 Test Soil and Sulfate Content

The natural soil used for this study was collected from Irving, Texas, and is classified as highly plastic clay (CH) as per the Unified Soil Classification System (USCS). All the cylindrical samples were identically prepared via static compaction to the corresponding maximum Proctor density and optimum moisture content. The samples were mellowed; prepared with different dosages of cement, lime, and/or fly ash; cured, and then tested under multiple stress path. The test results were used to experimentally calibrate some of the key constitutive parameters of natural and treated soils, hence assess the most effective treatment method for highly plastic, sulfate-rich clay.

The goal of this research was to investigate the effects of different treatment methods on the strength and constitutive parameters of expansive clay. The sulfate content of the soil was crucial for this study, since the main objective was to investigate the role of the lime + fly ash and cement V + fly ash in suppressing the detrimental effects of calcium-based stabilizers on high sulfate clay. Basic soil tests were required to determine the soil Classification and sulfate content in order to achieve this goal and make informed decisions about the appropriate treatment methods. Those tests included sieve analysis and hydrometer analysis, Atterberg limit, Proctor compaction, specific gravity, and the sulfate content determination test. The sieve analysis and hydrometer analysis presented in Figure 4.1 were performed according to ASTM D422 to determine the coarse and fine grain distribution of the soil. Figure 4.2 shows the tools utilized for the tests.

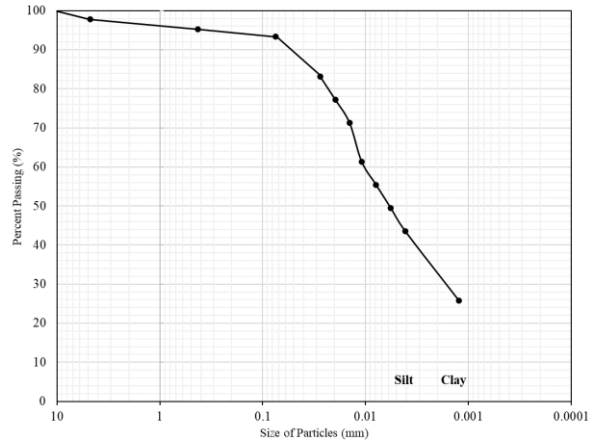


Figure 4.1 Grain size distribution



Figure 4.2 Hydrometer test

The Atterberg limit test was performed as per ASTM D 4318, and the soil was categorized as a plastic clay. Table 4.1 shows the Atterberg limit tabulations, and Figure 4.3 presents the test's tools and soil rolls of the plastic limit test.



Figure 4.3 Atterberg limit test

A specific gravity test also was conducted according to ASTM D854, and the result is reported in Table 4.1; the tools used for the test are presented in Figure 4.4.

Table 4.1 Atterberg and Specific Gravity Test Results

| Tests | | Values |
|------------------|----|--------|
| Atterberg limit | LL | 52 |
| | PL | 26 |
| | PI | 26 |
| Specific gravity | | 2.74 |

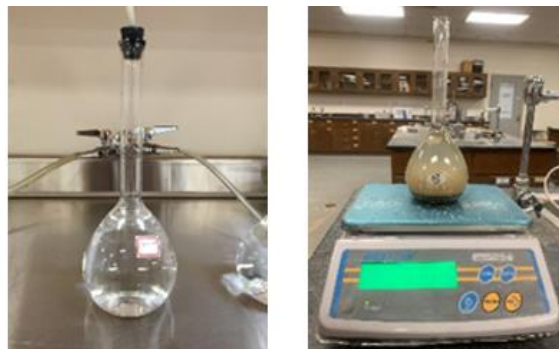


Figure 4.4 Illustration of specific gravity test

Since more than 50% of the soil passed through a No. 200 sieve, it was classified as CH, which is the USCS Classification for fat clay. The liquid limit of the soil was more than 50, and the plasticity index of the soil was more than 7.

Proctor compaction tests were conducted based on ASTM D698 to determine the maximum dry density and optimum moisture content of both the natural and treated soil, and the obtained values are presented in Table 4.2.

Table 4.2 Standard Proctor Test Results

| Soil Type | γ_d (max) (pcf) | ω_{opt} (%) |
|---------------------------------|------------------------|--------------------|
| Natural | 100 | 21 |
| 6% lime + 4% fly ash (F) | 91.8 | 22.5 |
| 5% cement (V) | 84.2 | 22.6 |
| 5% cement (V) + 15% fly ash (F) | 98.7 | 21.05 |

The colorimetric method was selected, based on TEX-145-E, to confirm that the area soil contained a high amount of sulfate content, and the tools utilized are presented in Figure 4.5. The primary sulfate content of the soil was around 1500 ppm, which was low; therefore, sulfate was added in the next step.

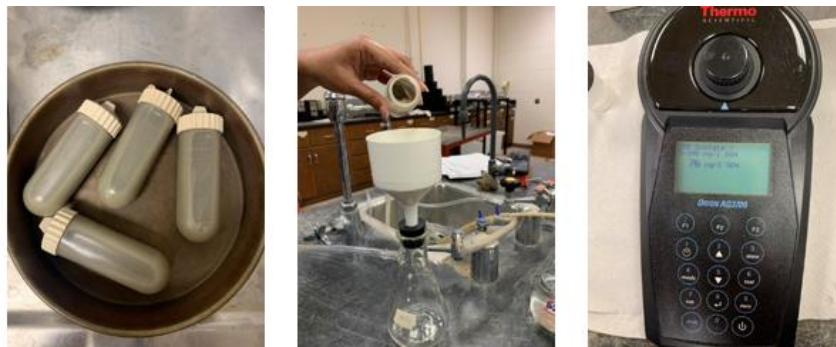


Figure 4.5 Steps for setting up the sulfate test

Sodium sulfate (Na_2SO_4) was added to the soil, as shown in Figure 4.6. The required amount of Na_2SO_4 was 50 grams per 2 kg soil, which was determined based on trial and error and led to reaching a sulfate concentration of more than 16000 ppm. The amount of water required to dissolve the Na_2SO_4 was calculated based on the lab room temperature, the formula for which was obtained from a study conducted by Fang et al. (2018). The utilized curve is shown in Figure 4.7.



Figure 4.6 Na_2SO_4

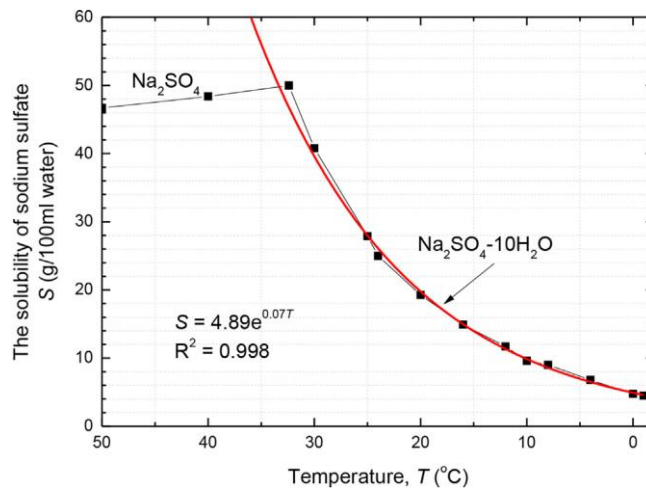


Figure 4.7 Solubility of sodium sulfate (Fang et al., 2018)

4.2 Chemical Treatments

The treatment methods used in this study were 6% lime + 4% fly ash (Class F), 5% sulfate-resistant cement or Type V cement, and 5% cement (V) + 15% fly ash (Class F). Hydrated Lime or calcium hydroxide with the chemical composition of $\text{Ca}(\text{OH})_2$, and the chemical composition of cement (V) and fly ash (Class F) were used, as reported in Tables 4.3 and 4.4, respectively.

Table 4.3 Chemical Composition of Type V Cement Used in this Research (Vasudev, 2007)

| Chemical Composition | Percent |
|---|---------|
| Calcium Oxide (CaO) | 53.10 % |
| Silicon Dioxide (SiO ₂) | 29.33 % |
| Aluminum Oxide (Al ₂ O ₃) | NA |
| Sulfur Trioxide (SO ₃) | 3.30 % |
| Magnesium Oxide (MgO) | 1.44 % |
| Loss of Ignition (LI) | 0.93% |
| Total Alkalies (Na ₂ O _{eq}) | 0.59 % |
| Insoluble Residue (IR) | 13,72 % |
| Class F Ash | 20.75 % |
| Sulfate Expansion (C-1012) | NA |

Table 4.4 Chemical Composition of Class F Fly Ash Used in this Research (Vasudev, 2007)

| Chemical Analysis | Results |
|---|----------------|
| Silicon Dioxide (SiO ₂), % | 56.7 |
| Aluminum Oxide (Al ₂ O ₃), % | 29.5 |
| Iron Oxide (Fe ₂ O ₃), % | 4.9 |
| Sum of SiO ₂ , Al ₂ O ₃ , Fe ₂ O ₃ , % | 91.1 |
| Calcium Oxide (CaO), % | 1.1 |
| Magnesium Oxide (MgO), % | 0.8 |
| Sulfur Trioxide (SO ₃), % | 0.1 |

4.3 Experimental Variables

The experimental variables considered in this work are summarized in Table 4.5: compaction specifications, mellowing time (days), curing time (days), initial confining pressure (psi), and type of stress path.

Table 4.5 Chemical Treatments and Experimental Variables

| Chemical Treatment | Compaction Specs. | | Mellowing (days) | Curing (days) | Initial Confining Pressure (psi) | | Stress path |
|-------------------------|-------------------|-----------|------------------|---------------|----------------------------------|-------|-------------|
| | OMC (%) | MDD (PCF) | | | | | |
| Natural Soil (CH) | 21 | 100 | - | - | 0 | | PL |
| | | | | | 2 – 100 | | HC |
| | | | | | 11.6 | 23.2 | CTC |
| | | | | | 23.2 | 31.9 | TC |
| | | | | | 23.2 | 31.9 | TE |
| 5% Type V Cement | 22.6 | 84 | 5 | 7 | 11.6 | - | CTC |
| | | | | | 23.21 | - | TC |
| | | | | | 23.21 | 31.9 | TE |
| 6% Lime + 4% Fly Ash | 22.5 | 92 | 5 | 7 | 0 | | PL |
| | | | | | 2 – 100 | | HC |
| | | | | | 11.6 | 23.2 | CTC |
| | | | | | - | 31.9 | TC |
| | | | | | - | 31.9 | TE |
| 5% Type V Cement+15% FA | 21.05 | 98.7 | 0 | 7 | 2-100 | | HC |
| | | | | | 10 | 23.21 | CTC |
| | | | | | 31.9 | 50 | TC |
| | | | | | 31.9 | 50 | TE |

4.4 Triaxial System: Main Components and Added Features

The triaxial device used in this research, the LoadTrac-II/FlowTrac-II system, is presented in Figure 4.8. Its main components are LoadTrac-II, two FlowTrac-II flow pumps, and triaxial software. The LoadTrac-II possesses a motor that can be used to apply the vertical load to the specimen. The two FlowTrac-II pumps also use a motor to apply the desired amount of pressure and volume to the cell or specimen. The precision for pressure and volume maintenance are ± 0.35 kPa and ± 0.001 cc, respectively. Two electrical output valves are responsible for controlling the direction of the flow, while two manual supply valves are used for the fill/ drain operation.

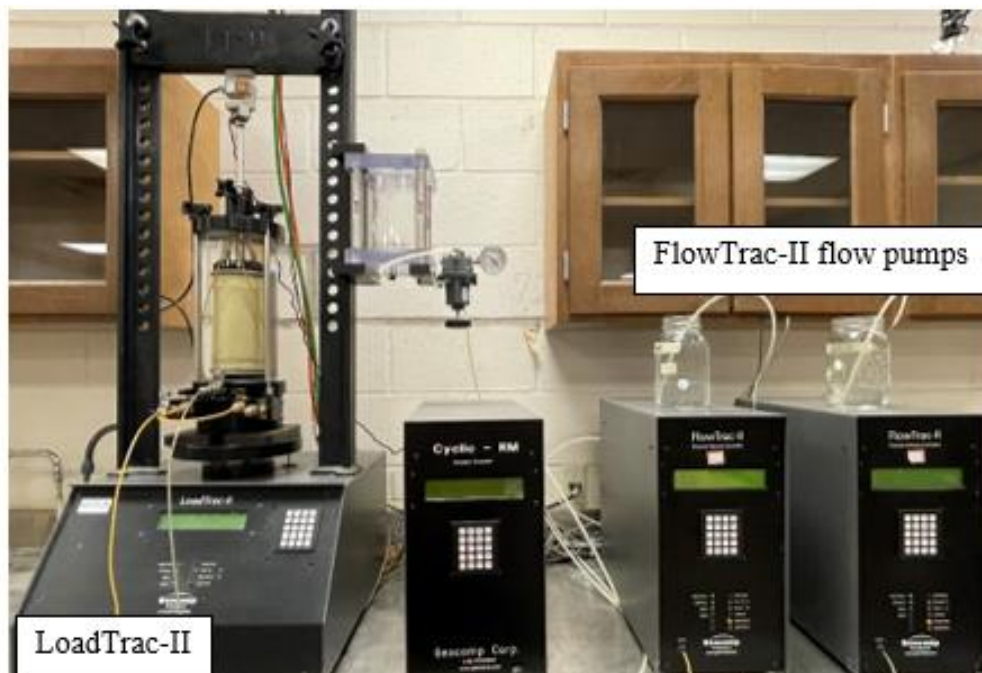


Figure 4.8 Main components of the triaxial device

Figure 4.9 presents the setup of the LoadTrac-II, and triaxial cell before the consolidated drained test was performed. The FlowTrac-II pumps were filled with distilled water up to 85% of the pump's capacity and were connected to the triaxial cell through pressure tubing and valves.

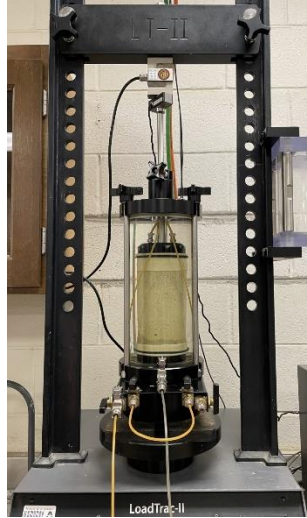


Figure 4.9 Setup of LoadTrac-II and triaxial cell before commencement of a consolidated drained test

A property page in the triaxial software was used to dictate the conditions of the test to the LoadTrac-II and FlowTrac-II pumps, and during the test, the data and status of the pumps could be observed on the screen. Figure 4.10 presents an example of the property page of one of the tests. At the end of the test, reports and graphs were created that were used to calculate the strength parameters of the variable stress path.

Some modifications had to be made to the LoadTrac-II before the triaxial extension test of the stress path could be conducted during this study. The LoadTrac-II's base platen was secured to the triaxial base with two clamps, as presented in Figure 4.11, and the interface cap was removed and the load cell was secured to the triaxial piston with a coupler adapter, as illustrated in Figure 4.12.

TRIAxIAL :REPORT(1) - C:\Documents and Settings\computer\My Documents\Azadeh\Stress Paths template\CTC.dat

File Calibrate Report Options Window Help

| Project | Specimen | Water Content | Read Table | Test Parameters | Initialization | Consolidation/A Table | | | | |
|------------|-------------------------|-----------------------|-------------|----------------------------|-----------------|-----------------------|-------------|--------------------|---------------------|------------|
| Saturation | | Consolidation/B Table | | | Shear Table | | | | | |
| | Horizontal Stress (psi) | Vertical Stress (psi) | Stress Type | Pore Pressure Change (psi) | Shear Step Type | Shear Step Control | Rate (/min) | Maximum Strain (%) | Maintain Time (min) | Read Table |
| 1 | 0 | 1000 | Relative | 0 | Undrained | Strain | 0.1 | 20 | 0 | Strain |
| 2 | 0 | 0 | Absolute | 0 | Undrained | Strain | 0 | 0 | 0 | Time |
| 3 | 0 | 0 | Absolute | 0 | Undrained | Strain | 0 | 0 | 0 | Time |
| 4 | 0 | 0 | Absolute | 0 | Undrained | Strain | 0 | 0 | 0 | Time |
| 5 | 0 | 0 | Absolute | 0 | Undrained | Strain | 0 | 0 | 0 | Time |
| 6 | 0 | 0 | Absolute | 0 | Undrained | Strain | 0 | 0 | 0 | Time |
| 7 | 0 | 0 | Absolute | 0 | Undrained | Strain | 0 | 0 | 0 | Time |
| 8 | 0 | 0 | Absolute | 0 | Undrained | Strain | 0 | 0 | 0 | Time |
| 9 | 0 | 0 | Absolute | 0 | Undrained | Strain | 0 | 0 | 0 | Time |
| 10 | 0 | 0 | Absolute | 0 | Undrained | Strain | 0 | 0 | 0 | Time |

Figure 4.10 Triaxial software’s property page for a CTC test

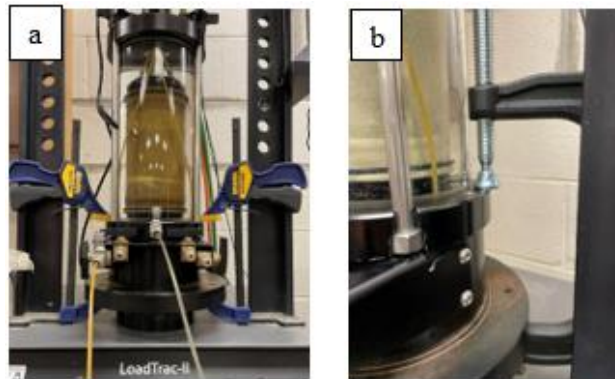


Figure 4.11 Modifications of LoadTrac-II for triaxial extension test: (a) Illustration for triaxial extension test setup, (b) Securing the LoadTrac-II’s base platen to the triaxial base with clamps



Figure 4.12 Load cell modifications for triaxial extension test: (a) Load cell interface cap for compression tests, (b) Coupler adapter for extension test, (c) Coupler adapter secured to the load cell (c)

4.5 Repeatability of Test Results

The reliability and repeatability of the test results were assessed by repeating the initial tests. A comparison of the two CTC tests under 11.6 psi initial confining of the natural samples is shown in Figure 4.13 and illustrates that the stress-strain behavior exhibited during the two tests was similar.

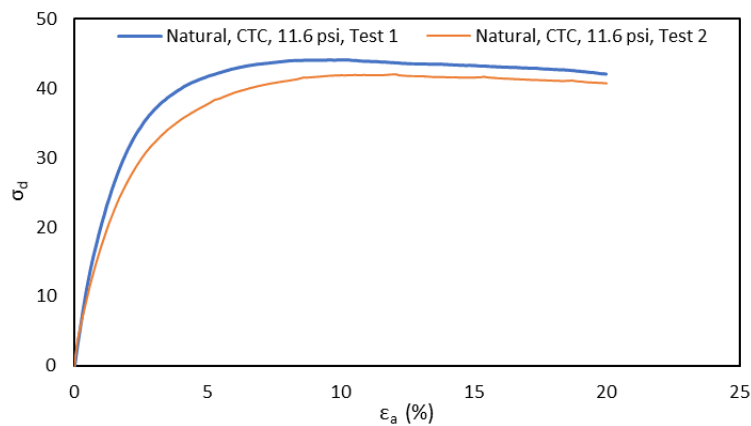


Figure 4.13 Repeatability test for the natural sample with CTC stress path under 11.6 psi initial confining

CHAPTER 5

ANALYSIS OF RESULTS: CONVENTIONAL TRIAXIAL TESTING

5.1 Stress-Strain Response: Natural and Treated Clay

The stress-strain responses (σ_d versus ϵ_a) are depicted and compared in this chapter for soil treated with 5% cement (V), 6% lime + 4% fly ash, and 5% cement (V) + 15% fly ash, as well as for natural soil. The curves were obtained from the CTC test results, during which σ_3 was kept constant and equal to the initial confining pressure, while σ_1 increased. The influence of the increasing initial confining pressure and different treatment methods on the peak stress or failure points is also discussed.

Figures 5.1 and 5.2 demonstrate the stress-strain response for natural soil under 11.6 and 23.21 psi initial confining pressure, respectively. The natural soil failed at approximate deviatoric stress and axial deformation of 44.10 psi and 10.2%, respectively, while the values increased to 54.39 psi and 15.8 % for initial confining of 23.21 psi.

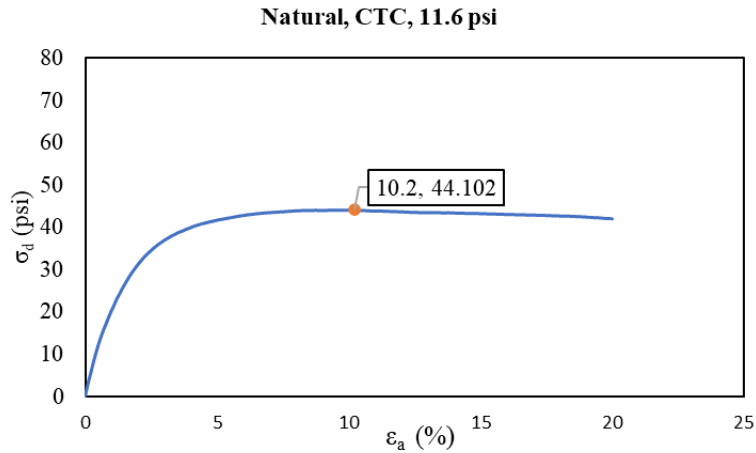


Figure 5.1 Stress-strain response for natural soil under CTC stress path with 11.6 psi initial confining pressure

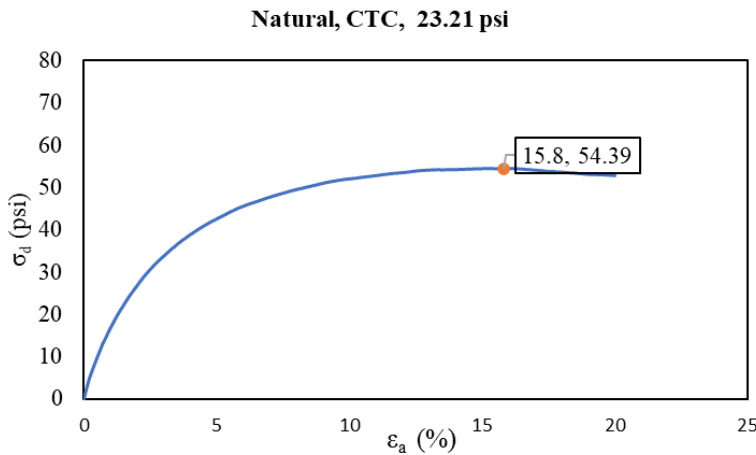


Figure 5.2 Stress-strain response for natural soil under CTC stress path with 23.2 psi initial confining pressure

Figure 5.3 shows the stress-strain response of soil treated with 5% cement (V) under 11.6 psi initial confining pressure. Based on the presented peak shear stress, the sample failed at 14.05 psi deviator stress. A comparison of the peak failure strength under 11.6 psi initial confining for natural soil and soil treated with 5% cement (V) is presented in Figure 5.4. The results showed that the soil

treated with cement (V) was not any stronger than the natural soil; therefore, the efficacy of 6% lime + 4% fly ash and 5% cement (V) + 15% fly ash were determined as the best treatments for the current study. The stress-strain behavior corresponding to these treatment methods is reported in the subsequent figures.

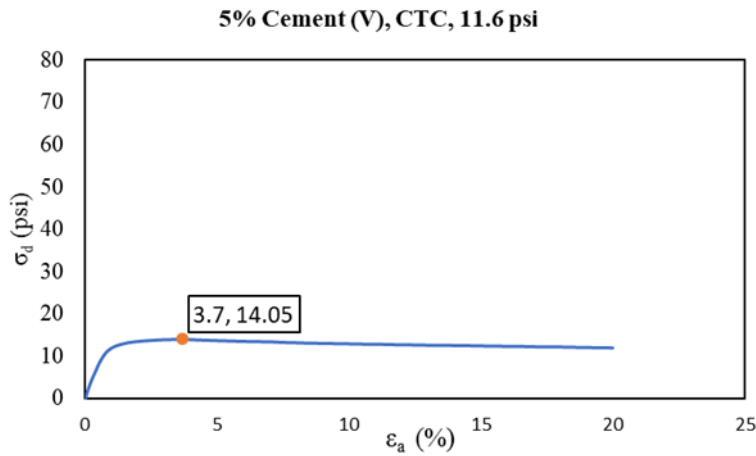


Figure 5.3 Stress-strain response for soil treated with 5% cement (V) under CTC stress path with 11.6 psi initial confining pressure

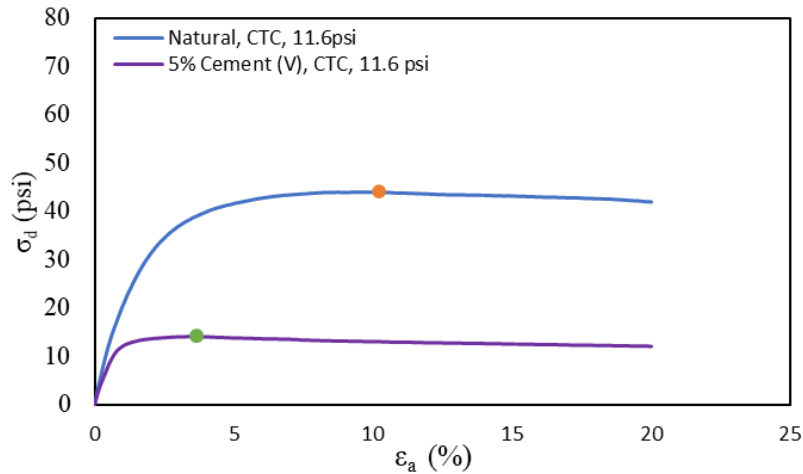


Figure 5.4 Stress-strain response for natural soil versus soil treated with 5% cement (V) under CTC stress path with 11.6 psi initial confining pressure

Figures 5.5 and 5.6 illustrate that as the initial confining pressure of the soil treated with 6% lime + 4% fly ash increased from 11.6 to 23.2, the peak values of the stress and strain also increased. The increase in deviator stress from 12.4 psi to 13.7 psi is indicative of the strength gain that occurred as the confining pressure intensified.

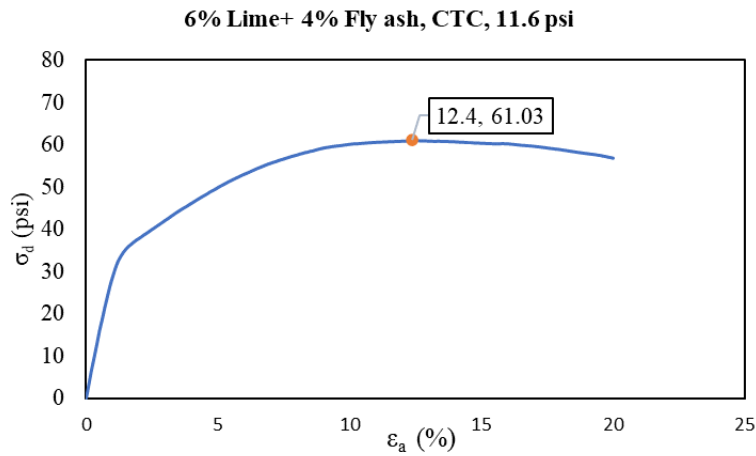


Figure 5.5 Stress-strain response for soil treated with 6% lime + 4% fly ash under a CTC stress path with 11.6 psi initial confining pressure

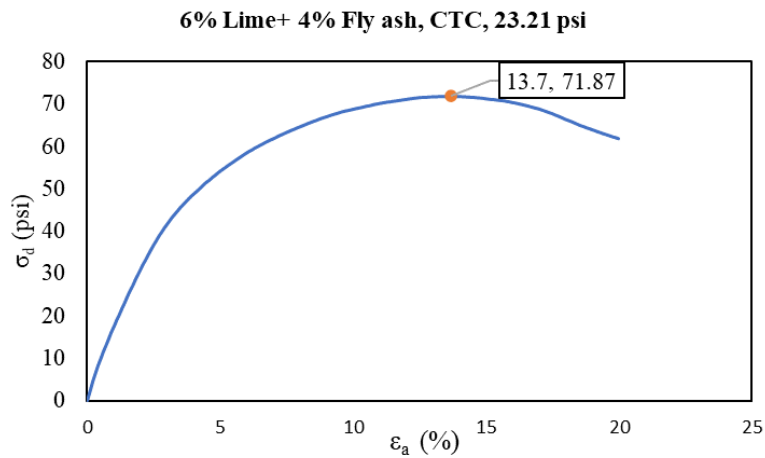


Figure 5.6 Stress-strain response for soil treated with 6% lime + 4% fly ash under a CTC stress path with 23.2 psi initial confining pressure

Similarly, as presented in Figures 5.7 and 5.8, clay treated with 5% cement (V) + 15% Fly ash demonstrated a strength gain (61.10 to 71.80 psi) as the confining pressure increased from 10 psi to 23.21 psi.

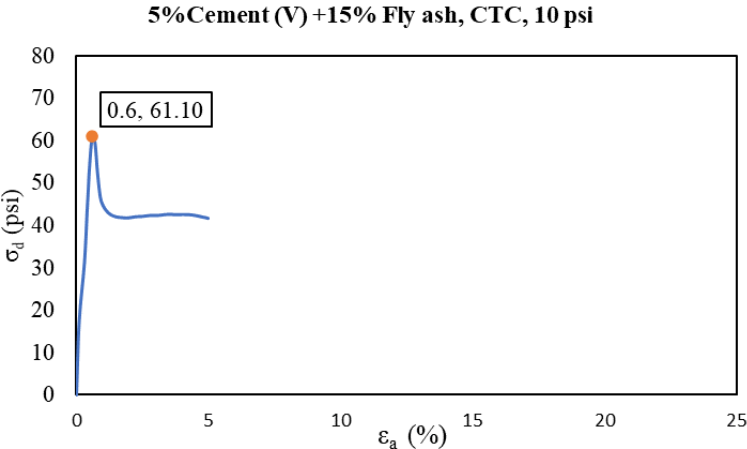


Figure 5.7 Stress-strain response for soil treated with 5% cement (V) + 15% fly ash under CTC stress path with 10 psi initial confining pressure

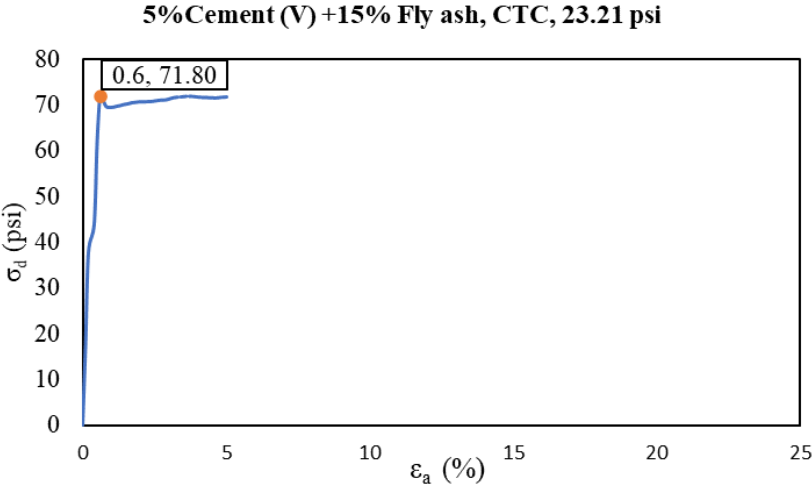


Figure 5.8 Stress-strain response for soil treated with 5% cement (V) + 15% fly ash under CTC stress path with 23.21 psi initial confining pressure

Figure 5.9 shows the stress-strain responses under 11.6 initial confining pressure for natural soil and the soil treated with 6% lime + 4% fly ash, and 5% cement. As can be observed, the soil treated with 6% lime+ 4% fly ash exhibited the highest strength, and the soil treated with 5% cement (V) exhibited less strength than the natural soil.

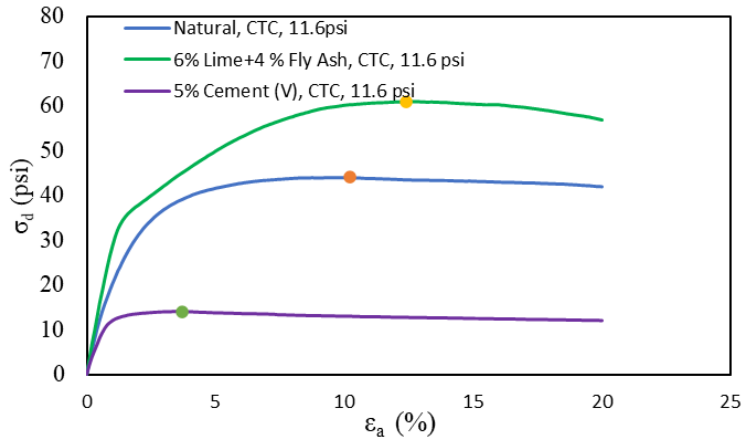


Figure 5.9 Stress-strain responses for natural soil, soil treated with 6% lime + 4% fly ash, and soil treated with 5% cement (V) with CTC stress path under 11.6 psi initial confining pressure

Comparisons of the stress-strain responses of the natural soil, the soil treated with 6% lime + 4% fly ash, and soil treated with 5% cement (V) + 15% fly ash under 23.2 psi confining pressure are depicted in Figure 5.10. It can be observed that the soil treated with 5% cement (V) + 15% fly ash and soil treated with 6% lime + 4% fly ash had failure strength values that were almost identical and were higher than the natural soil's failure deviatoric stress. This confirms that these two treatments are capable of improving the natural soil's strength; however, the treatment with 6% lime + 4% fly ash is preferable since the behavior of the soil treated with 5% cement (V) + 15% fly ash is more brittle than either the 6% lime + 4% fly ash treated soil or the natural soil.

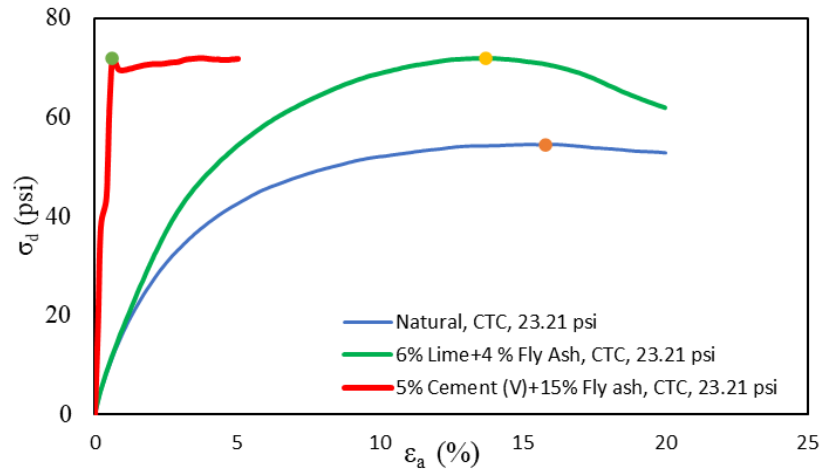


Figure 5.10 Stress-strain responses for natural soil, soil treated with 6% lime + 4% fly ash, and soil treated with 5% cement (V) + 15% fly ash with CTC stress path under 23.21 psi initial confining pressure

5.2 Mohr Circles at Failure: Natural and Treated Clay

Based on the Mohr-Coulomb failure theory, the most severe normal and shear stress combination that soil can undergo is at the intersection of the failure envelope and the Mohr circle. This point is named shear stress at failure and is denoted by τ_{ff} . The slope of the failure envelope is named the angle of friction angle, and the intercept exhibits soil cohesion, which is two important strength parameters and is shown on the Mohr circles for natural soil and all treated soils and summarized in a table later.

Figure 5.11 illustrates the Mohr circles and the cohesion and friction angles obtained for natural soil. It can be seen that the Mohr circle enlarged as the initial confining pressure increased, which leads to the conclusion that the shear strength at failure is higher for soil with 23.21 psi initial confining pressure than for soil with 11.6 psi initial confining pressure.

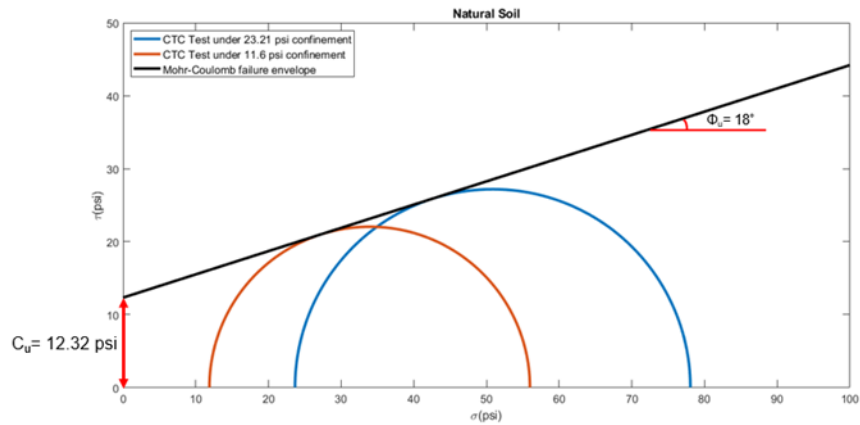


Figure 5.11 Mohr circles for natural soil with 11.6 psi and 23.21 psi initial confining pressures

Figure 5.12 depicts the Mohr circles corresponding to soil treated with 5% cement (V) with 11.6 psi initial confining pressure.

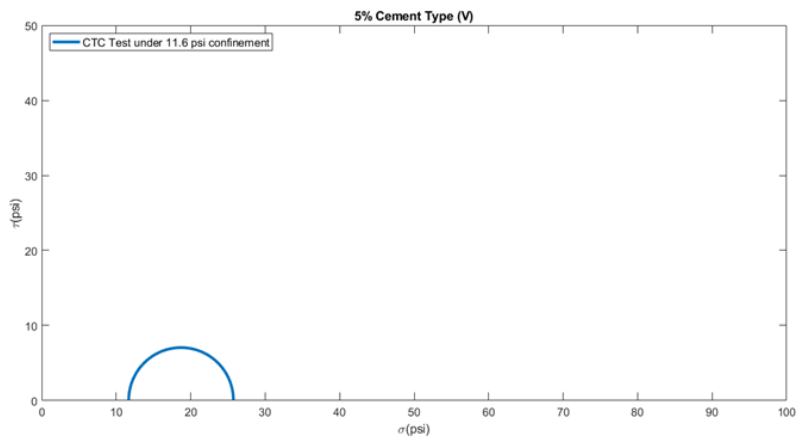


Figure 5.12 Mohr circles for soil treated with 5% cement (V) with 11.6 psi initial confining pressure

Figures 5.13 and 5.14 demonstrate the Mohr circles for soil samples treated with 6% lime + 4% fly ash and 5% cement (V) + 15% fly ash, respectively, where it is exhibited that the shear strength

at failure was higher for the larger values of the initial confining pressure for both treatment methods.

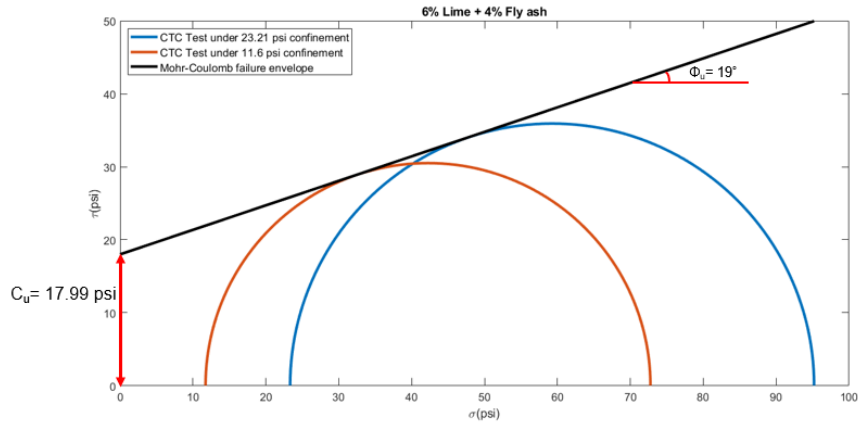


Figure 5.13 Mohr circles for soil treated with 6% lime+ 4% fly ash with 11.6 psi and 23.21 psi initial confining pressures.

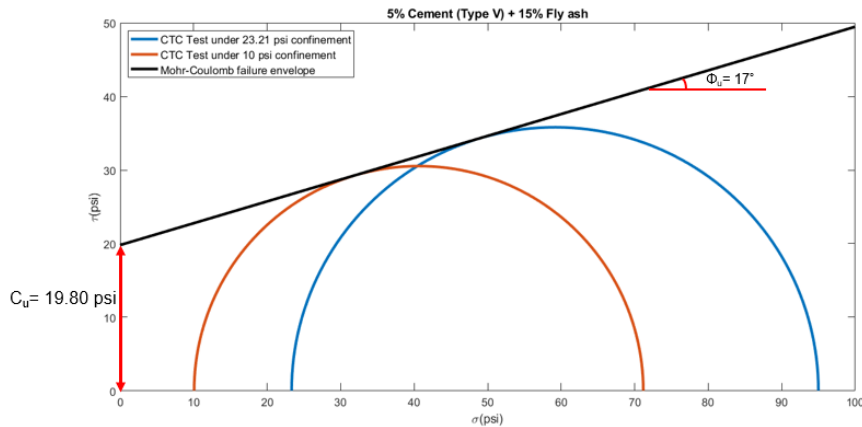


Figure 5.14 Mohr circles for soil treated with 5% cement (V) + 15% fly ash with 11.6 psi and 23.21 psi initial confining pressures

Comparisons of the Mohr circles corresponding to the natural soil, soil treated with 6% lime + 4% fly ash, and soil treated with 5% cement (V) under initial confining of 11.6 psi are presented in Figure 5.15. The soil treated with cement (V) exhibited the least shear strength at failure, and the soil treated with 6% lime + 4% fly ash exhibited the most shear strength at failure, leading to the conclusion that the treatment improved the soil's strength.

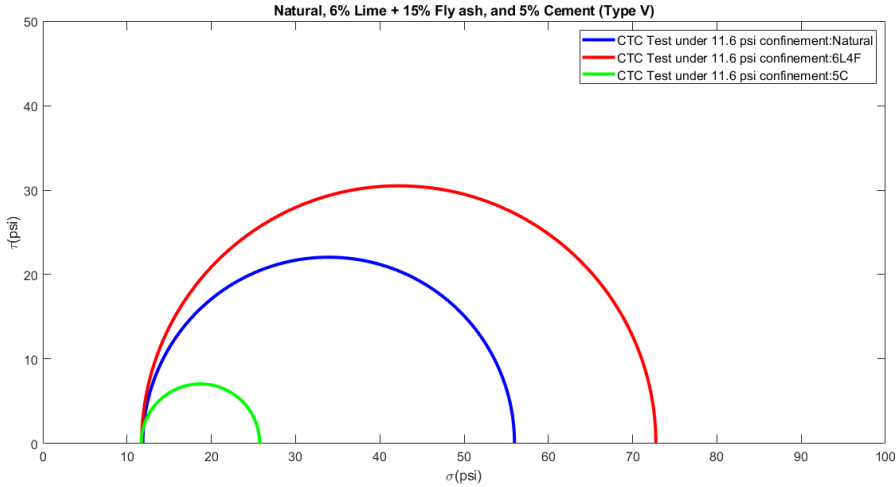


Figure 5.15 Mohr circles corresponding to natural soil, soil treated with 6% lime + 4% fly ash, and soil treated with 5% cement (V) with 11.6 psi initial confining pressure

By comparing the Mohr circles depicted in Figure 5.16 for the natural soil and the soil treated with 6% lime +4% fly ash for both 11.6 psi and 23.21 psi, it can be seen that the Mohr circles for the treated soil are larger than natural soil. This suggests that the soil gained more strength after being stabilized with 6% lime+ 4% fly ash.

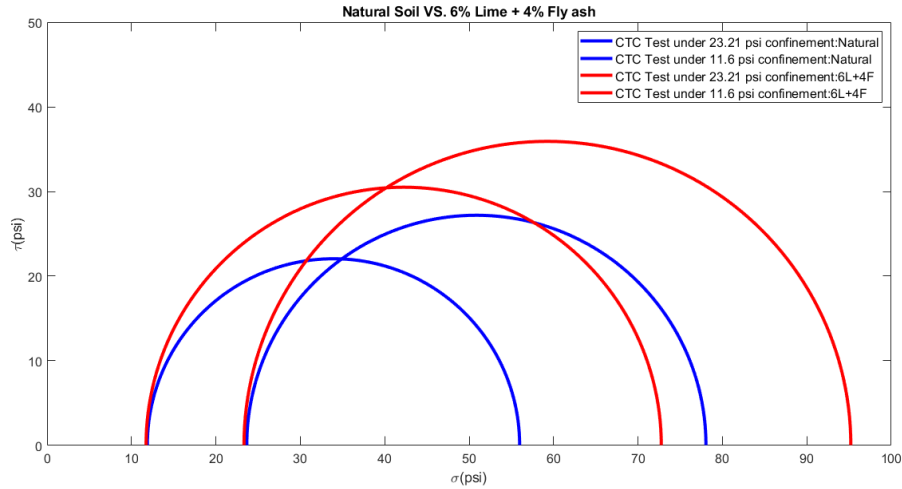


Figure 5.16 Mohr circles for natural soil versus soil treated with 6% lime + 4% fly ash with 11.6 psi and 23.21 psi initial confining pressure

Figures 5.17 and 5.18 present the Mohr circles of soil treated with 5% cement (V) + 15% fly ash versus natural soil and soil treated with 5% cement (V) + 15% fly ash versus soil treated with 6% lime + 4% fly ash under 23.21 psi confining pressures. The sizes of the Mohr circles indicate that the sample treated with 5% cement (V) + 15% fly ash exhibited more shear strength at failure than the natural soil, while its strength at failure was almost equal to the failure strength of the soil treated with 6% lime + 4% fly ash under 23.21 initial confining pressure.

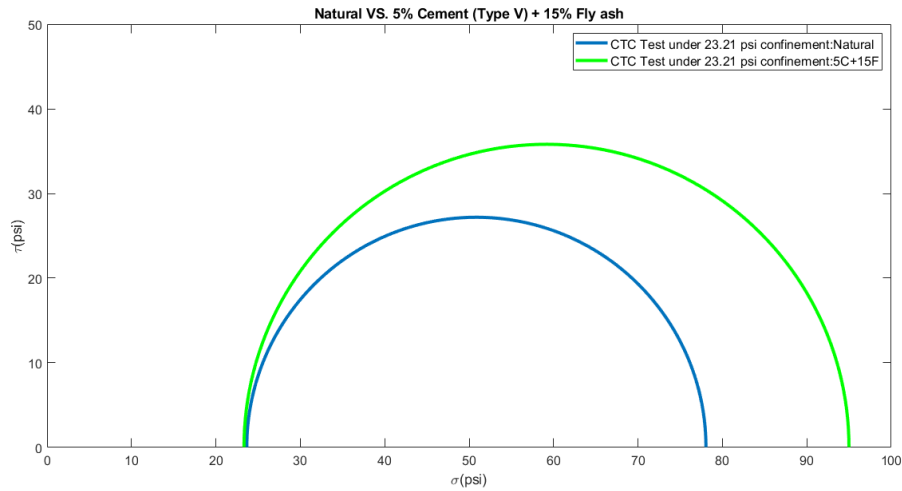


Figure 5.17 Mohr circles for natural soil versus soil treated with 5% cement (V) + 15 % fly ash with 23.21 psi initial confining pressure

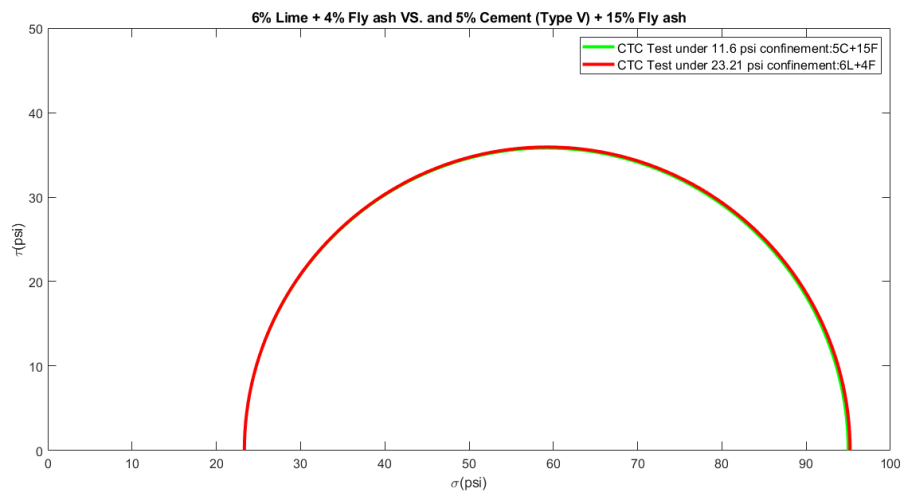


Figure 5.18 Mohr circles for soil treated with 6% lime + 4% fly ash versus soil treated with 5% cement (V) +15% fly ash with 23.21 psi initial confining pressures.

Figure 5.19 shows a comprehensive comparison of the Mohr circles of the natural soil, soil treated with 6% lime + 4% fly ash, and soil treated with 5% cement (V) + 15% fly ash soil under 23.21 confining pressure. The treated soils exhibited almost identical maximum shear strength, which

was higher than that of the natural soil. It can be concluded that based on Mohr-Coulomb failure criteria, the two treatment methods are equally effective for enhancing the strength of the soil.

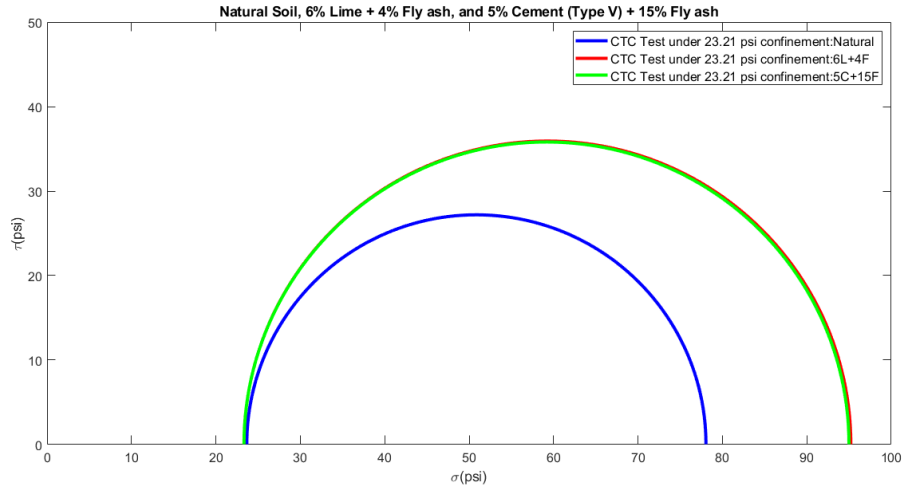


Figure 5.19 Mohr circles for natural soil, soil treated with 6% lime+ 4% fly ash, and soil treated with 5% cement (V) + 15% fly ash with 23.21 psi initial confining pressure

5.3 Failure Envelopes: Natural and Treated Clay

The Mohr-Coulomb criterion, which is the most popular strength parameter, can be written as Eq. 7. It can predict the soil’s stress state at failure on sliding surfaces so that the angle of the failure plane for each soil element can be calculated by Eq. 8.

$$\tau_{ff} = \tan \varphi + C \tag{7}$$

$$\alpha_{ff} = 45^\circ + \frac{\varphi}{2} \tag{8}$$

A comparison of the Mohr-Coulomb failure envelopes for the natural soil, soil treated with 6% lime + 4% fly ash, and soil treated with 5% cement (V) + 15% fly ash is presented in Figure 5.20. The corresponding strength parameters are reported in Table 5.1. Based on the results, the

soil treated with 5% cement (V) + 15% fly ash had the highest cohesion. Both the soils treated with 6% lime + 4% fly ash and with 6% lime + 4% fly ash showed higher cohesion than the natural soil. The friction angles did not reflect any specific pattern.

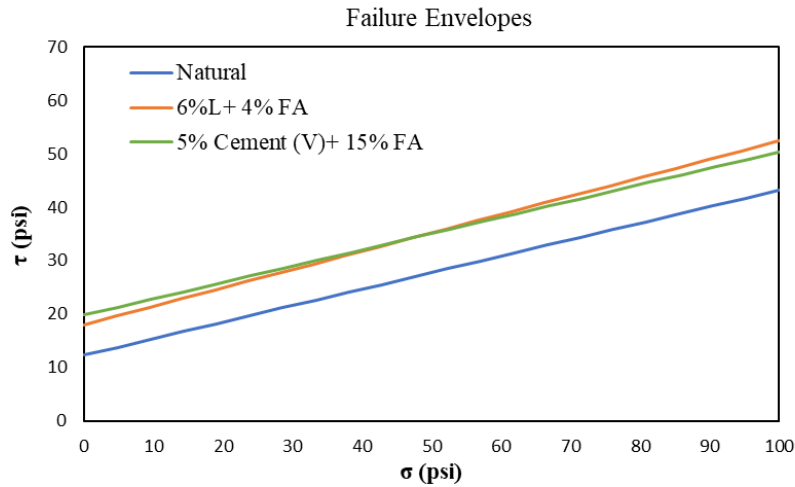


Figure 5.20 Mohr-Coulomb envelope for natural soil, soil treated with 6% lime + 4% fly ash, and soil treated with 5% cement (V) + 15% fly ash

Table 5.1 Strength Parameters Obtained from Mohr-Coulomb Failure Envelopes

| Treatment Method | Cohesion (psi) | Friction Angle (Degrees) |
|------------------|----------------|--------------------------|
| Natural | 12.31 | 18 |
| 6L+4% FA | 17.99 | 19 |
| 5% C (V) +15% FA | 19.81 | 17 |

CHAPTER 6

ANALYSIS OF RESULTS: MULTIPLE TRIAXIAL TESTING

6.1 Stress path and Stress-Strain-Work Response: Natural and Treated Clay

The results of the triaxial tests and the curves generated from their results are reported and discussed in this chapter. The stress path are reported in the q - p plane for each test and the stress-strain responses are reported in the q - ϵ_a plane beside them and are used for calculating the elastic modulus and obtaining the yield and peak or residual points. The P-W (work) curves shown for each test were also used for obtaining the yield points. The first set of curves belongs to natural soil, the second set is for 5% cement (V) treated soils, the third is for 6% lime + 4% fly ash, and the last set of curves are the results obtained from 5% cement (V) + 15% fly-ash-treated soil.

6.1.1 Natural Soil

The results obtained from hydrostatic compression (HC) and proportional loading (PL) are shown in Figures 6.1 and 6.2. Based on these two curves the pre-consolidation pressure or maximum stress that the natural soil experienced during compaction was identified at $p = 29$ psi. Figure 6.3 shows the CTC stress path for the natural soil under initial 11.6 psi confining pressure. The soil behaved linear elastic up to the yield point ($q = 13$ psi) since 11.6 psi is less than the pre-consolidation pressure. After the yield point, the natural soil behaved elastic-plastic up to the peak point ($q = 21$ psi), after which the behavior was purely plastic; the soil experienced huge plastic shear strain but did not experience any plastic volume change. Figure 6.4 shows the q -W for this test, which was used to confirm the yield point. The q - p , stress-strain, and p -W or q -W responses are presented in the rest of the figures. The method for obtaining the yield point is shown for a few curves as examples.

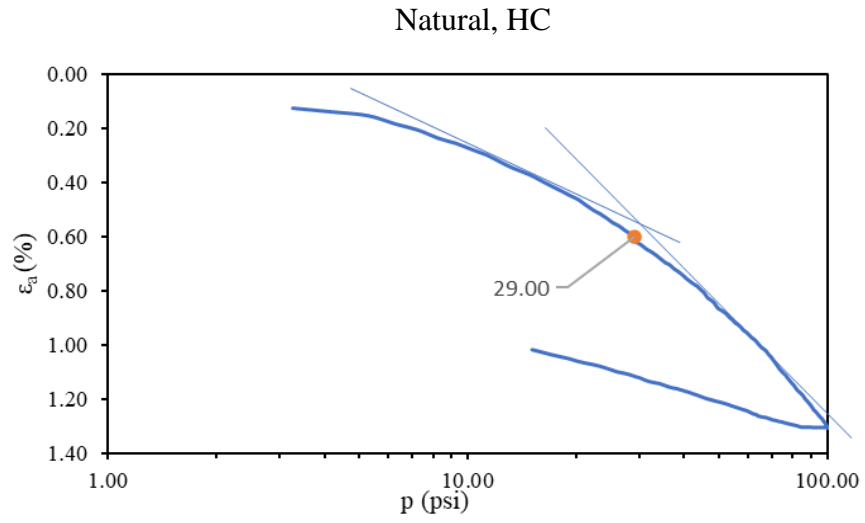


Figure 6.1 HC stress path for natural soil

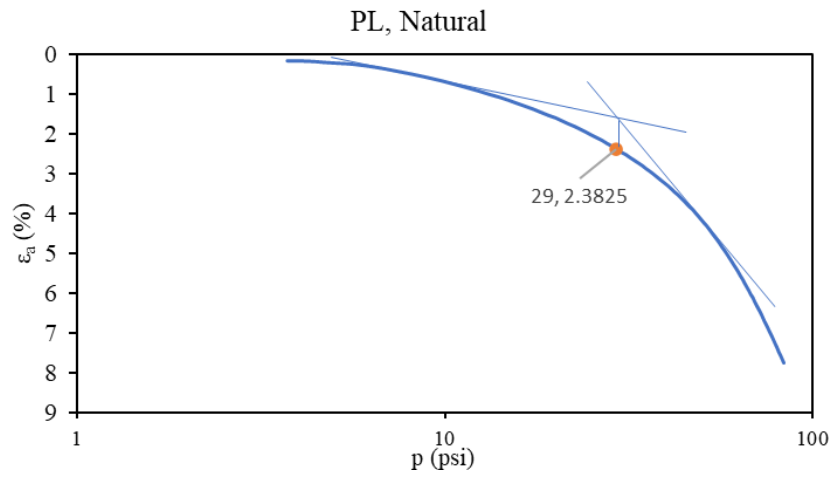


Figure 6.2 PL stress path for natural soil

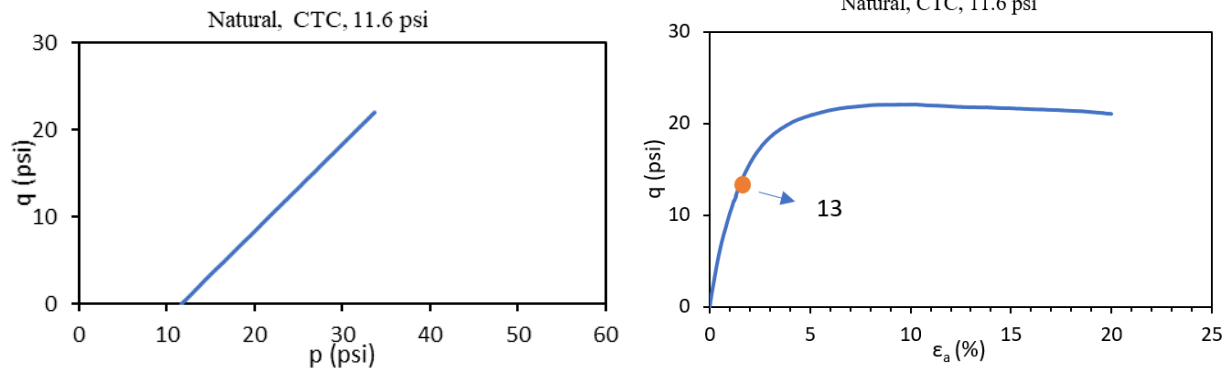


Figure 6.3 CTC stress path with 11.6 psi initial confining pressure for natural soil: (a) q-p plane, (b) q- ϵ_a plane

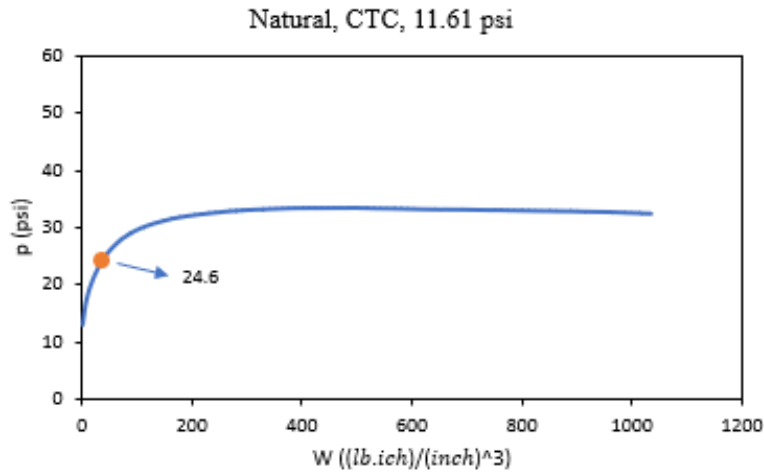


Figure 6.4 CTC stress path with 11.6 psi initial confining pressure for natural soil: p-W response

The stress-strain behavior of natural soil under the CTC stress path with a higher initial confining pressure (23.21 psi) is illustrated in Figure 6.5, and Figure 6.6 shows the corresponding p-W response. The soil behaved linearly elastic up to the yield point which was identified at $p = 30.01$ psi and $q = 6.8$ psi.

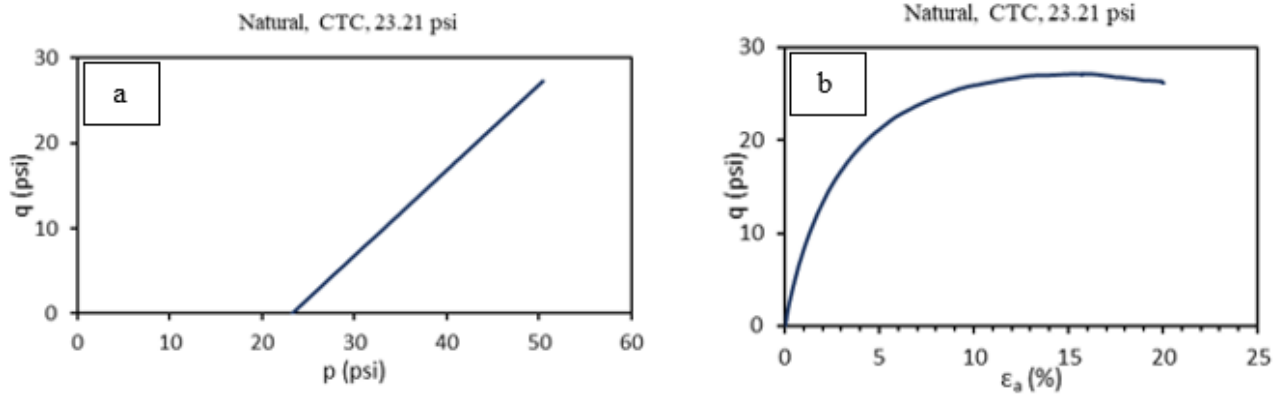


Figure 6.5 CTC stress path with 23.21 psi initial confining pressure for natural soil: (a) q-p plane, (b) q- ϵ_a plane

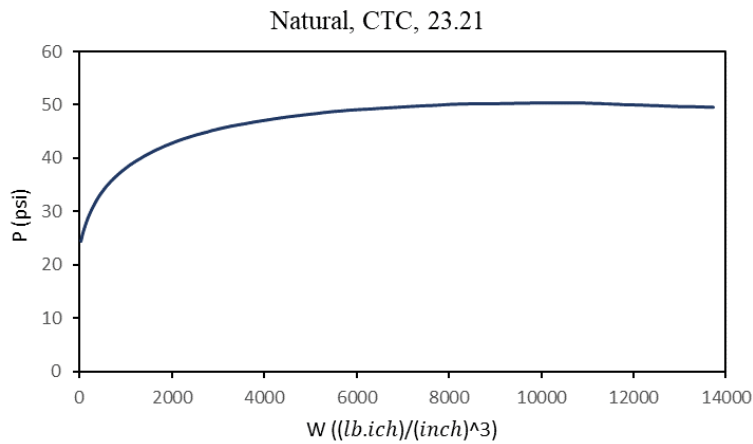


Figure 6.6 CTC stress path with 23.21 psi initial confining pressure for natural soil: p-W response

Figures 6.7 and 6.8 show the stress path, q-p and p-W, for natural soil under the TC stress path with 23.21 psi initial confining. The soil's behavior was elastic up to the yield point ($q=14$ psi) and elastoplastic up to the residual point ($q=16$ psi).

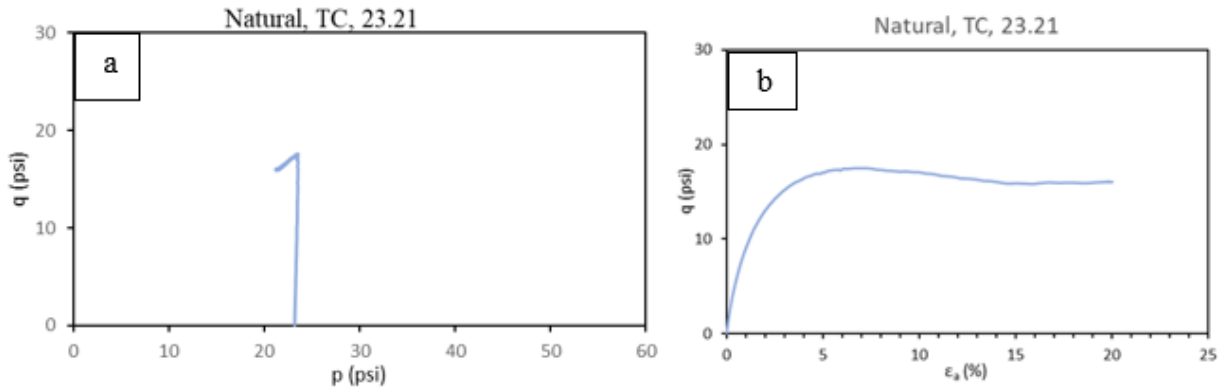


Figure 6.7 TC stress path with 23.21 psi initial confining pressure for natural soil: (a) q-p plane, (b) q- ϵ_a plane

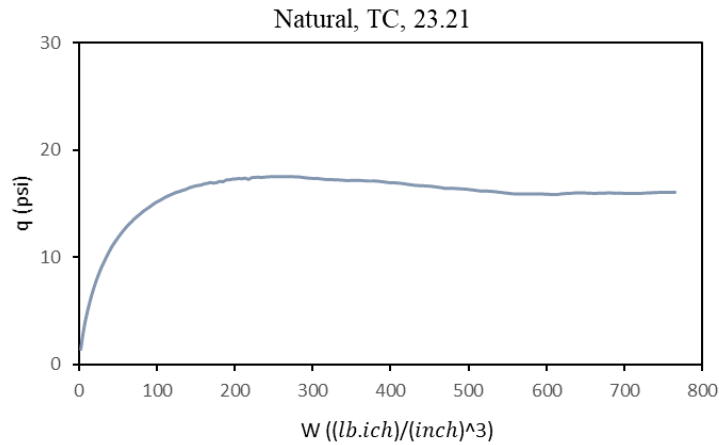


Figure 6.8 TC stress path with 23.21 psi initial confining pressure for natural soil: q-W response

The curves corresponding to the TC stress path for natural soil with 31.9 initial confining pressure are presented in Figures 6.9 and 6.10. Because the initial confining stress was higher than the pre-consolidation stress (29 psi), the soil behavior was elastoplastic from the beginning up to the critical point ($q = 20$ psi); there was no elastic portion in the stress-strain response.

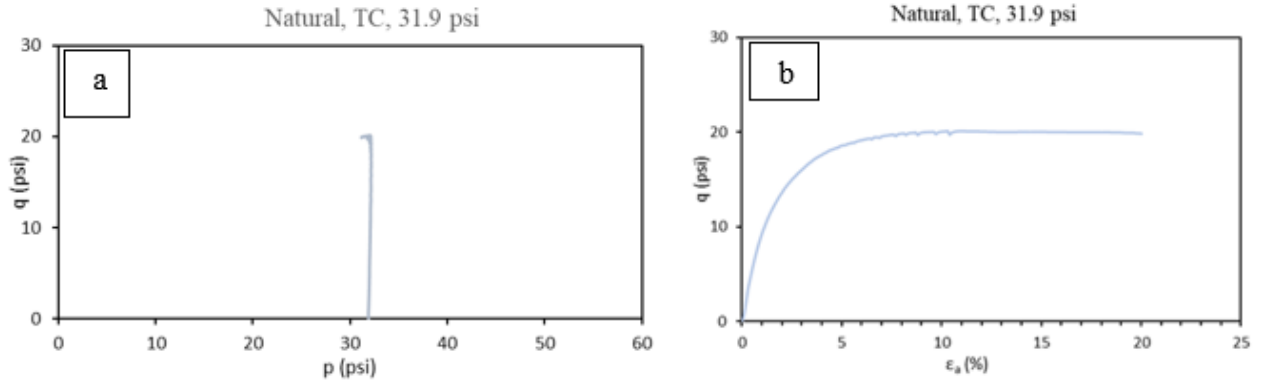


Figure 6.9 TC stress path with 31.9 psi initial confining pressure for natural soil: (a) q-p plane, (b) q- ϵ_a plane

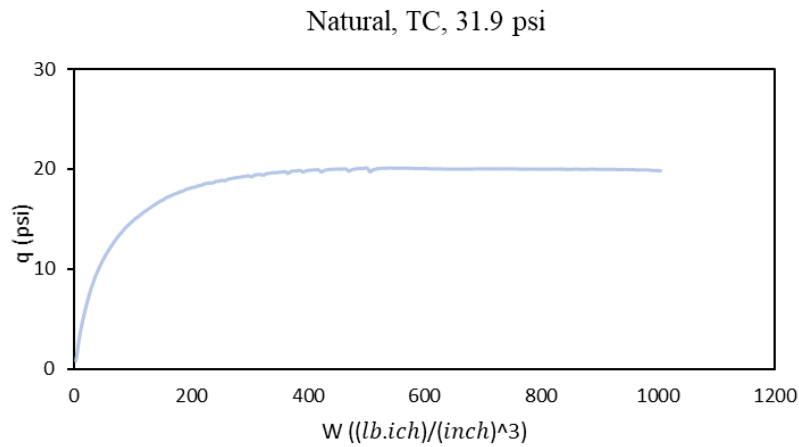


Figure 6.10 TC stress path with 31.9 psi initial confining pressure for natural soil: q-W response

Figure 6.11 and Figure 6.12 present the stress path, stress-strain, and q-w for natural soil with a triaxial extension (TE) stress path under 23.21 psi initial confining pressure. The soil reached the yield point ($q = -4$ psi) and critical point ($q = -6$ psi) in less time than the sample tested under the TC stress path with the same initial confining.

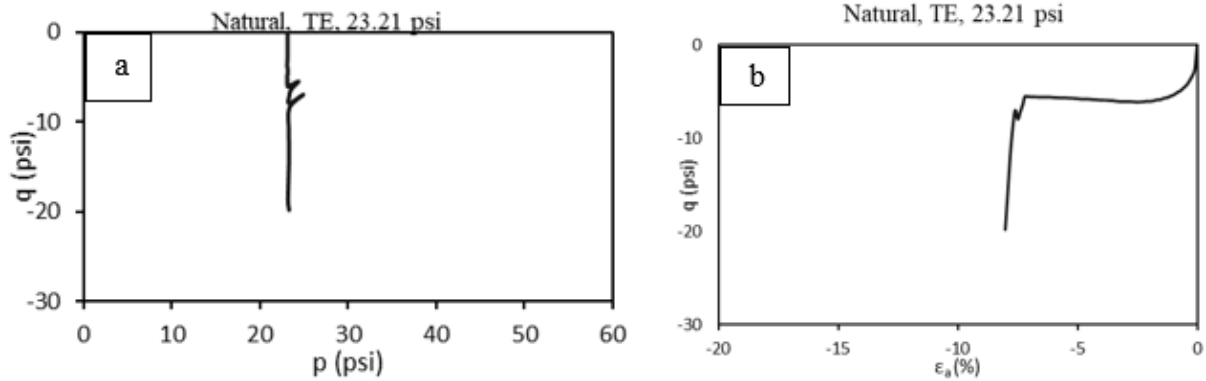


Figure 6.11 TE stress path with 23.21 psi initial confining pressure for natural soil: (a) q-p plane, (b) q- ϵ_a plane

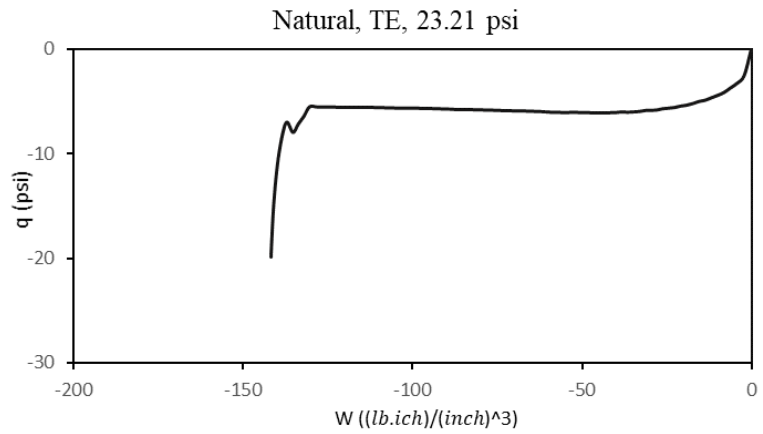


Figure 6.12 TE stress path with 23.21 psi initial confining pressure for natural soil: q-W response

The results obtained from the TE stress path for natural soil under higher initial confining pressure (31.9 psi) are presented in Figures 6.13 and 6.14. The soil behaved elastoplastic from the beginning since the confining pressure was higher than the pre-consolidation pressure and at the critical point, q was -9 psi.

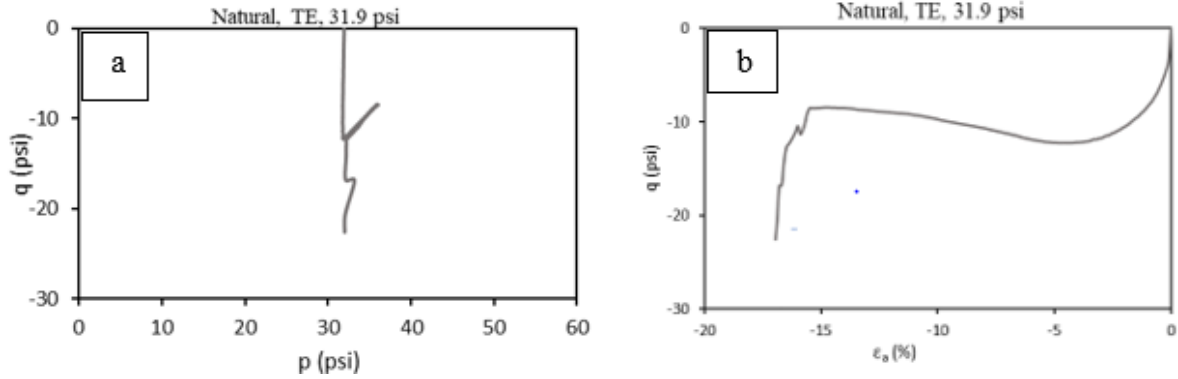


Figure 6.13 TE stress path with 31.9 psi initial confining pressure for natural soil: (a) q-p plane, (b) q- ϵ_a plane

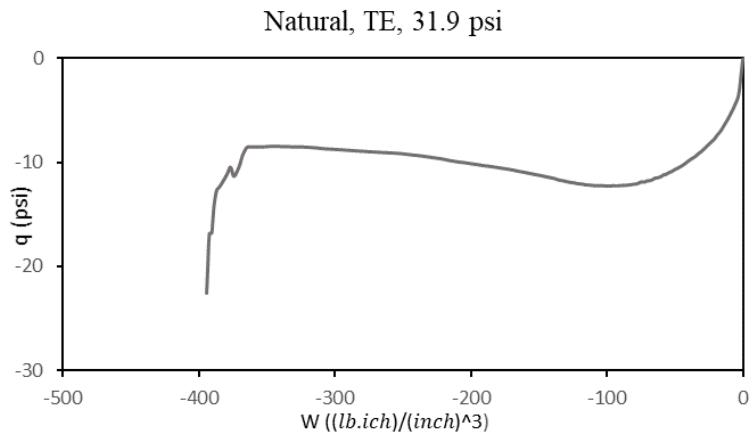


Figure 6.14 TE stress path with 31.9 psi initial confining pressure for natural soil: q-W response

6.1.2 Soil treated with 5% Cement (V)

As previously discussed, the soil treated with 5% cement did not exhibit high strength. Figures 6.15 and 6.16 show the stress path, the stress-strain response, and the p-W response for the sample treated with 5% cement (V) under the CTC stress path with 11.6 psi confining. The critical point or the peak point was identified at $p = 18.67$ and $q = 7$ psi. This value is much lower

than the q and p values of natural soil (21, 32.64) with the same stress path and same initial confining pressure. The initial linear elastic part of the stress-strain responses for this soil was greater than for natural soil, and the behavior was more brittle.

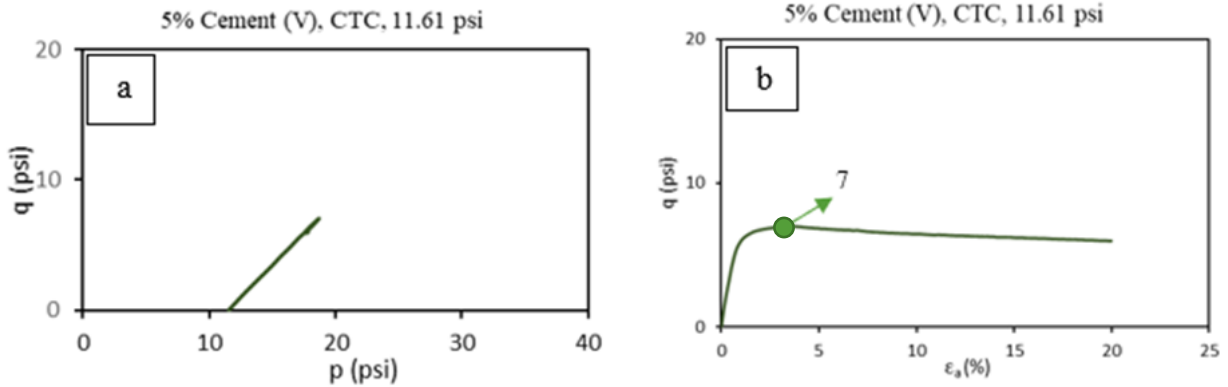


Figure 6.15 CTC stress path with 11.6 psi initial confining pressure for soil treated with 5% cement (V): (a) q - p plane, (b) q - ϵ_a plane

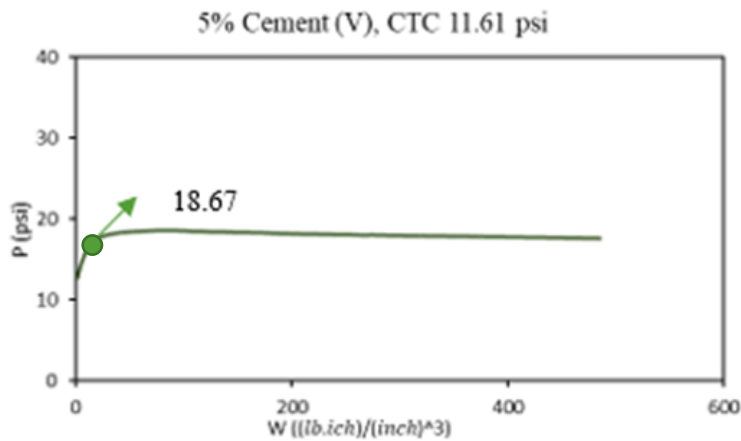


Figure 6.16 CTC stress path with 11.6 psi initial confining pressure for soil treated with 5% cement (V): p - W response

Figures 6.17 and 6.18 show the stress path, stress-strain, and q - w for the soil treated with 5% cement (V) under a TC stress path with 27.55 psi initial confining. The q value at the peak was

identified at 8.5 psi, which was higher than for the same soil tested under CTC with 11.6 psi initial confining pressure.

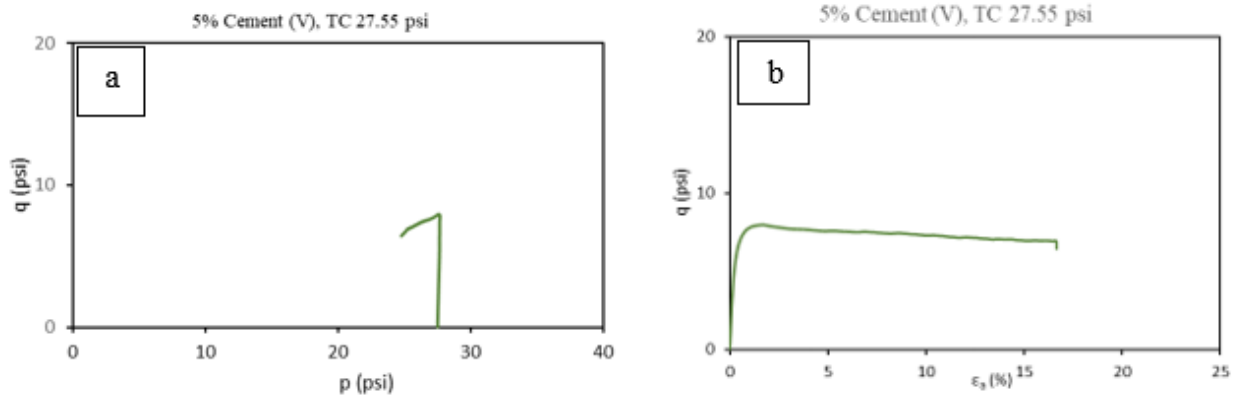


Figure 6.17 TC stress path with 27.55 psi initial confining pressure for soil treated with 5% cement (V): (a) q-p plane, (b) q-ε_a plane

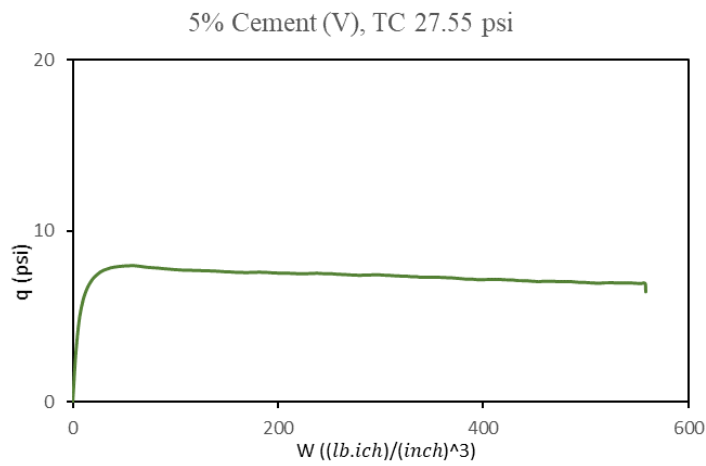


Figure 6.18 TC stress path with 27.55 psi initial confining pressure for soil treated with 5% cement (V): q-W response

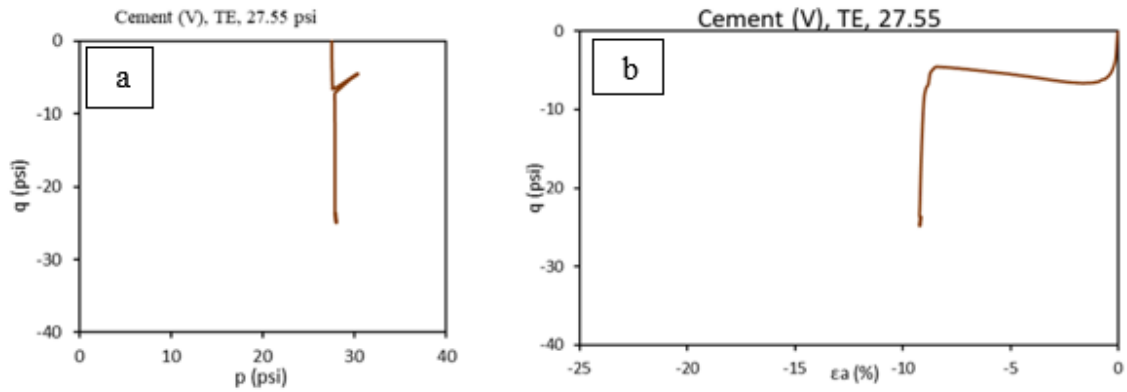


Figure 6.19 TE stress path with 27.55 psi initial confining pressure for soil treated with 5% cement (V): (a) q-p plane, (b) q- ϵ_a plane

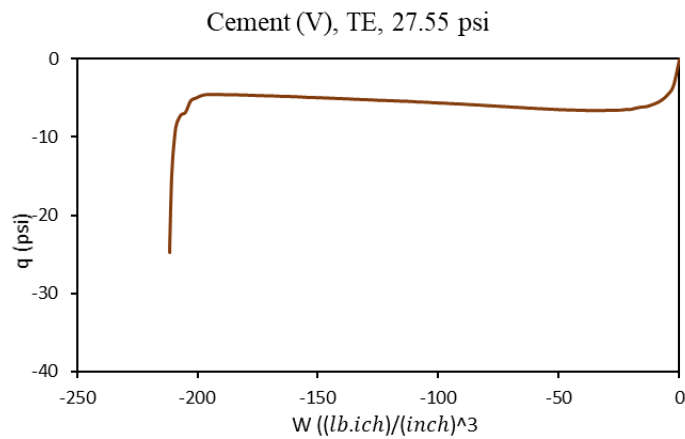


Figure 6.20 TE stress path with 27.55 psi initial confining pressure for soil treated with 5% cement (V): q-W response

Figures 6.19 and 6.20 show the stress path, stress-strain, and q-w for the soil treated with 5% cement (V) under the TE stress path with 27.55 initial confining. The critical point or residual point for this test was identified at $q = -4$ psi, and the soil reached the critical state line in less time than the TC stress path with the same confining pressure.

The TE stress path for the soil treated with 5% cement (V) with higher initial confining is presented in Figure 6.21, and Figure 6.22 shows the q-W response for this test. The peak value was identified at $q = -5$ psi was higher than the peak value for the same test under 27.55 psi initial confining pressure.

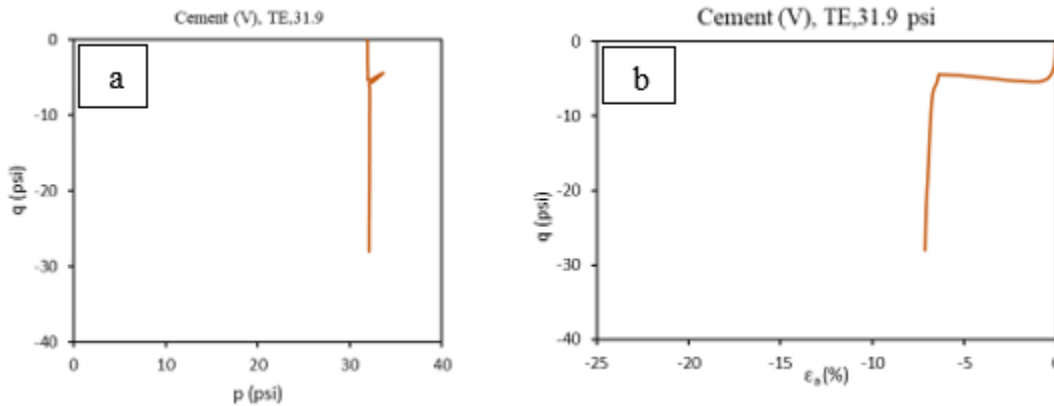


Figure 6.21 TE stress path with 31.9 psi initial confining pressure for soil treated with 5% cement (V): (a) q-p plane, (b) q- ϵ_a plane

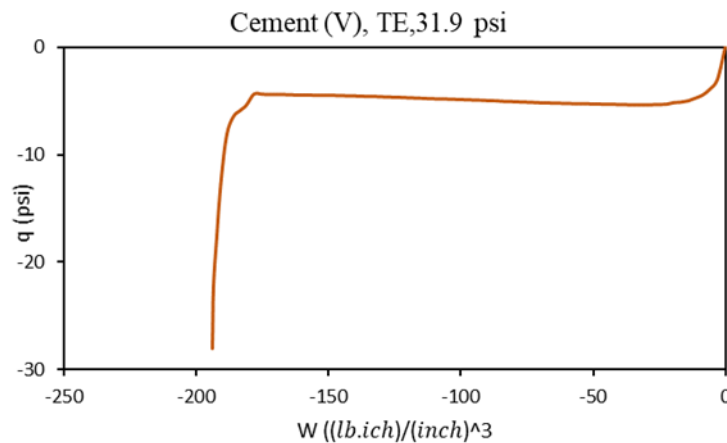


Figure 6.22 TE stress path with 31.9 psi initial confining pressure for soil treated with 5% cement (V): q-W response

6.1.3 Soil treated with 6% Lime + 4% Fly ash

The soil treated with 6% lime + 4% fly ash had greater strength than the natural soil. Figures 6.23 and 6.24 show the curves generated from HC and PL test results. The pre-consolidation pressure was identified at $p = 40$ psi, and the initial yield surface was larger than that of natural soil with pre-consolidation of 29 psi.

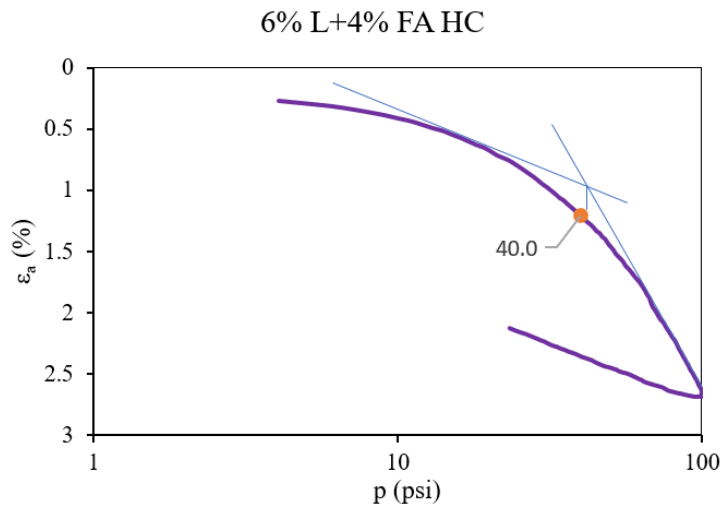


Figure 6.23 HC stress path for soil treated with 6% lime + 4% fly ash

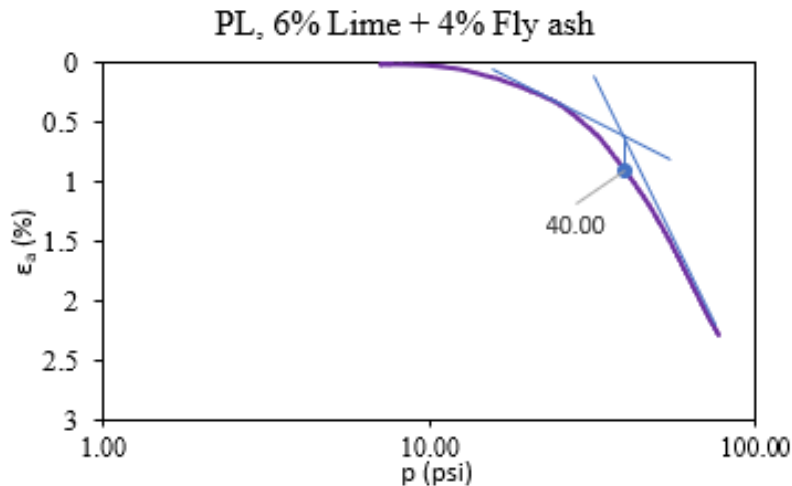


Figure 6.24 PL stress path for soil treated with 6% lime + 4% fly ash

Figures 6.25 and 6.26 show the stress path, stress-strain response, and p-W response for the soil treated with 6% lime + 4% fly ash. The soil exhibited elastic behavior before the yield point, which was identified at $q=18.5$ psi and $p = 30.10$ psi; the critical state point was at the residual point, which was identified at $q = 28$ psi and $p = 39.54$ psi.

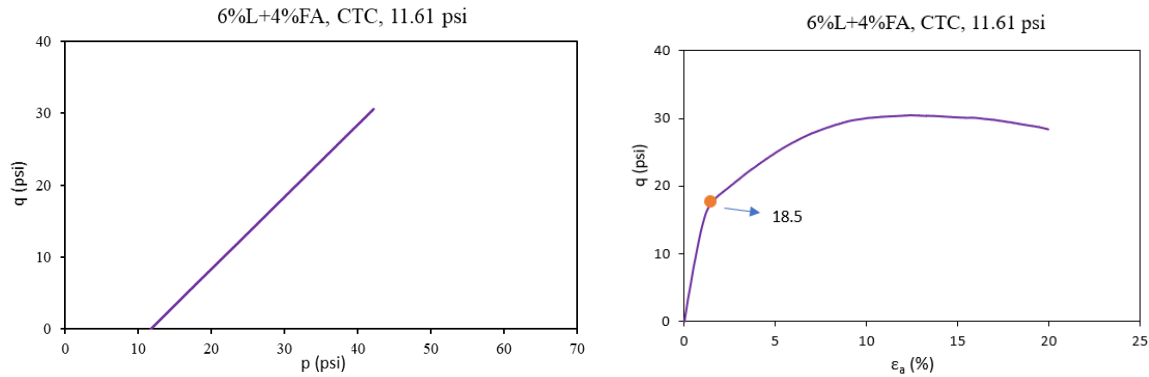


Figure 6.25 CTC stress path with 11.6 psi initial confining pressure for soil treated with 6% lime + 4% fly ash: (a) q - p plane, (b) q - ϵ_a plane

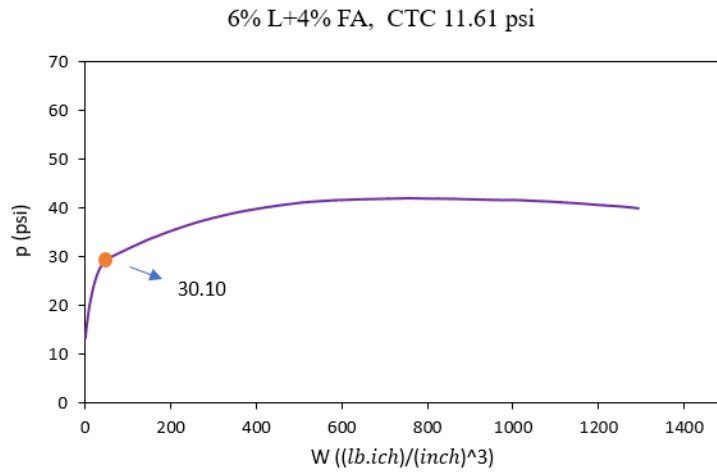


Figure 6.26 CTC stress path with 11.6 psi initial confining pressure for soil treated with 6% lime + 4% fly ash: p - W response

The stress path, stress-strain response, and p-W response for the soil treated with 6% lime + 4% fly ash under a CTC stress path with higher confining pressure of 23.21 psi are shown in Figures 6.27 and 6.28, respectively. The yield point was identified at $q = 23.21$ psi and $p = 23$, and the critical or residual point was identified at $q = 32$ psi and $p = 55.27$ psi, which was higher than the residual point for the same soil with a CTC stress path under 11.6 psi initial confining pressure.

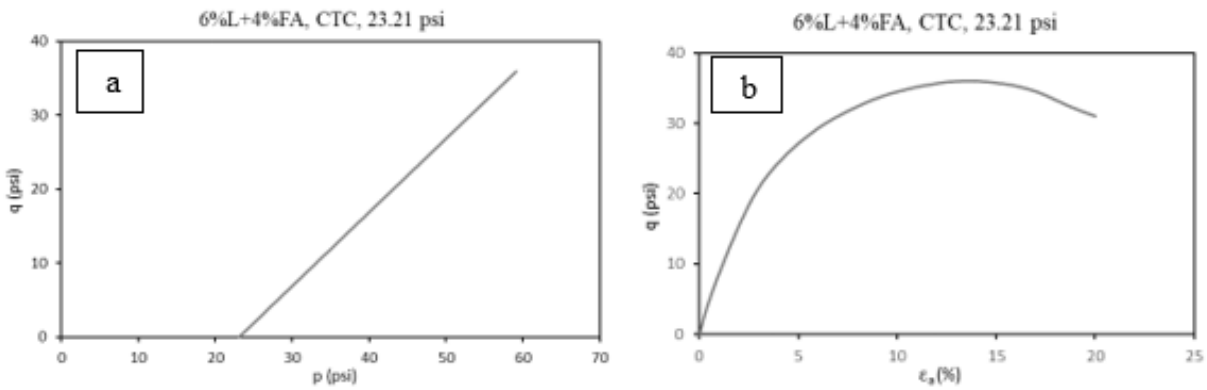


Figure 6.27 CTC stress path with 23.21 psi initial confining pressure for soil treated with 6% lime + 4% fly ash: (a) q-p plane, (b) q-ε_a plane

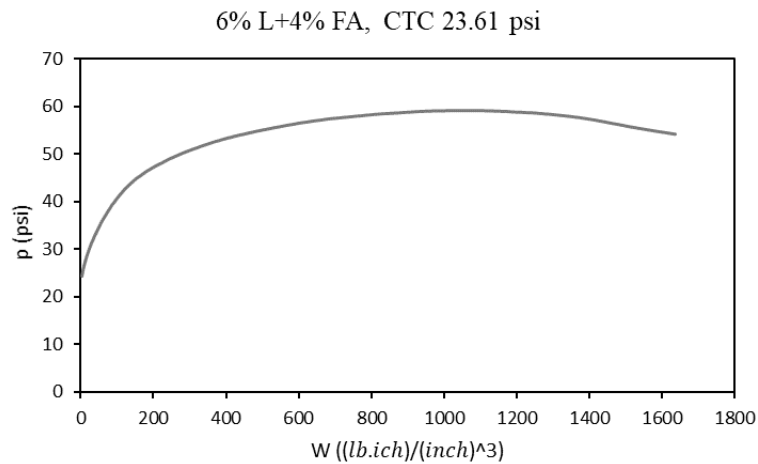


Figure 6.28 CTC stress path with 23.21 psi initial confining pressure for soil treated with 6% lime + 4% fly ash: p-W response

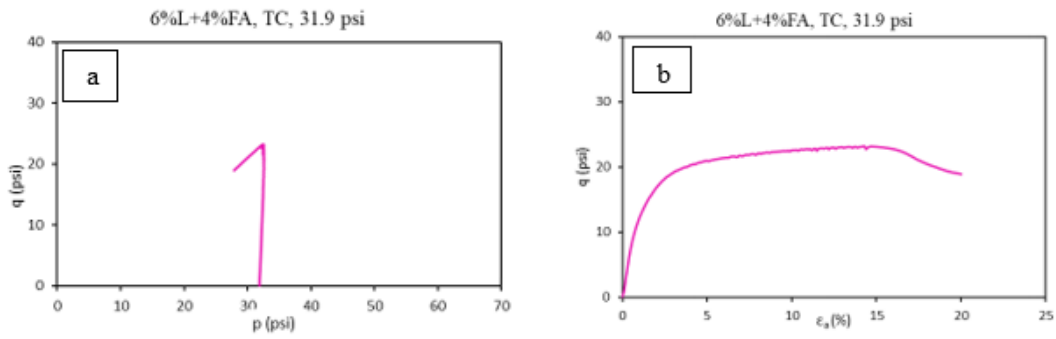


Figure 6.29 TC stress path with 31.9 psi initial confining pressure for soil treated with 6% lime + 4% fly ash: (a) q - p plane, (b) q - ϵ_a plane

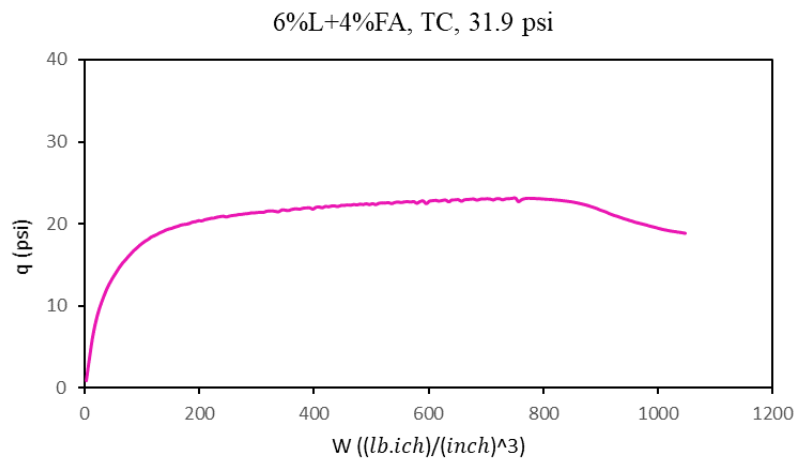


Figure 6.30 TC stress path with 31.9 psi initial confining pressure for soil treated with 6% lime + 4% fly ash: q - W response

Figures 6.29 and 6.30 show the TC stress path for the soil treated with 6% lime + 4% fly ash under 31.9 psi initial confining pressure, stress-strain, and the q - W generated from the results. The soil behaved elastic up to $q = 18$ psi and reached the critical state line at the peak point, which was identified at $q = 23$ psi and $p = 32.39$ psi.

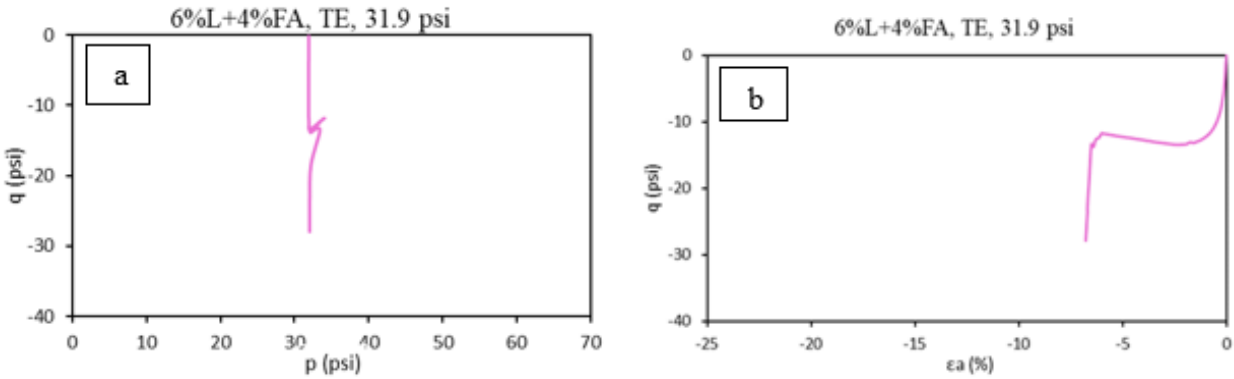


Figure 6.31 TE stress path with 31.9 psi initial confining pressure for soil treated with 6% lime + 4% fly ash: (a) q-p plane, (b) q-ε_a plane

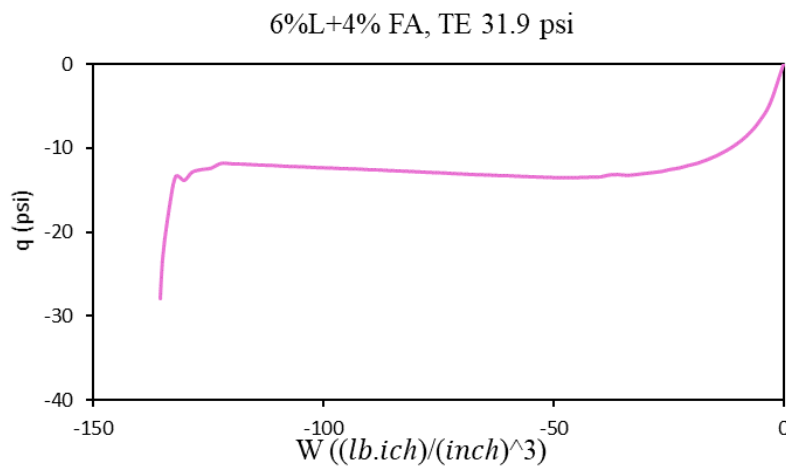


Figure 6.32 TE stress path with 31.9 psi initial confining pressure for soil treated with 6% lime + 4% fly ash: q-W response

The q-p plane, stress-strain response, and q-W response for the soil treated with 6% lime + 4% fly ash under 31.9 psi initial confining pressure are shown in Figures 6.31 and 6.32, respectively. The soil reached the yield point at q = -9 psi and reached the peak point at q = -12 psi, which is less than the yield and peak value for the TC stress path for the same soil.

6.1.4 Soil treated with 5% Cement (V) + 15% Fly ash

The soil treated with 5% cement (V) + 15% fly ash showed higher strength than the natural soil; however, the soil behavior was brittle. The curves generated from the HC test results for this treatment are shown in Figures 6.33; the pre-consolidation pressure was identified at $p = 62$ psi, which was the highest among the previous treatments.

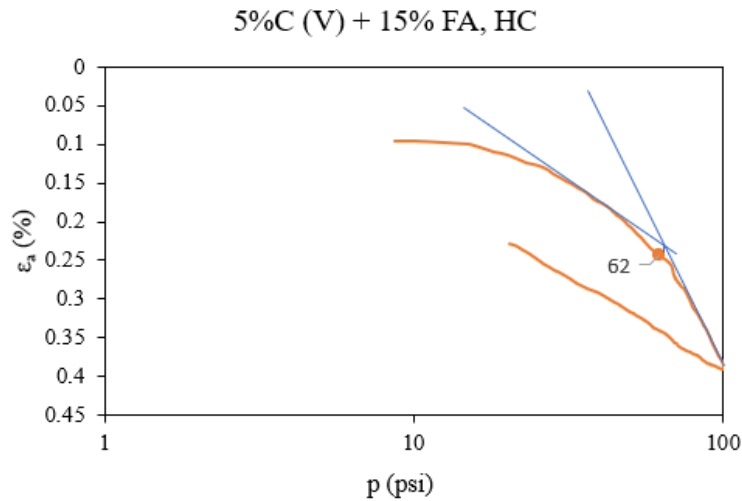


Figure 6.33 HC stress path for soil treated with 5% cement (V) + 15% fly ash

Figures 6.34 and 6.35 show the stress path, stress-strain, and p - W for the soil treated with 5 % cement (V) + 15 % fly ash under the CTC stress path with initial confining pressure of 10 psi. The yield value was identified at $q = 30$ psi, which was the peak value for this curve, meaning that the soil behaves purely elastic up to failure.

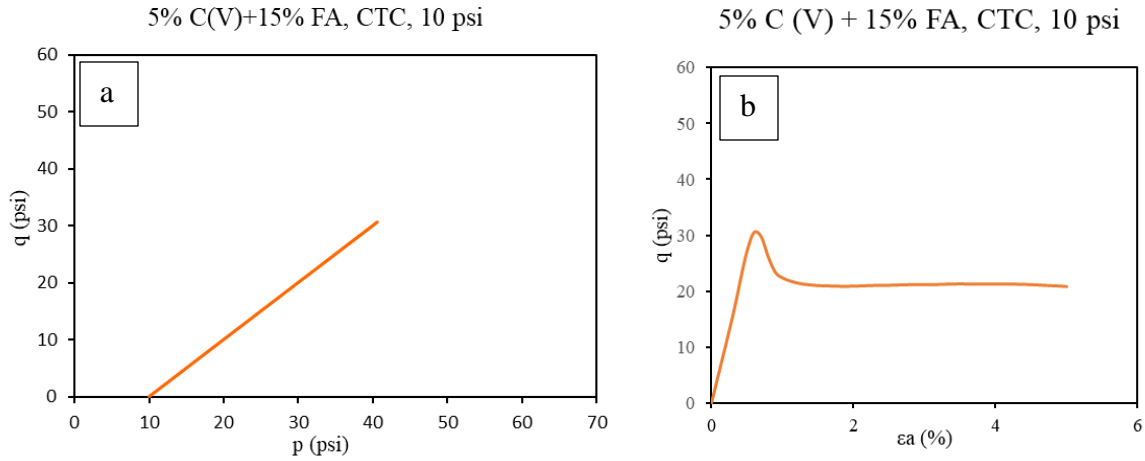


Figure 6.34 CTC stress path with 10 psi initial confining pressure for the soil treated with 5% cement (V) + 15% fly ash: (a) q-p plane, (b) q- ϵ_a plane

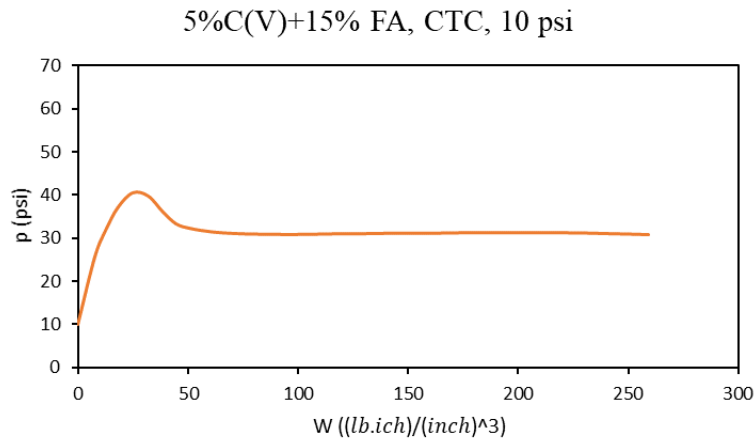


Figure 6.35 CTC stress path with 10 psi initial confining pressure for the soil treated with 5% cement (V) + 15% fly ash: p-W response

Figures 6.36 and 6.37 show the stress path, stress-strain response, and p-W response for the soil treated with 5% cement (V) + 15% fly ash with CTC stress path under 23.21 initial confining pressure. The yield point was identified at $q = 29.5$ psi and $p = 52.71$ psi, and the peak point was identified at $q = 36$ psi.

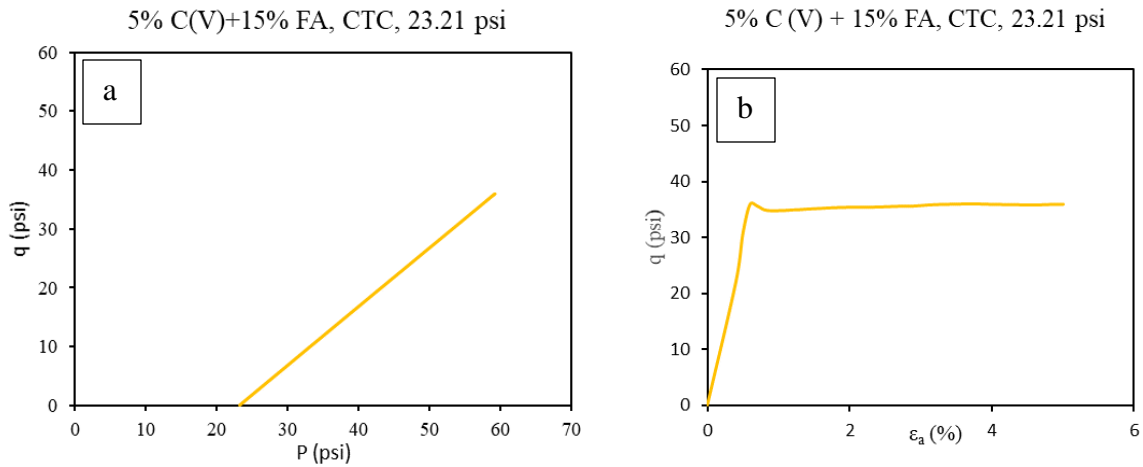


Figure 6.36 CTC stress path with 23.21 psi initial confining pressure for soil treated with 5% cement (V) + 15% fly ash: (a) q-p plane, (b) q- ϵ_a plane

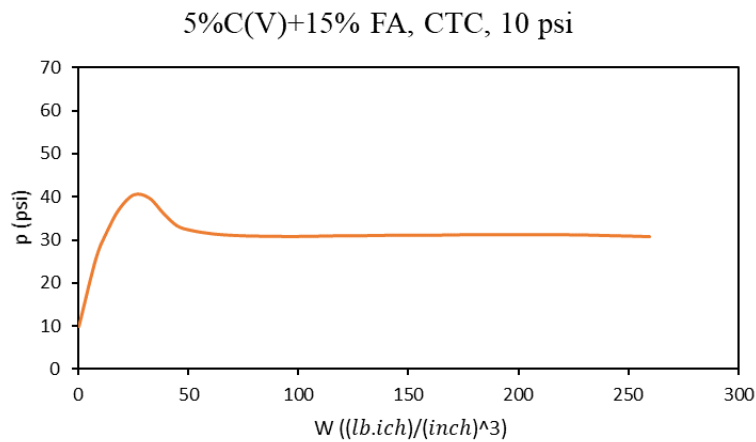


Figure 6.37 CTC stress path with 23.21 psi initial confining pressure for soil treated with 5% cement (V) + 15% fly ash: p-W response

Figure 6.38 shows the stress path for the soil treated with 5% cement (V) + 15% fly ash under the TC stress path with initial confining pressure of 31.9 psi, based on the stress-strain

response in Figure 6.38 and the q-W response in Figure 6.39. The yield point was identified at $q = 27$ psi, which was the same as the peak point.

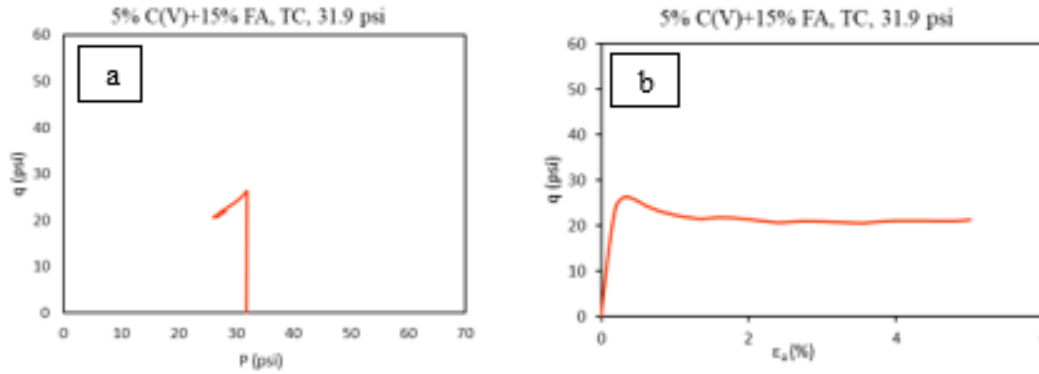


Figure 6.38 TC stress path with 31.9 psi initial confining pressure for soil treated with 5% cement (V) + 15% fly ash: (a) q-p plane, (b) q- ϵ_a plane

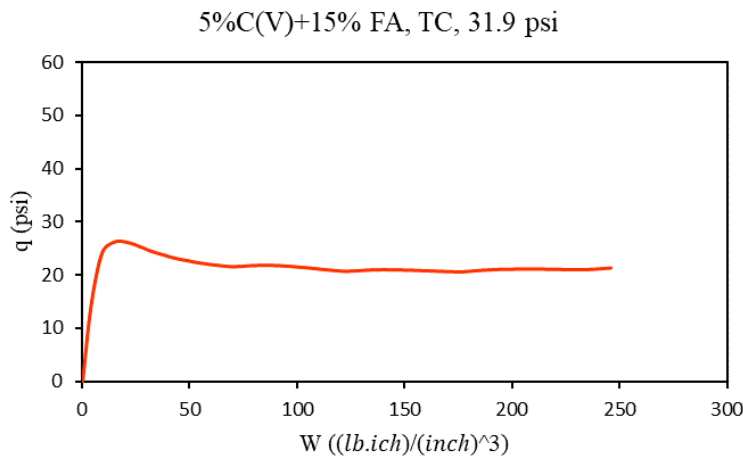


Figure 6.39 TC stress path with 31.9 psi initial confining pressure for soil treated with 5% cement (V) + 15% fly ash: q-W response

Figure 6.40 and Figure 6.41 show the stress path, stress-strain response, and p-W response for the soil treated with 5 % cement (V) + 15% fly ash under TC stress path with initial confining

pressure of 50 psi. The yield point was identified at $q = 30$ psi and the residual point was identified at $q = 34$ psi. The q value for the yield point was higher for this test than for the same test under 31.9 psi initial confining pressure for the same soil.

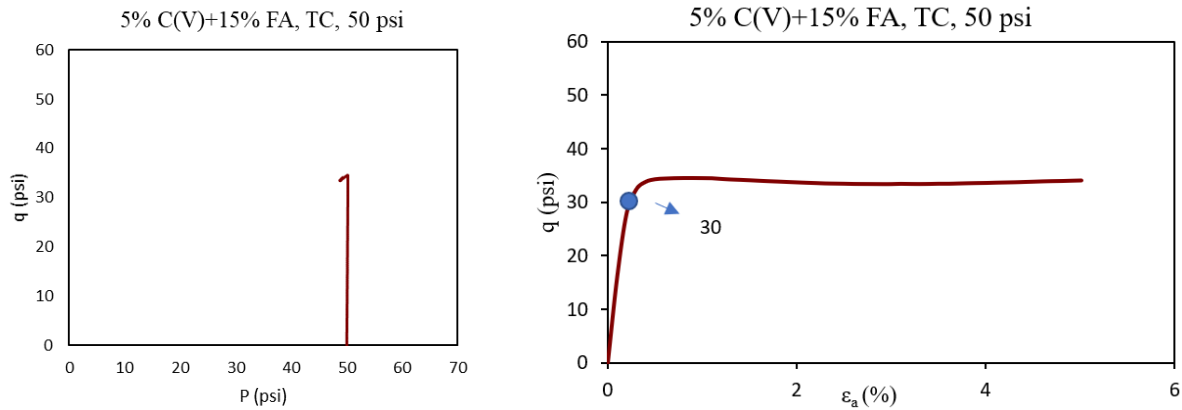


Figure 6.40 TC stress path with 50 psi initial confining pressure for soil treated with 5% cement (V) + 15% fly ash: (a) q - p plane, (b) q - ϵ_a plane

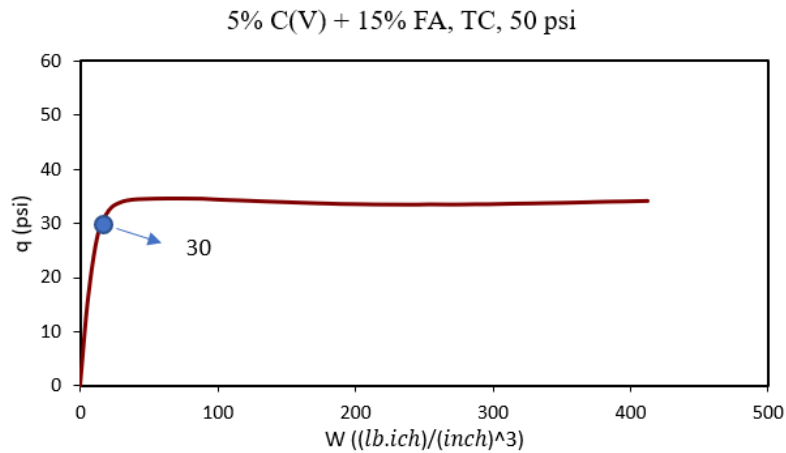


Figure 6.41 TC stress path with 50 psi initial confining pressure for soil treated with 5% cement (V) + 15% fly ash: q - W response

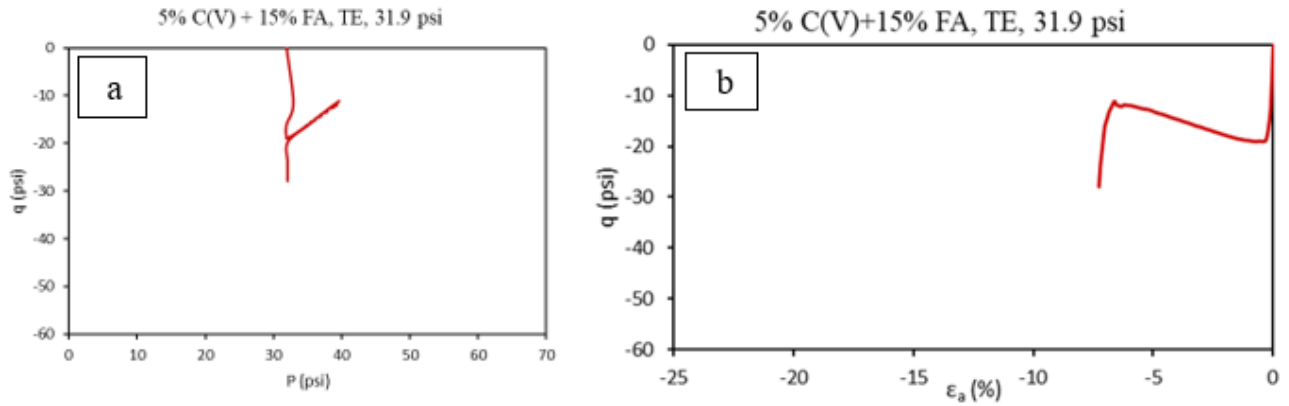


Figure 6.42 TE stress path with 31.9 psi initial confining pressure for soil treated with 5% cement (V) + 15% fly ash: (a) q - p plane, (b) q - ϵ_a plane

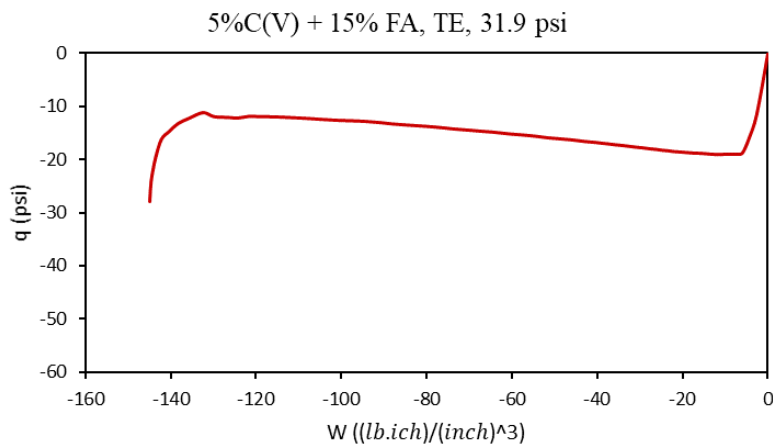


Figure 6.43 TE stress path with 31.9 psi initial confining pressure for soil treated with 5% cement (V) + 15% fly ash: q - W response

Figures 6.42 and 6.43 show the stress path, stress-strain response, and p - W response for 5% cement (V) + 15% fly ash under a TE stress path with initial confining pressure of 31.9 psi, respectively. The yield point was identified at $q = -14$ psi; the yield point for soil treated with 5% cement (V) + 15% fly ash under the same stress path under higher initial confining of -50 psi was

identified at $q = -15$ psi. The stress path, stress-strain response, and p - W response are presented in Figures 6.44 and 6.45.

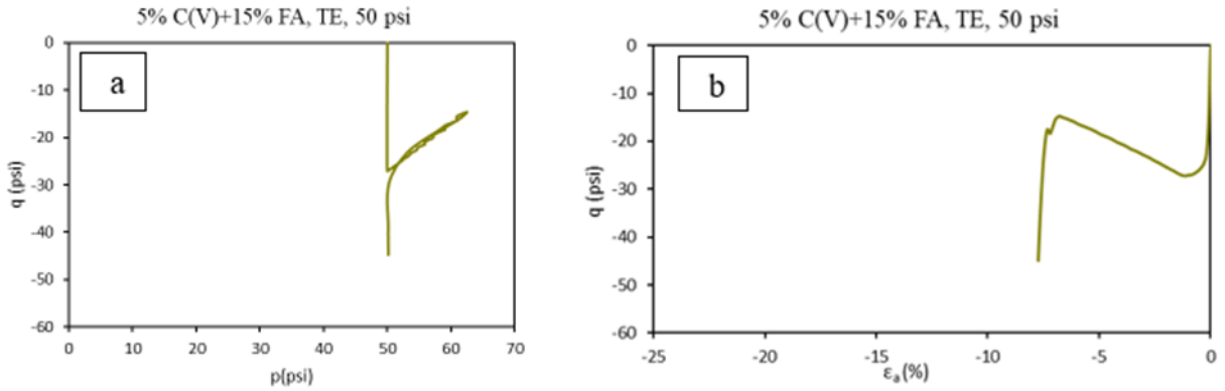


Figure 6.44 TE stress path with 50 psi initial confining pressure for soil treated with 5% cement (V) + 15% fly ash: (a) q - p plane, (b) q - ϵ_a plane

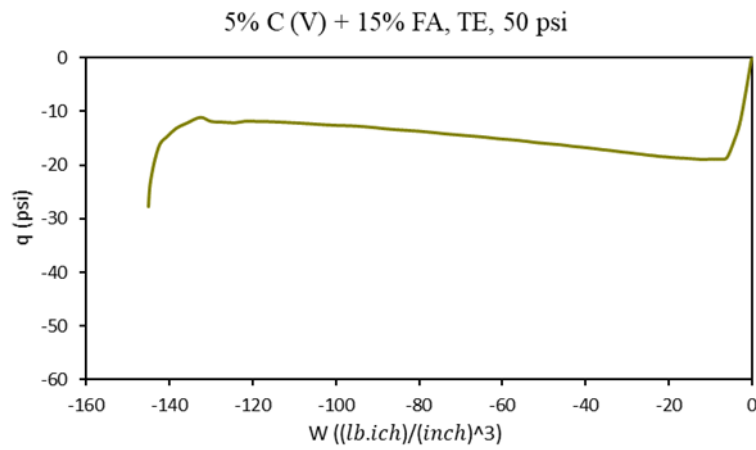


Figure 6.45 TE stress path with 50 psi initial confining pressure for soil treated with 5% cement (V) + 15% fly ash: q - W response

6.2 Proportional Loading (PL) Stress path

Two proportional loading tests were conducted: one on natural soil with a specific K_0 coefficient and one on the soil treated with 6% lime and 4% fly ash. The importance of this test is that the stress path can model a more realistic form of consolidation that occurs in the field because K_0 (at-rest pressure coefficient) is considered, the increase in the horizontal and vertical stresses is not identified during the test, and the ratio of q top is a constant value. For natural soil, K_0 and μ values are calculated and exhibited in formulas 9 and 10; for the soil treated with 6% lime + 4% fly ash, they are calculated and shown in formulas 11 and 12. The values are larger for the PL stress path of the soil treated with 6% lime + 4% fly ash because the friction angle is larger than in the natural soil.

$$K_0 = 1 - \sin(18^\circ) = 0.69 \quad (9)$$

$$\eta = \frac{q}{p} = \frac{(1-0.69)}{(1+0.69)} = 0.183 \quad (10)$$

$$K_0 = 1 - \sin(19^\circ) = 0.674 \quad (11)$$

$$\eta = \frac{q}{p} = \frac{(1-0.674)}{(1+0.674)} = 0.194 \quad (12)$$

Figure 6.46 shows a comparison of the PL stress path in the $p - \epsilon_a$ plane. The volumetric rebound index and volumetric compression index were calculated for natural soil and the soil treated with 6% lime + 4% fly ash from the slope of these curves, as shown in the figure, and the values are summarized in Table 6.1.

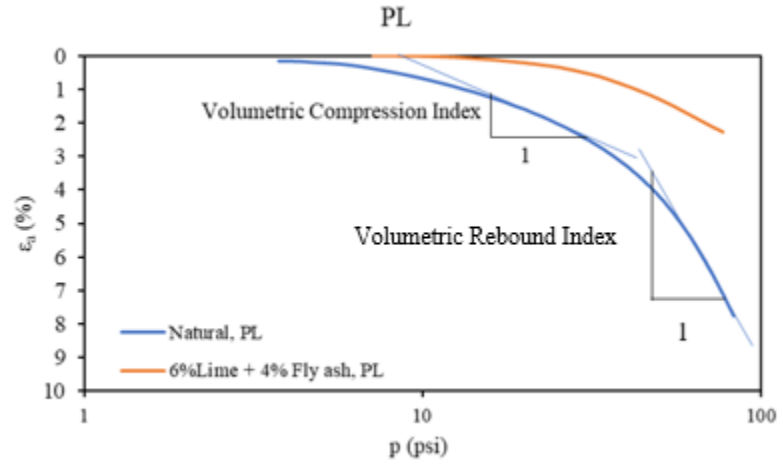


Figure 6.46 PL stress path in p - ϵ_v for natural soil and soil treated with 6% lime + 4% fly ash

Table 6.1 Volumetric Compression Index and Volumetric Rebound Index for Natural Soil and Soil Treated with 6% Lime + 4% Fly Ash

| Treatment Method | Volumetric Compression Index | Volumetric Rebound Index |
|----------------------|------------------------------|--------------------------|
| Untreated | 4.2 | 19.4 |
| 6% lime + 4% fly ash | 0.7 | 4.8 |

6.3 Typical Failure Modes: Compression vs. Extension

The typical failure modes for the samples treated with 5% cement (V) + 15% fly ash under different stress paths are shown in Figure 6.47. The soil experienced bulging deformation at the bottom of a sample under the CTC stress path, while p increased as the deviator intensified. Similarly, the sample shows bulging deformation in the upper part of the sample under the TC stress path where p was kept constant as the deviator stress increased. The failure zone in both of the CTC tests was the same in the lower part of the sample. The sample tested under the TE stress path exhibited necking at the failure zone. Figure 6.48 shows that all of the samples exhibited a barreling form of failure under the CTC stress path. The bulging deformation was in the lower part

of the sample for the soil treated with 5% cement (V) + 15% fly ash and the sample treated with 6% lime + 45 fly ash, while it was in the middle section of the natural soil.

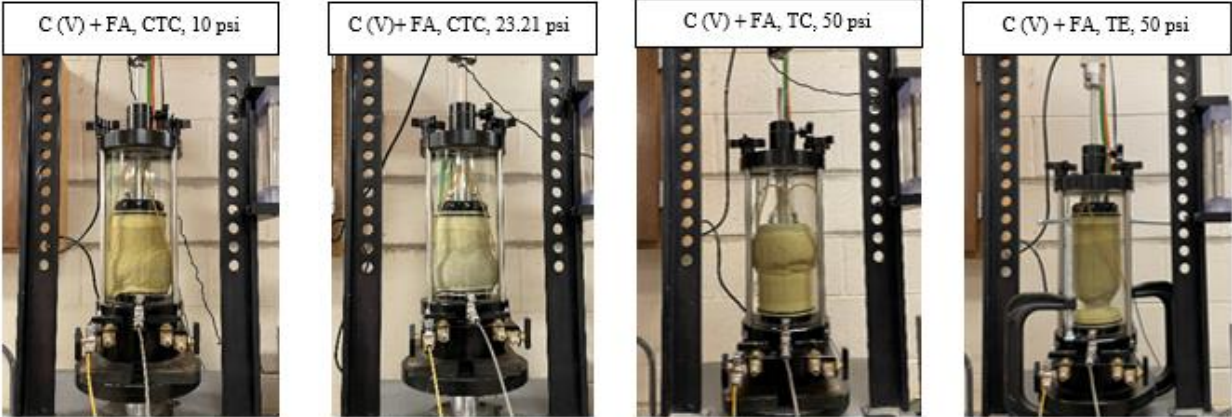


Figure 6.47 Different failure modes for the sample treated with 5% cement (V) + 15 % fly ash under different stress path

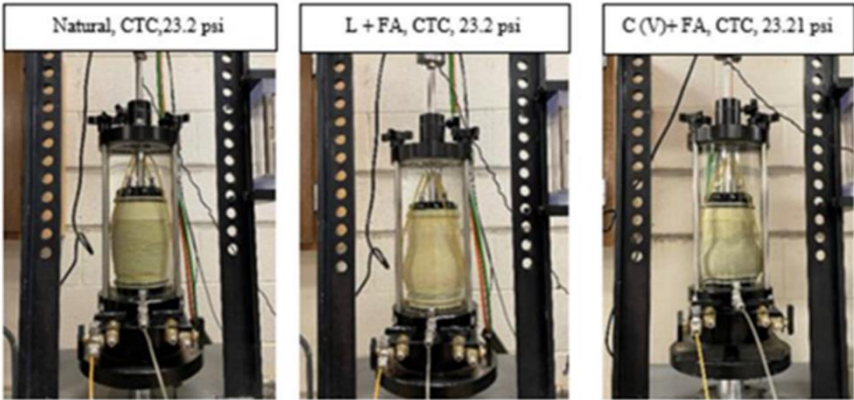

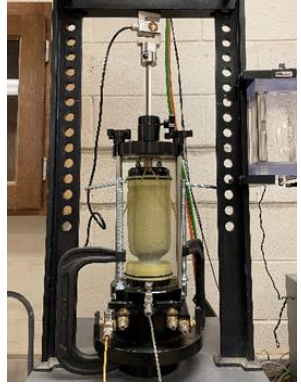
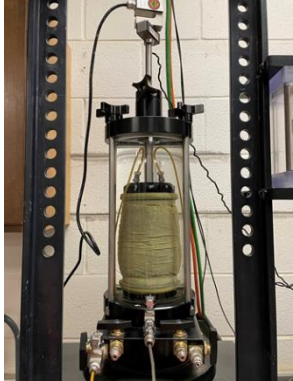



Figure 6.48 Barreling failure mode under CTC for natural sample, sample treated with 6% lime + 4% fly ash, and sample treated with 5% cement (V) + 15% fly ash

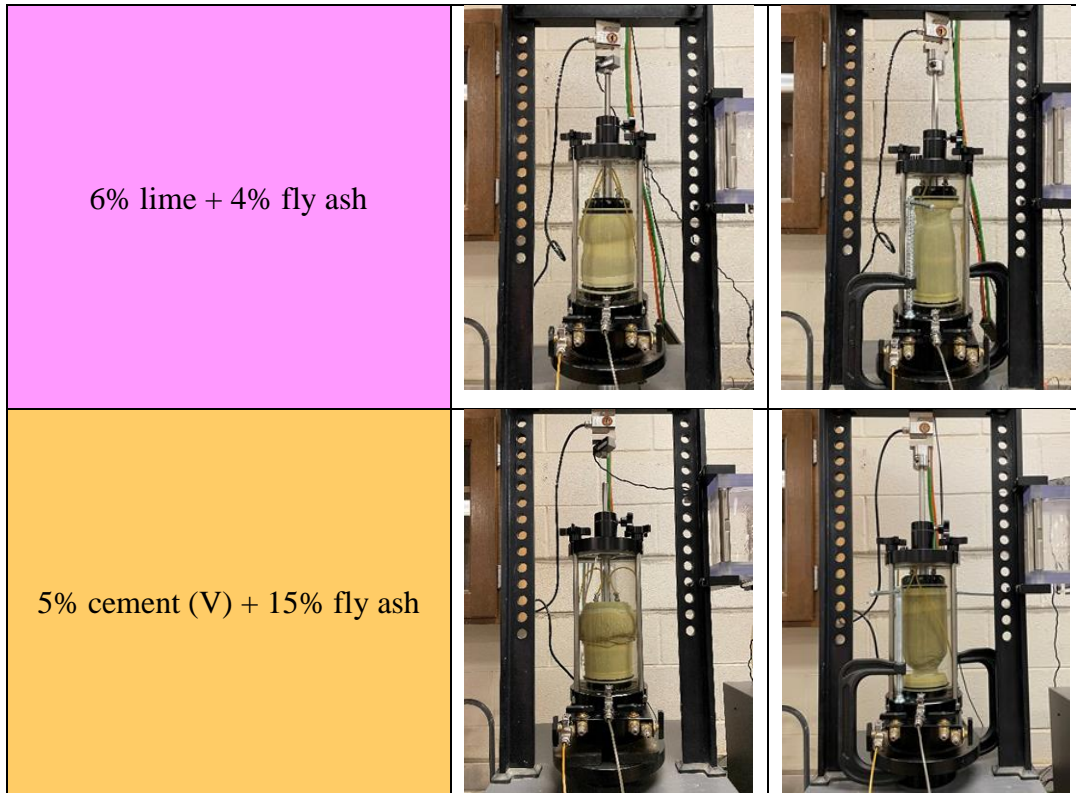
A comparison of the failure modes of the natural soil, the soil treated with 6% lime + 4% fly ash, and the soil treated with 5% cement (V) + 15% fly ash under TC and TE stress path is

depicted in Table 6.2. For natural soil and the sample treated with 5% cement (V), the failure zone and bulging form were in the middle part of the sample, while for the samples treated with 5% cement (V) + 15% fly ash and 6% lime + 4% fly ash, the failure zone was at the bottom of the sample. Under the TE stress path, the failure zones for the natural soil and the soil treated with 5% cement + 15% fly ash were at the bottom part of the sample, while it was at the top part for the soil treated with 5% cement (V) and 6% lime + 4% fly ash.

Table 6.2 Failure Modes Under TC and TE Stress Path for Untreated and Treated Samples

| Soil | TC | TE |
|---------------|--|---|
| Natural |  |  |
| 5% cement (V) |  |  |

**Table 6.2 Failure Modes Under TC, VS, and TE Stress Path
for Untreated and Treated Sample (Continued)**



6.4 Unconsolidated-Undrained Critical State Lines: Natural and Treated Clay

The critical state line or CSL line shows the state of the stress of failure on the q-p plane. The parameters obtained from this line are the slope of the critical state line (M) and the intercept of the critical state line (μ), which are reported in all the figures in this section. The line was generated with the peak and residual points obtained from the stress-strain responses in section 6.1.

Figure 6.49 shows the unconsolidated undrained critical state line for natural soil that is the result of connecting residual points for the UU tests conducted on natural soil in compression; μ is equal to 7.5 psi and M is 0.4 in compression.

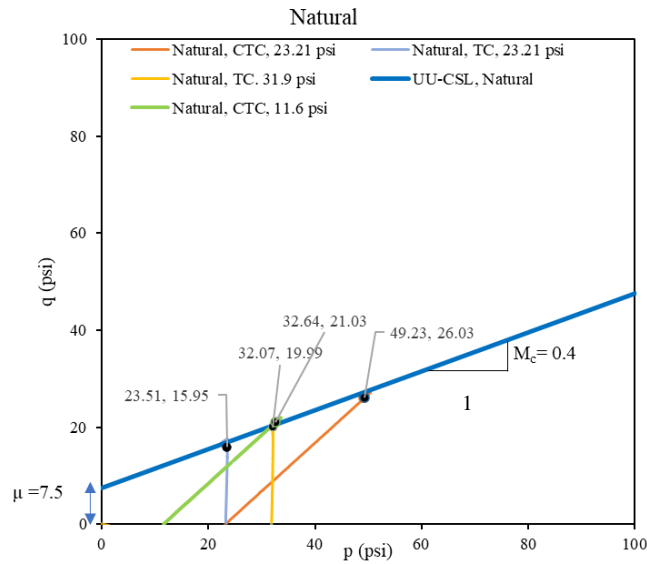


Figure 6.49 CSL line for natural soil in compression

Figure 6.50 shows the CSL line for natural soil that connects the residual points on the q-p plane for extension; M and μ values are smaller in extension as shown in Figure 6.51.

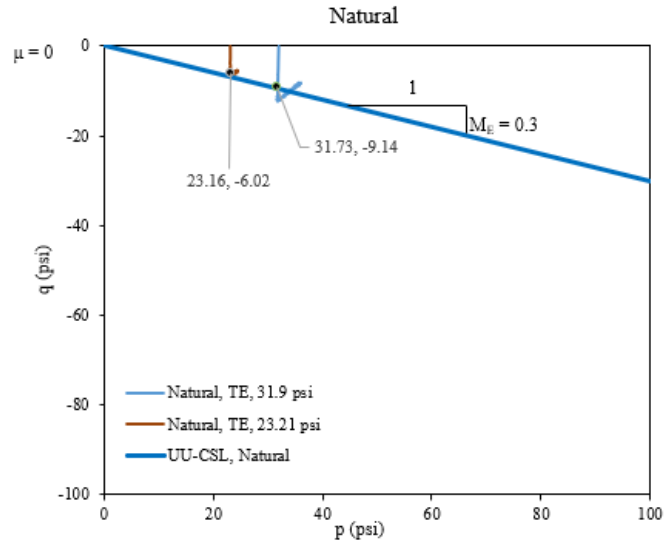


Figure 6.50 CSL line for natural soil in extension

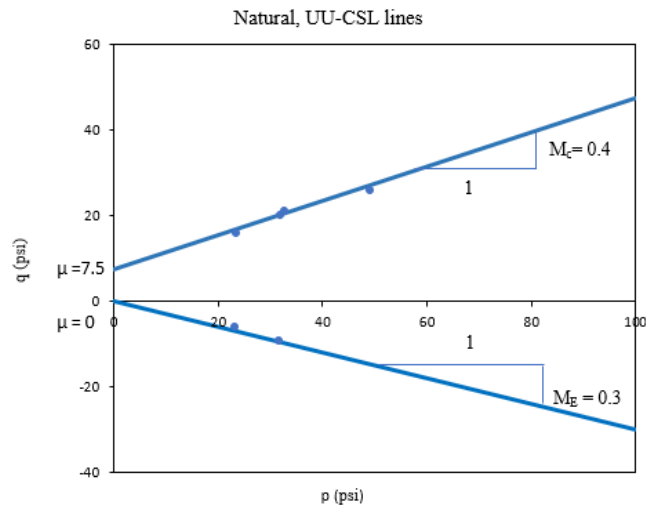


Figure 6.51 CSL lines for natural soil in compression and extension

Figures 6.52 and 6.53 show the critical state lines for the soil treated with 5% cement (V) in compression and extension, respectively. This line connects the peak points obtained from the test results conducted on the soil treated with 5% cement (V). Figure 6.54 shows that the μ value is zero for both lines and the slope of the critical state line is smaller in extension for this soil.

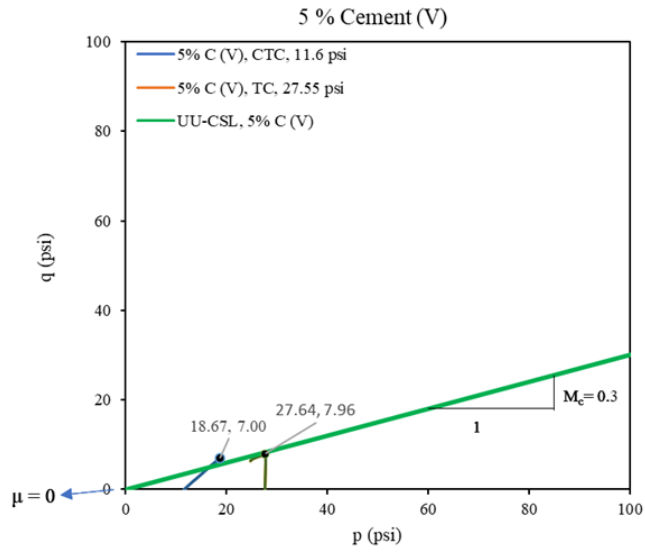


Figure 6.52 CSL line for soil treated with 5% cement (V) in compression

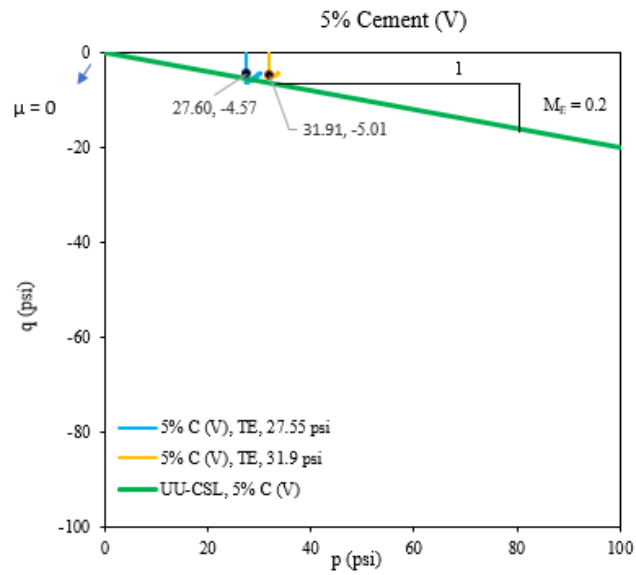


Figure 6.53 CSL line for soil treated with 5% cement (V) in extension

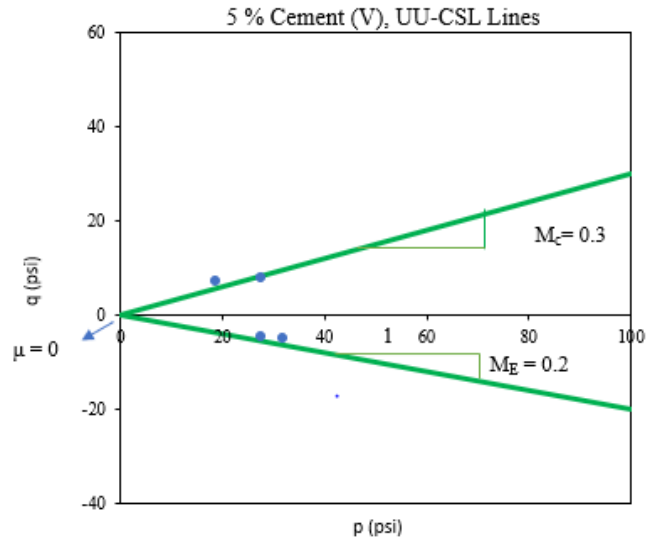


Figure 6.54 CSL lines for soil treated with 5% cement (V) in compression and extension

Figures 6.55 and 6.56 show the CSL lines in compression and extension, respectively, for the soil treated with 6% lime + 4% fly ash. The critical points are the peak and residual points from the stress-strain responses and the slope of this line; the μ value was higher in compression than the extension as presented in Figure 6.57.

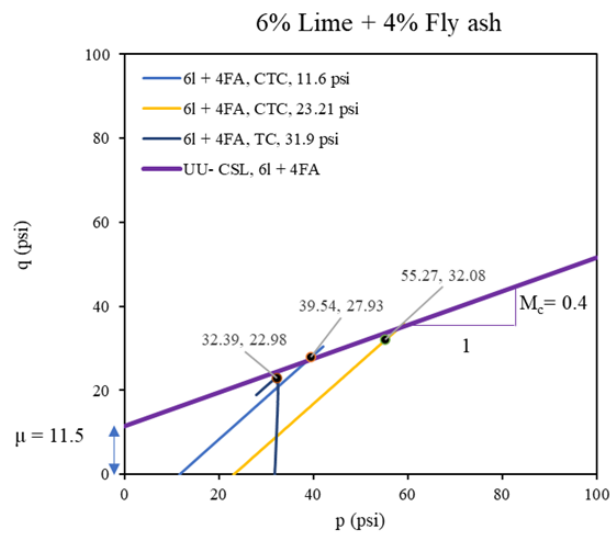


Figure 6.55 CSL line for soil treated with 6% lime + 4% fly ash in compression

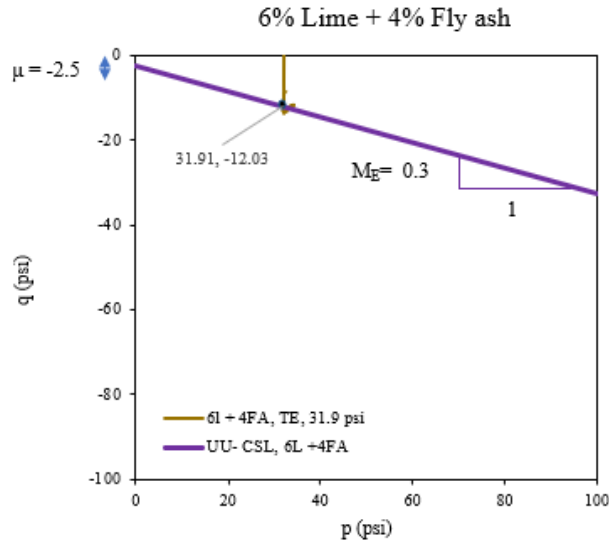


Figure 6.56 CSL line for soil treated with 6% lime + 4% fly ash in extension

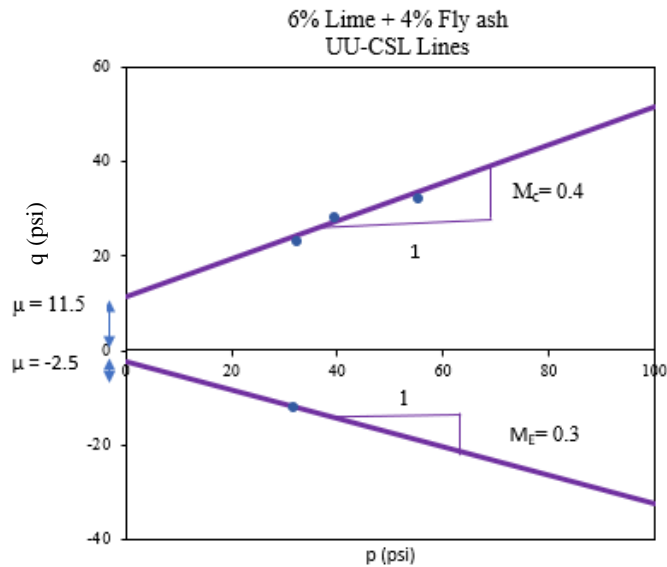


Figure 6.57 CSL lines for soil treated with 6% lime + 4% fly ash in compression and extension

Figures 6.58 and 6.59 show the CSL lines for the soil treated with 5% cement (V) + 15 % fly ash that result from connecting the peak values of the stress-strain responses. As Figure 6.60 shows, the M and μ values are higher in compression than in extension for this soil.

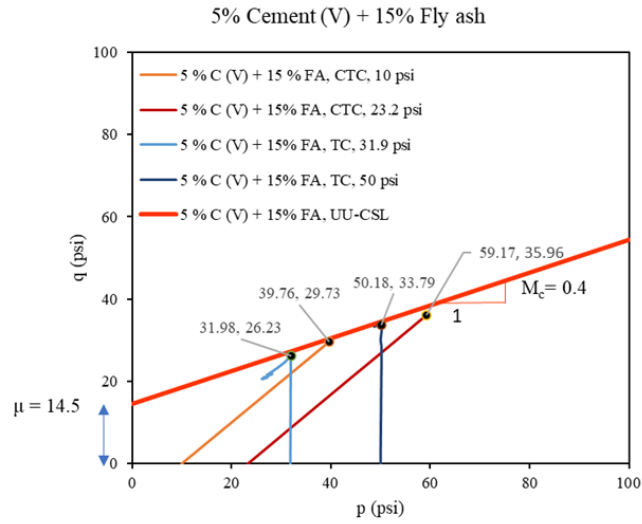


Figure 6.58 CSL line for soil treated with 5% cement (V) + 15 % fly ash in compression

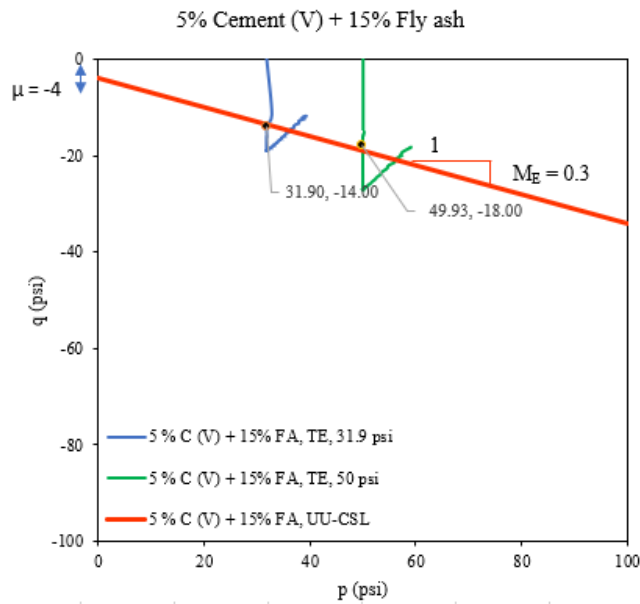


Figure 6.59 CSL line for soil treated with 5% cement (V) + 15 % fly ash in extension

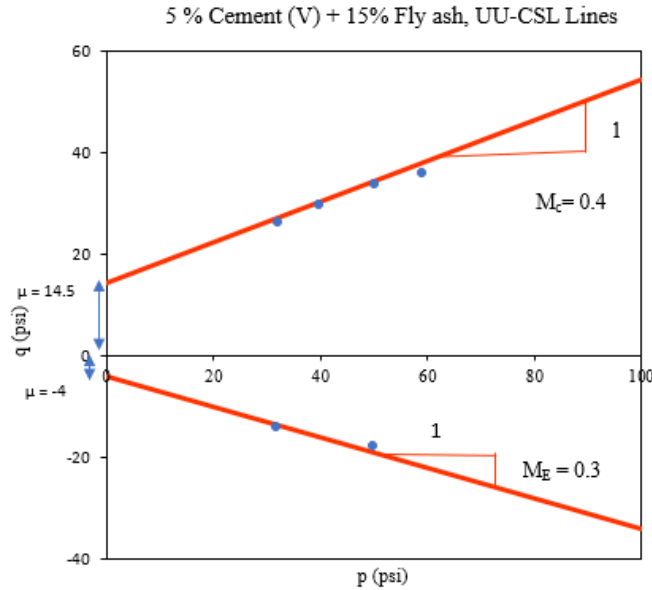


Figure 6.60 CSL lines for soil treated with 5% cement (V) + 15 % fly ash in compression and extension

Figure 6.61 shows a comprehensive illustration of all the CSL lines obtained from the test results of natural soil and the three treatment methods. The highest μ value was for the soil treated with 5% cement (V) + 15 % fly ash and the lowest was for the soil treated with 5% cement (V) (zero). The slope of the critical state line was identical for natural soil, the soil treated with 5% cement (V) + 15 % fly ash, and the soil treated with 6% lime + 4% fly ash; the soil treated with 5% cement (V) exhibited the lowest M value of all of the soils. This observation indicates that the soil treated with 5% cement (V) + 15 % fly ash can sustain more stress before failing than the other treatment methods.

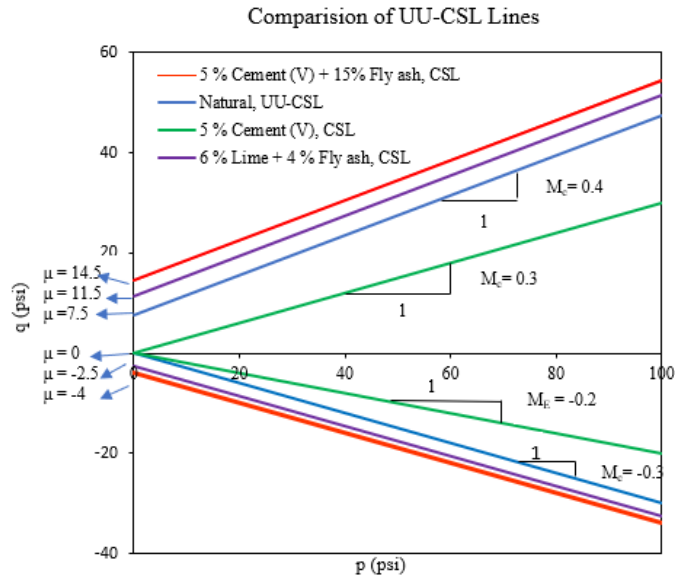


Figure 6.61 Comprehensive illustration of all the CSL lines

6.5 Yielding in Compression and Extension: Natural and Treated Clay

The yield surface is a 2-D or 3-D surface that is produced from connecting the yield points induced from different stress path on a soil. The soil shows elastic behavior before the q and p -value reach the yield surface and exhibits elastoplastic behavior beyond the yield surface up to the CSL line, where it fails. The method for obtaining the yield point was illustrated in section 6.1, and the yield surfaces were generated and compared for the natural soil, the soil treated with 5% cement (V), the soil treated with 6% lime + 4% fly ash, and the soil treated with 5% cement (V) + 15% fly ash.

Figure 6.62 shows the yield surface generated from the yield points for natural soil in compression, and Figure 6.63 shows the yield surface obtained from triaxial extension tests; the complete yield surface for natural soil is illustrated in Figure 6.64. The pre-consolidation pressure for the natural soil calculated from the HC test was 26 psi, and for the tests which had initial confining below this value, the soil exhibited purely elastic behavior up to the yield surface.

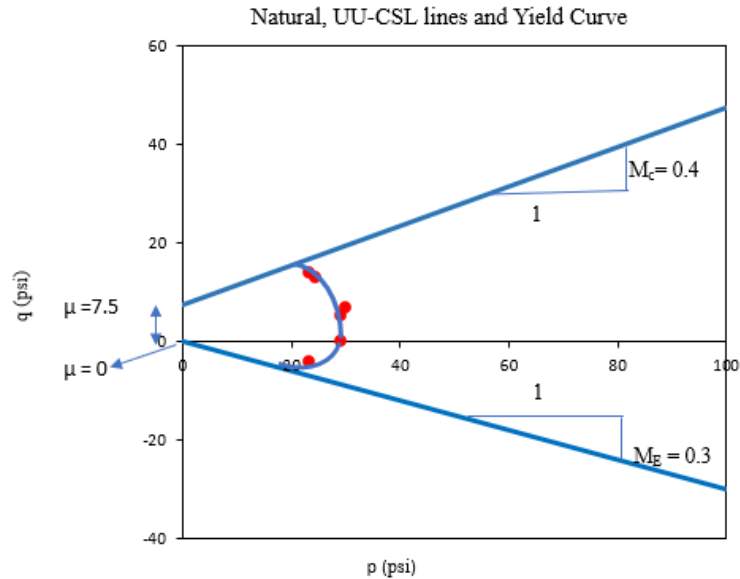


Figure 6.64 Total yield surface for natural soil

Figure 6.65 shows the yield surface generated from the yield points for soil treated with 6% lime + 4% fly ash in compression, and Figure 6.66 shows the yield surface obtained from the triaxial extension tests; the complete yield surface is illustrated in Figure 6.67. The pre-consolidation pressure calculated from the HC test was 40 psi. The soil showed elastic behavior for the stress path with an initial confining below 40 psi up to the yield surface, and the behavior changed to elastoplastic up to the critical state line. The compaction-induced yield surface for the soil treated with 6% lime + 4% fly ash was larger than that of the natural soil's compaction-induced yield surface, which means that the soil's strength-stiffness improved after it was stabilized with 6% lime + 4% fly ash.

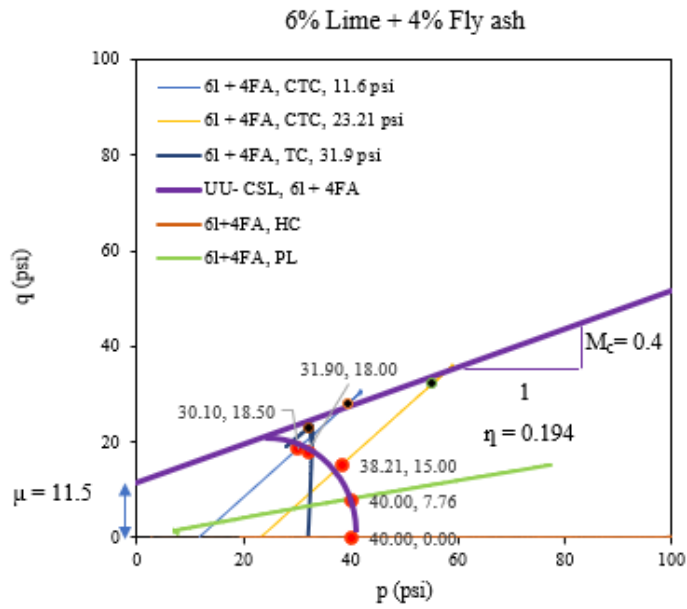


Figure 6.65 Compaction-induced yield surface of soil treated with 6% lime + 4% fly ash in compression

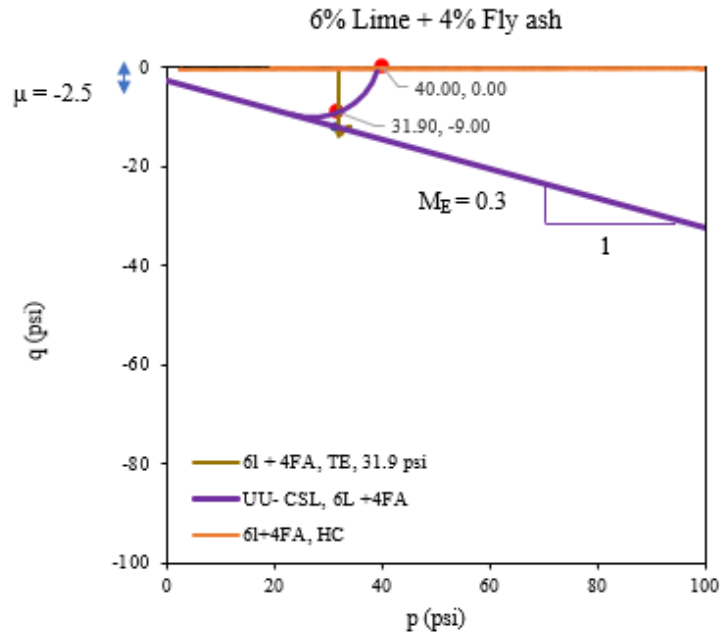


Figure 6.66 Compaction-induced yield surface of soil treated with 6% lime + 4% fly ash in compression

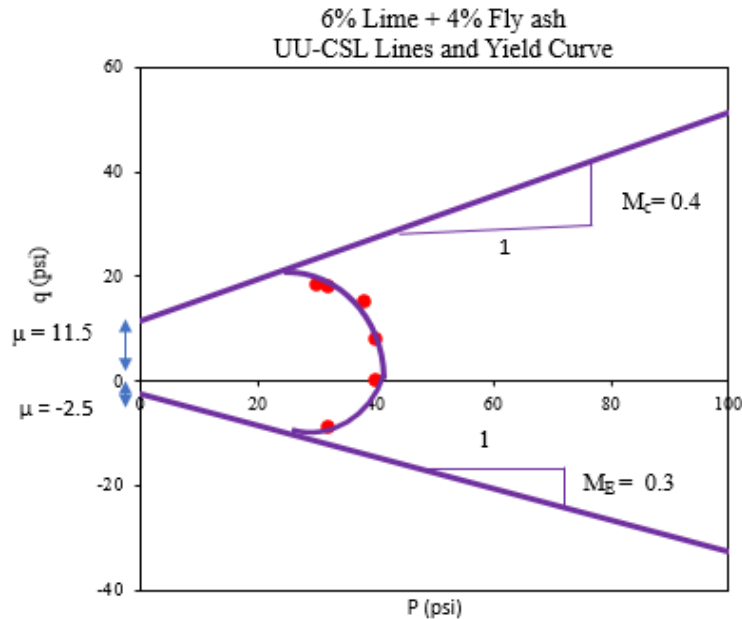


Figure 6.67 Compaction-induced yield surface of soil treated with 6% lime + 4% fly ash

Figure 6.68 shows the yield surface generated from the yield points for or the soil treated with 5% cement (V) + 15% fly ash, and Figure 6.69 shows the yield surface obtained from triaxial extension tests. The pre-consolidation pressure calculated from the HC test for the soil treated with 5% cement (V) + 15% fly ash was 62 psi. For the tests with initial confining below this value, the soil exhibited purely elastic behavior up to the yield surface. The soil exhibited elastoplastic behavior beyond the yield surface up to the critical state line. The complete yield surface for the soil treated with 5% cement (V) + 15% fly ash is illustrated in Figure 6.70.

A comparison of the yield surfaces generated for the natural soil, the soil treated with 6% lime + 4% fly ash, and the soil treated with 5% cement + 15% fly ash is illustrated in Figure 6.71. The yield surface expanded as it was treated with 6% lime + 4% fly ash and 5% cement + 15% fly ash; the largest yield surface was for the soil treated with 5% cement (V) + 15% fly ash. This indicates that the soil treated with 5% cement + 15% fly ash exhibited highest strength-stiffness.

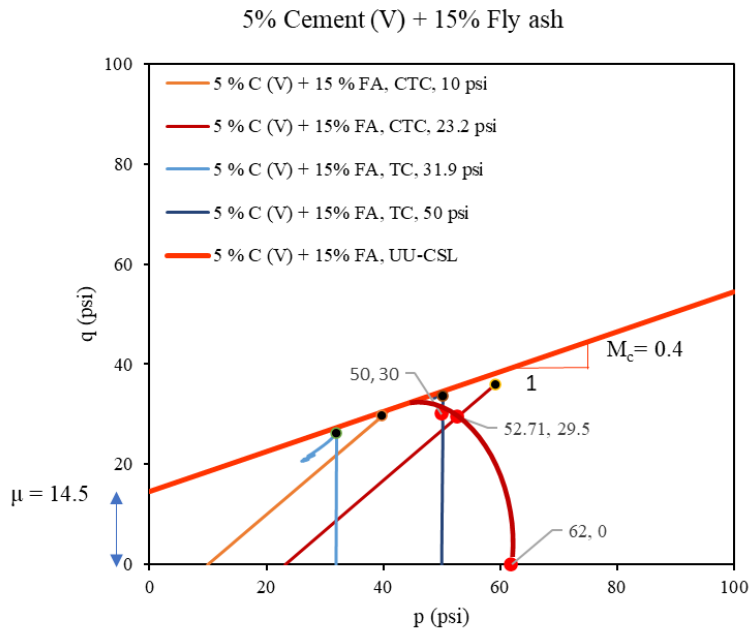


Figure 6.68 Yield surface of the soil treated with 5% cement (V) + 15% fly ash in compression

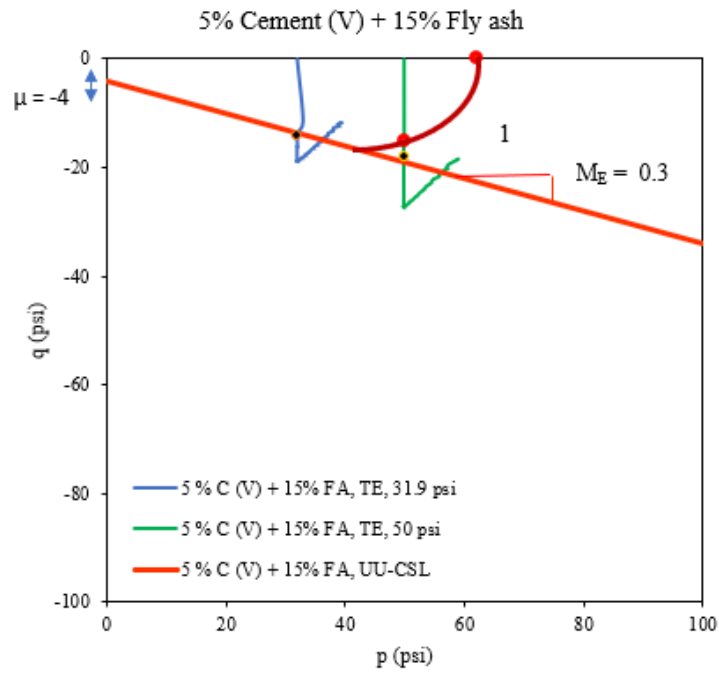


Figure 6.69 Yield surface of the soil treated with 5% cement (V) + 15% fly ash in extension

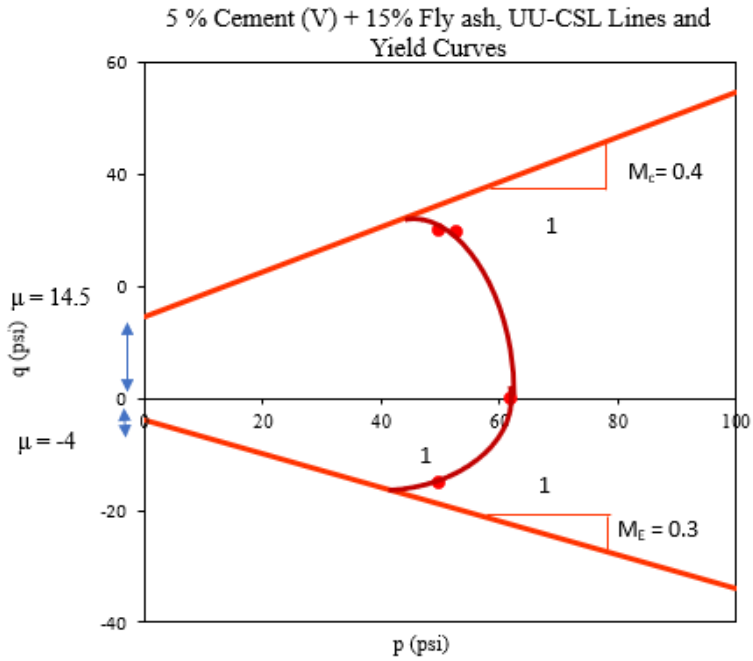


Figure 6.70 Compaction-induced yield surface of the soil treated with 5% cement (V) + 15% fly ash

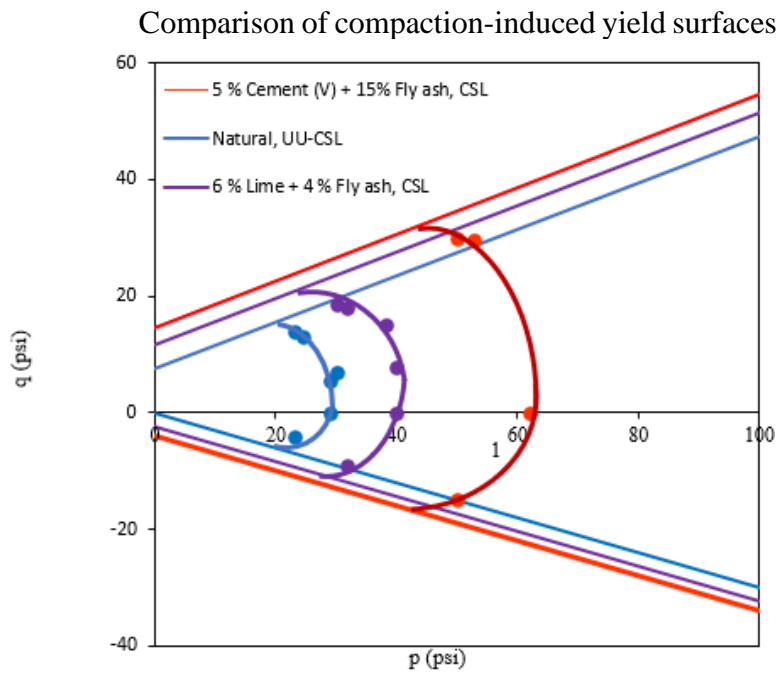


Figure 6.71 Comparison of compaction-induced yield surfaces for untreated and treated soil

6.6 Calibration of Constitutive Parameters

The elastic modulus of soil is the soil's resistance to elastic deformation when stress is applied. This parameter can be obtained from the initial slope of the stress-strain response for each test. Table 6.3 is a summary of the undrained elastic modulus (E_u) and the undrained shear modulus (G_u) calculated from the elastic modulus for each test. Based on the reported values, the samples treated with 5% cement (V) + 15% fly ash exhibited higher undrained elastic modulus and shear modulus than the natural soil, the soil treated with 5% cement (V), and the soil treated with 6% lime + 4% fly ash. For each treatment method and constant initial confining pressure, the E_u and G_u values were higher for TE than either TC or CTC, and the CTC stress path showed the least shear modulus and elastic modulus.

Figure 6.72 shows an example of calculating E_u for natural soil under a CTC stress path with initial confining of 11.6 psi; the calculation of G_u for this test is shown as an example in formula 13.

$$G_u = \frac{E_u}{3} = \frac{10.34}{3} = 3.45 \text{ psi} \quad (13)$$

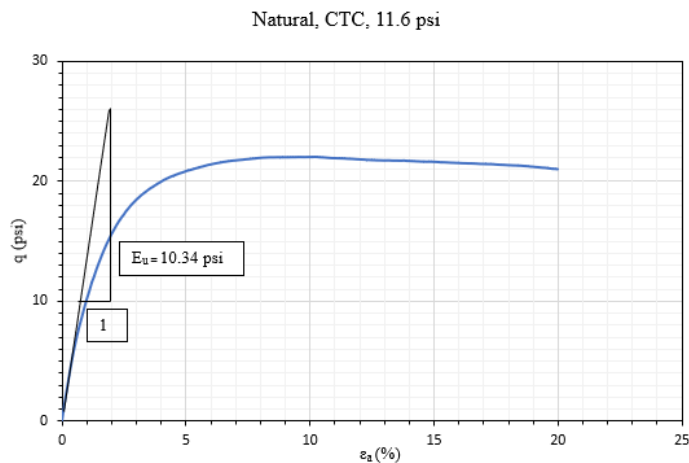


Figure 6.72 Illustration for calculating elastic modulus for natural soil under CTC stress path with 11.6 psi initial confining pressure

**Table 6.3 Elastic Modulus and Shear Modulus for Untreated and Treated Soil
with Variable Stress Path**

| Chemical Treatment | Stress Path | Confining pressure (psi) | E_u (psi) | G_u (psi) |
|----------------------------|-------------|--------------------------|--------------|-------------|
| Natural | TC | 23.21 | 11.54 | 3.85 |
| | CTC | 11.6 | 10.34 | 3.45 |
| | | 23.21 | 9.09 | 3.03 |
| | TE | 23.21 | 34.09 | 11.36 |
| | | 31.9 | 39.47 | 13.16 |
| 5% Type V Cement | TC | 23.21 | 20 | 6.67 |
| | CTC | 11.6 | 7.69 | 2.56 |
| | TE | 23.21 | 44.11 | 14.70 |
| | | 31.9 | 36.14 | 12.05 |
| 6% Lime + 4% Fly ash | TC | 31.9 | 14.63 | 4.88 |
| | CTC | 11.6 | 15 | 5.00 |
| | | 23.21 | 8 | 2.67 |
| | TE | 31.9 | 37.04 | 12.35 |
| 5% Type V Cement+15% FA | TC | 31.9 | 133.33 | 44.44 |
| | | 50 | 120 | 40.00 |
| | CTC | 10 | 97.22 | 32.41 |
| | | 23.21 | 114.28 | 38.09 |
| | TE | 31.9 | 217.4 | 72.47 |
| | | 50 | 192.31 | 64.10 |

A summary of all the parameters obtained for treated and untreated samples is depicted in Table 6.4, where VCI stands for the volumetric compression index and VRI stands for the volumetric rebound index. The rest of the parameters are elastic modulus, shear modulus, friction angle, cohesion, and the slope and intercept of the critical state line.

**Table 6.4. Constitutive Parameters Obtained from Triaxial Tests
on Untreated and Treated Soil**

| Chemical Treatment | Stress Path | Confining pressure (psi) | E _u (psi) | G _u (psi) | c _u (psi) | Φ (°) | η | μ _c | μ _E | M _c | M _E | VCI | VRI |
|----------------------|-------------|--------------------------|----------------------|----------------------|----------------------|-------|-------|----------------|----------------|----------------|----------------|-----|-------|
| Natural | TC | 23.21 | 11.54 | 3.85 | 12.31 | 18 | 0.183 | 7.5 | 0 | 0.4 | 0.3 | 4.2 | 19.4 |
| | | 31.9 | - | - | | | | | | | | | |
| | CTC | 11.6 | 10.34 | 3.45 | | | | | | | | | |
| | | 23.21 | 9.09 | 3.03 | | | | | | | | | |
| | TE | 23.21 | 34.09 | 11.36 | | | | | | | | | |
| | | 31.9 | - | - | | | | | | | | | |
| 5% Type V Cement | TC | 23.21 | 20 | 6.67 | - | - | - | 0 | 0 | 0.3 | 0.2 | - | - |
| | | 31.9 | - | - | | | | | | | | | |
| | CTC | 11.6 | 7.69 | 2.56 | | | | | | | | | |
| | | 23.21 | 44.11 | 14.70 | | | | | | | | | |
| TE | 31.9 | 36.14 | 12.05 | | | | | | | | | | |
| | 23.21 | 8 | 2.67 | | | | | | | | | | |
| 6% Lime + 4% Fly ash | TC | 31.9 | 14.63 | 4.88 | 17.99 | 19 | 0.194 | 11.5 | -2.5 | 0.4 | 0.3 | 0.7 | 4.8 |
| | | 31.9 | 15 | 5.00 | | | | | | | | | |
| | CTC | 11.6 | 15 | 5.00 | | | | | | | | | |
| | | 23.21 | 8 | 2.67 | | | | | | | | | |
| TE | 31.9 | 37.04 | 12.35 | | | | | | | | | | |
| | 31.9 | 133.33 | 44.44 | 19.81 | 17 | - | 14.5 | -4 | 0.4 | 0.3 | - | - | |
| TC | 50 | 120 | 40.00 | | | | | | | | | | |
| | CTC | 10 | 97.22 | | | | | | | | | | 32.41 |
| 23.21 | | 114.28 | 38.09 | | | | | | | | | | |
| TE | 31.9 | 217.4 | 72.47 | | | | | | | | | | |
| | 50 | 192.31 | 64.10 | | | | | | | | | | |

CHAPTER 7

TRUE TRIAXIAL TESTING: PRELIMINARY RESULTS

7.1 Cubical Device: Main Components

The main components of the mixed boundary type of true triaxial device that was used in the present Work are described in this chapter, and the results of a preliminary test performed on cement-treated high-PI clay and natural soil are reported in the final part of the chapter.

The mixed boundary type of true triaxial device used in this study has five flexible sides and one rigid side. The major components of the device are the cubical frame, lateral and top wall assemblies' sections, and flexible membranes. Figure 7.1.a shows the core aluminum frame that accommodates the cubical sample.

As illustrated in Figure 7.1.b, the lateral and top walls have flexible silicon membranes on the inner side and nylon tubes that are connected to transmit water from pistons to the membranes on the outer side. There is a fluid outlet on each side for expelling excess water and air bubbles from the membranes.

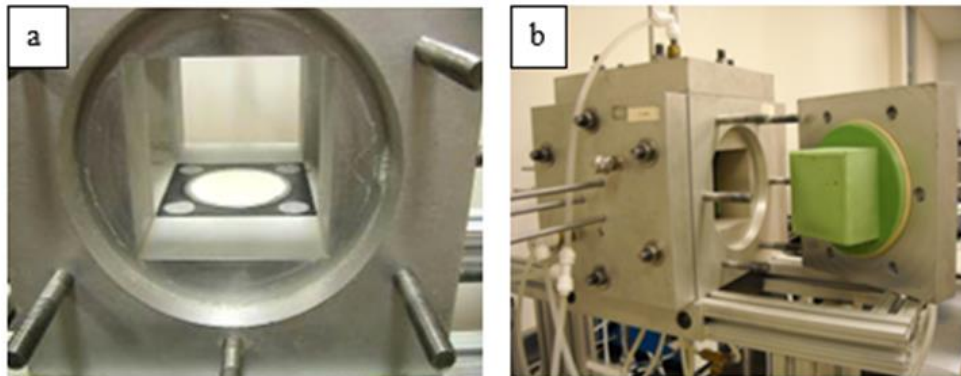


Figure 7.1 True triaxial device: (a) Cubical frame, (b) Wall assemblies (Hoyos et al., 2012)

The flexible membranes that apply hydraulic pressure to the sample are the product of mixing 10 units of Dow Corning silicone rubber with one unit of J-RTV silicone rubber curing agent. After casting the mixture in the mold, it is vacuumed for two hours in a vacuum chamber, until there are no visible bubbles in the membrane. The chamber is then bolted for two days to allow the membranes to cure, after which it is ready to be installed on the cubic walls. The preparation procedure is illustrated in Figure 7.2.

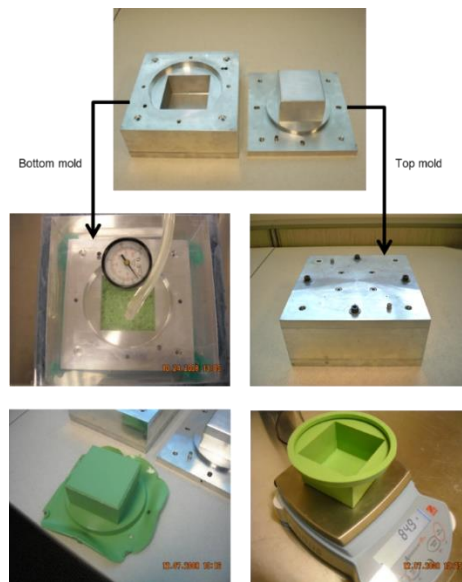


Figure 7.2 Fabrication of custom-made cubical (latex) membranes (Hoyos et al., 2012)

The hydraulic pressure is supplied and controlled by computer-driven PCP-5000 and PVC 100 panels that are depicted in Figure 7.3. The soil sample deformation is equal to the volume change of water in the pistons that is measured by a DC-750-5000 model LVDT that is attached to the hydraulic pistons (Hoyos et al., 2012). After the volume change is measured by the three LVDTs, the output is recorded and processed by the DA/PCS. The system uses a DAS-16 analog-

to-digital converter that converts the analog input signals (volts) delivered by the LVDT and pressure sensor in each hydraulic piston into digital output (Hoyos et al., 2012).

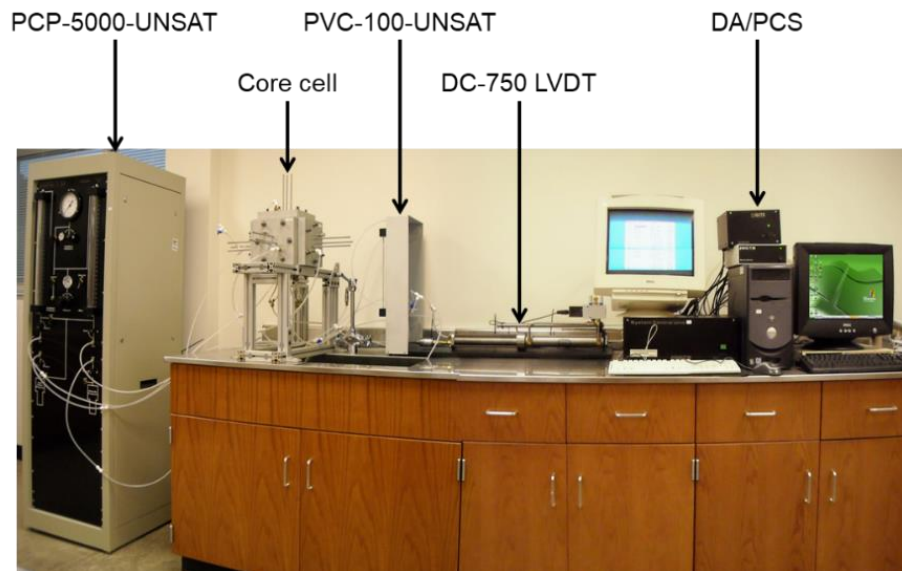


Figure 7.3 Panoramic view of true triaxial test layout (Hoyos et al., 2012)

7.2 Response of Chemically Treated Clay

High-PI clay with a dry density of (γ_d) = 102 lb./ft² and optimum moisture content (ω) of 13.5% was used in the preliminary tests. The cubical soil samples illustrated in Figure 7.4 were prepared by static compaction at a rate of 1 mm/min. Optimum water content and the highest Proctor dry density (γ_d) values were used to gain the target volume by compaction.

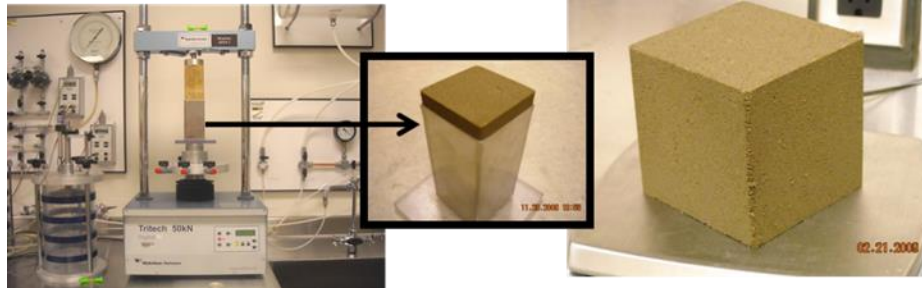


Figure 7.4 Static compaction of typical 3-in side cubical sample (Hoyos et al., 2012)

The stress path chosen for the preliminary test was HC and σ_1 . σ_2 , and the σ_3 increased from 0 to 100 kPa simultaneously with a ramp loading mode for one hour. The first test was conducted on an untreated sample, and the second was performed on the same clay treated with 3% cement +2% fly ash. The bulk modulus (K) is the slope of the tangent at origin in volumetric strain (ϵ_v) versus the net mean stress (p) curve, and its calculation is illustrated in Figure 7.5 and Figure 7.6. The formulas for the parameters are listed in Eq. 14, 15, and 16.

$$p = k_u \times \epsilon_v \quad (14)$$

$$\epsilon_v = \epsilon_1 + \epsilon_2 + \epsilon_3 \quad (15)$$

$$p = \frac{\sigma_1 + \sigma_2 + \sigma_3}{3} \quad (16)$$

The bulk modulus (K) is a strength parameter that estimates the strength of the soil under compression; stiffer samples have a higher bulk modulus. In the current experiments, K was $1/0.00003=33333.33$ kPa for the untreated soil sample and $1/0.014=71.42$ kPa for the treated sample, which means that stabilizing the clay with 3% cement + 2% fly ash, with 5 days of mellowing did not boost the stiffness of the soil. This might be due to eliminating the curing period.

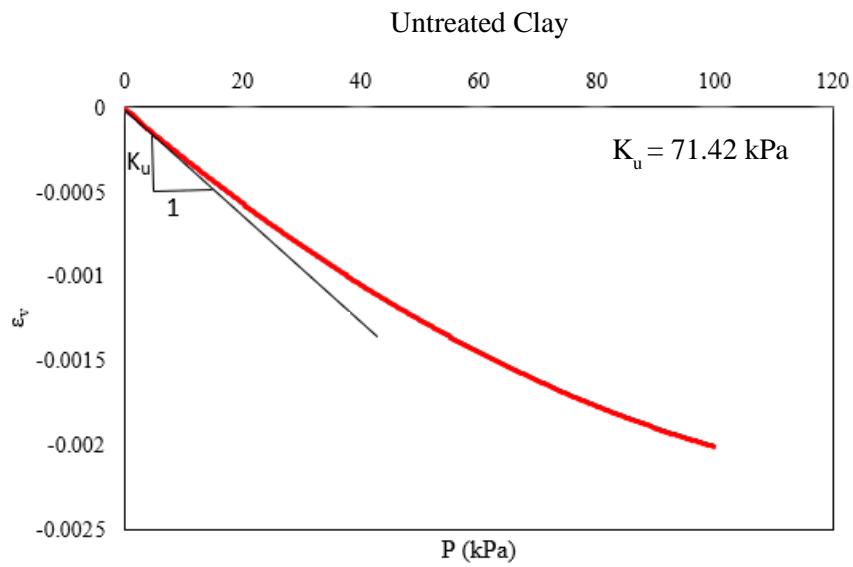


Figure 7.5 Volumetric response of untreated clay from hydrostatic compression (HC) test

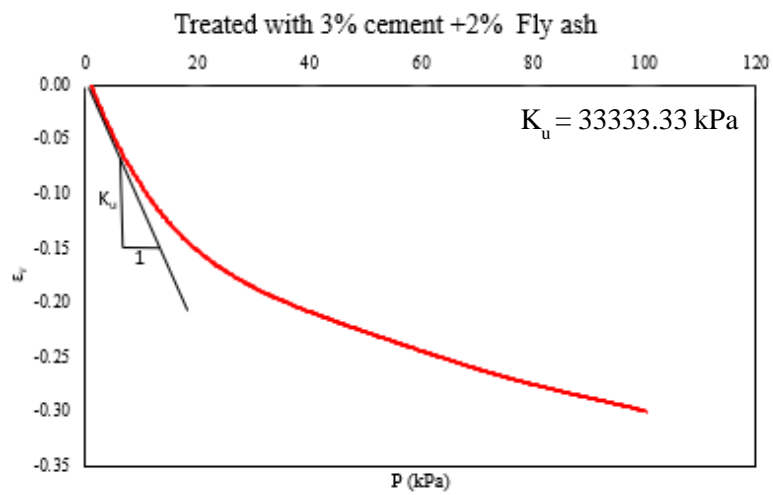


Figure 7.6 Hydrostatic compression (HC) test's volumetric response of clay treated with cement and fly ash with no days of curing

CHAPTER 8

CONCLUSIONS AND FUTURE WORK

8.1 Summary

A series of unconsolidated undrained (UU) and consolidated drained (CD) tests were conducted under multiple stress path and initial confining pressures on treated high-PI, sulfate-rich clay, using a fully servo-controlled triaxial apparatus. The stress path included CTC, TC, TE, PL, and HC, and the additives selected for stabilizing the sulfate-rich clay were 5% Type V cement, 6% lime + 4% Class F fly ash, and 5% Type V cement + 15% Class F fly ash. The test results were used to experimentally calibrate the key mechanical properties and constitutive parameters of natural and treated soils, including the assessment of corresponding critical state lines (CSL) and compaction-induced yield loci.

8.2 Conclusions

The main conclusions drawn from the analysis of the triaxial test results are summarized below.

1. The soil treated with 5% cement (V) exhibited less strength than the natural soil; on the other hand, the other two treatments, namely 6% lime + 4% fly ash and 5% cement (V) + 15% fly ash, exhibited higher strength than the natural soil. This may be attributed to the fact that cement treatments do not require long mellowing periods for stabilizing soil, and the 5 days of mellowing adopted for all of the treatments performed in this work might have hurt the efficacy of the treatment, while a 7-day curing may not be long enough.

2. The samples treated with both 6% lime + 4% fly ash and 5% cement (V) + 15% fly ash exhibited identical maximum shear failures that were higher than that of the natural soil, according to Mohr-Coulomb failure criteria. The undrained cohesion was also almost identical in both treatments, yet higher than that of natural soil, while the friction angle did not exhibit a definitive trend upon chemical treatment.
3. Based on the comparison of the quantitative assessment of the proportional loading (PL) results, the soil treated with 6% lime + 4% fly ash exhibited more volumetric stiffness than the natural soil.
4. Based on the critical state lines (CSLs), the samples treated with 5% cement (V) + 15% fly ash exhibited a higher intercept value than the rest of the soil, and the samples treated with 6% lime + 4% fly ash exhibited a higher intercept value than the natural soil, while the samples treated with 5% cement (V) showed zero value at the intercept. The slope of the CSL line was virtually the same for all of the soil samples, natural or treated, except that the slope was smaller for the samples treated with 5% cement (V).
5. According to the compaction-induced yield curves generated from the yield points on the stress-strain responses of different stress path, the samples treated with 5% cement (V) + 15% fly ash showed the largest yield loci. This indicates that, compared to 6% lime + 4% fly ash treatment, the soil treated with 5% cement (V) + 15% fly ash can sustain higher stresses before the soil yields into an elasto-plastic regime with irrecoverable plastic deformations. Both treatments, however, exhibited a larger compaction-induced yield locus than that of natural soil.
6. Overall, the samples treated with 5% cement (V) + 15% fly ash exhibited higher undrained elastic modulus and shear modulus than the natural soil, the soil treated with

5% cement (V), and the soil treated with 6% lime + 4% fly ash. Also, the natural soil with 23.21 psi initial confining pressure showed a higher undrained elastic modulus under TC than the CTC stress path.

7. The samples treated with 5% cement (V) + 15% fly ash showed higher strength based on CSL and yield curves, but a mixture of 6% lime + 4% fly ash is preferable because the stress-strain responses of the samples treated with 5% cement (V) + 15% fly ash were significantly more brittle.

8.3 Recommendations for Future Work

1. Perform additional triaxial tests for a more thorough, regression-based analysis of all of the experimental data, including the analytical relationships between soil strength-stiffness properties, mellowing periods, confining pressures, and stress path.
2. Analyze the effects of varying mellowing and curing durations on the strength-stiffness properties, constitutive parameters, critical state lines, and yield loci expansion.
- 3.
4. Assess the effect of long-term durability of the treated samples by subjecting them to wetting/drying cycles prior to multiple triaxial stress path.
5. Explore the suitability of existing constitutive models postulated for expansive and chemically modified expansive soils with the given set of constitutive parameters experimentally calibrated in the present work.
6. Apply different treatment methods to calculate the compaction energy during static compaction, using a load cell for natural and treated clay.

REFERENCES

Azadeh Asghariastaneh (2017). Performance of lime and cement-based treatment of sulfate-rich soil via RC testing. (Master thesis). The University of Texas at Arlington, Arlington, Texas.

Cammack, C. H. (1978). Triaxial shear of soil with stress path control by performance feedback.

Cheshomi, A., Eshaghi, A., & Hassanpour, J. (2017). Effect of lime and fly ash on swelling percentage and Atterberg limits of sulfate-bearing clay. *Applied Clay Science*, 135, 190-198.

Chittoori, B. C. S. (2009). Clay mineralogy effects on long-term performance of chemically treated expansive clays. (Ph.D. dissertation). The University of Texas at Arlington, Arlington, Texas.

Desai, C.S, and Siriwardane, H.J. (1984). Constitutive Laws for Engineering. Materials. Prentice_Hall.

Fang, J., Li, X., Liu, J., Liu, C., Liu, Z., & Ji, Y. (2018). The crystallization and salt expansion characteristics of a silty clay. *Cold Regions Science and Technology*, 154, 63-73.

Gaily, A. H. M. (2012). Engineering behavior of lime treated high sulfate soils. (Master Thesis). The University of Texas at Arlington, Arlington, Texas.

Gao, J., Wang, J., Wei, Y., Jiao, S., Jing, M., Gao, J., & Wang, C. (2020). Study on treatment of loess landslide based on nanosilica and fly ash composite stabilizer filling fissures. *Advances in Civil Engineering*, 2020.

He, S. (2019). *Chemical Stabilization of Expansive Soils Using Liquid Ionic Soil Stabilizers (LISS)* (Doctoral dissertation).

Holtz, R. D., Kovacs, W. D., & Sheahan, T. C. (1981). *An introduction to geotechnical engineering* (Vol. 733). Englewood Cliffs: Prentice-Hall.

Hoyos, L. R. & McCartney, J. (Eds.). (2017). Advances in characterization and analysis of expansive soils and rocks: Proceedings of the 1st GeoMEast International Congress and Exhibition, Egypt 2017 on Sustainable Civil Infrastructures. Springer.

Hoyos, L. R., Chainuwat, P., & Puppala, A. J. (2006). Dynamic characterization of chemically modified expansive soil (pp. 465-481). Taylor & Francis Group, London, UK.

Hoyos, L. R., Devabhaktuni, K., & Puppala, A. J. (2006). Assessment of heave induced infrastructure distress hazard potential in expansive soil environments using GIS technology. In *GeoCongress 2006: Geotechnical Engineering in the Information Technology Age* (pp. 1-6).

Hoyos, L. R., Laikram, A., & Puppala, A. J. (2006). Assessment of seasonal effects on engineering behavior of chemically treated sulfate-rich expansive clay. New York: Taylor & Francis.

Hoyos, L. R., Puppala, A. J., & Chainuwat, P. (2004). Dynamic properties of chemically stabilized sulfate rich clay. *Journal of Geotechnical and Geoenvironmental Engineering*, 130(2), 153-162.

Hoyos, L.R., and Puppala, A.J. (2009). Behavior of chemically stabilized sulfate-rich subgrade clays under quick aging environments. Keynote Paper, Springer, Proceedings of INDEX 2009: International Conference on Infrastructure Development on Expansive Soils, August 27-29, 2009, Adhiyamaan College of Engineering, Hosur, India, Eds: G. Ranganath, S. Suresh Babu, pp. 16-27.

Hoyos, Laureano R., Diego D. Pérez-Ruiz, & Anand J. Puppala. Refined true triaxial apparatus for testing unsaturated soils under suction-controlled stress path. *International Journal of Geomechanics* 12, no. 3 (2012): 281-291.

Huang, H., Huang, M., & Ding, J. (2018). Calculation of tangent modulus of soils under different stress path. *Mathematical Problems in Engineering*, 2018.

Jain, A., Choudhary, A. K., & Jha, J. N. (2020). Influence of rice husk ash on the swelling and strength characteristics of expansive soil. *Geotechnical and Geological Engineering*, 38(2), 2293-2302.

Jha, A. K., & Sivapullaiah, P. V. (2017). Physical and strength development in lime treated gypseous soil with fly ash-Micro-analyses. *Applied Clay Science*, 145, 17-27.

Khemissa, M. & Mahamedi, A. (2014). Cement and lime mixture stabilization of an expansive overconsolidated clay. *Applied Clay Science*, 95, 104-110.

Knopp, Julia & Moormann, Christian. Ettringite swelling in the treatment of sulfate-containing soils used as subgrade for road constructions. *Procedia Engineering* 143 (2016): 128-137.

Li, J., Cameron, D. A., & Ren, G. (2014). Case study and back analysis of a residential building damaged by expansive soils. *Computers and Geotechnics*, 56, 89-99.

Li, Y., Zou, W., Wu, W., Chen, L., & Chu, X. (2018). Triaxial compression tests of QH-E lunar soil simulant under constant mean principal stress path using discrete element method simulations. *Granular matter*, 20(4), 1-13.

Lucian, C. (2013). Effectiveness of mellowing time on the properties of two-stage lime-cement stabilized expansive soils. *International Journal of Engineering Research & Technology (IJERT)*, 2(5), 2278-0181.

Mariri, M., Ziaie Moayed, R., & Kordnaeij, A. (2019). Stress–Strain behavior of loess soil stabilized with cement, zeolite, and recycled polyester fiber. *Journal of Materials in Civil Engineering*, 31(12), 04019291.

Texas Department of Transportation. Guidelines for modification and stabilization of soils and base for use in pavement structures. Material and Test Division. (2019).

Matsuoka, H., Sun, D. A., Kogane, A., Fukuzawa, N., & Ichihara, W. (2002). Stress–strain behaviour of unsaturated soil in true triaxial tests. *Canadian Geotechnical Journal*, 39(3), 608-619.

McCartney, J. S. & Hoyos, L. R. (Eds.). (2018). Recent advancements on expansive soils: Proceedings of the 2nd GeoMEast International Congress and Exhibition on Sustainable Civil Infrastructures, Egypt 2018–The Official International Congress of the Soil-Structure Interaction Group in Egypt (SSIGE). Springer.

Pakbaz, M. S. & Alipour, R. (2012). Influence of cement addition on the geotechnical properties of an Iranian clay. *Applied Clay Science*, 67, 1-4.

Pedarla, A. (2009). Durability studies on stabilization effectiveness of soils containing different fractions of montmorillonite. (Master Thesis). The University of Texas at Arlington, Arlington, Texas.

Perez-Ruiz, D. D. (2009). *A refined true triaxial apparatus for testing unsaturated soils under suction-controlled stress path* (Doctoral dissertation, The University of Texas at Arlington).

Phanikumar, B. R. & Raju, E. R. (2020). Compaction and strength characteristics of an expansive clay stabilised with lime sludge and cement. *Soils and Foundations*, 60(1), 129-138.

Pinilla, J. D., Miller, G. A., Cerato, A. B., & Snethen, D. S. (2011). Influence of curing time on the resilient modulus of chemically stabilized soils. *Geotechnical Testing Journal*, 34(4), 364-372.

Puppala, A. J., Congress, S. S., Talluri, N., & Wattanasanthicharoen, E. (2019). Sulfate-heaving studies on chemically treated sulfate-rich geomaterials. *Journal of Materials in Civil Engineering*, 31(6), 04019076.

Semane, M. (2014). Stiffness response of chemically stabilized sulfate rich soil via resonant column test. (Master Thesis). The University of Texas at Arlington, Arlington, Texas.

Sirivitmaitrie, C. (2009). Novel stabilization methods for sulfate and non-sulfate soils. (Ph.D. dissertation). The University of Texas at Arlington, Arlington, Texas.

Talluri, N. (2013). Stabilization of high sulfate soils, (Ph.D. dissertation). The University of Texas at Arlington, Arlington, Texas.

Vasudev, D. (2007). Performance studies on rigid pavement sections built on stabilized sulfate soils. (Master Thesis). The University of Texas at Arlington, Arlington, Texas.

Ye, G. L., Ye, B., & Zhang, F. (2014). Strength and dilatancy of overconsolidated clays in drained true triaxial tests. *Journal of geotechnical and geoenvironmental engineering*, 140(4), 06013006.

Zhang, M., Zhao, M., Zhang, G., Nowak, P., Coen, A., & Tao, M. (2015). Calcium-free geopolymer as a stabilizer for sulfate-rich soils. *Applied Clay Science*, 108, 199-207.

Zhang, Y., Zuo, S., Li, R. Y. M., Mo, Y., Yang, G., & Zhang, M. (2020). Experimental study on the mechanical properties of Guiyang red clay considering the meso micro damage mechanism and stress path. *Scientific Reports*, 10(1), 1-20.